



Mohamed Khider University of Biskra  
Faculty of exact sciences and natural and life sciences  
Material sciences department

# MASTER MEMORY

Field of Material Sciences  
Physics  
Specialty: Energetic Physics and Renewable Energies  
Réf. : Entrez la référence du document

---

Presented by:

Fradj Zineb

Le : 18 June 2023

Investigation of Schottky barrier solar cell based  
on copper indium gallium (di) selenide (CIGS)  
alloy.

---

**Jury:**

Mr	Sengouga Nouredine	Professor	M <sup>ed</sup> Khider University of Biskra	President
Ms	Meftah Amjad	Professor	M <sup>ed</sup> Khider University of Biskra	Supervisor
Ms	Boudhib Wahiba	MCB	M <sup>ed</sup> Khider University of Biskra	Examiner

*Academic Year: 2022/2023*

## **ACKNOWLEDGEMENT**

This thesis was carried out at Mohammed Khider University of Biskra. First, I give thanks to ALLAH for protection and ability to do this work.

I am deeply grateful for the valuable guidance, continuous support, insight and patience of my supervisor, Pr. Meftah Amjad, without her constant trust and gentle prodding; this thesis would not have been completed. Additionally, I would like to thank the members of jury, Pr. Sengouga Nouredine and Dr. Boudhib Wahiba who have kindly accepted to read and examine my thesis.

I am also deeply thankful to my family and friends who encouraged me and prayed for me throughout the time of my research.

Finally, I would like to thank all who in one way or another contributed in the completion of this thesis.

May the Almighty ALLAH richly bless all of you.

## **Dedication**

*I dedicate this humble work to the one who gave me life, the symbol of tenderness, who sacrificed herself for my happiness and my success, for mom “Derradjia Debbakh”*

*To my father, “Saadi Fradj” who has been my shadow all along School years. My God protect them for me.*

*To my husband, “Omar” who supported and encouraged me.*

*To my sisters (Siham, Naziha, Madjda, Marwa) and their children (Heba Al-Rahman, Lujain, Ashwaq, Ayoub, Karim) and my brothers (Aissa, Imad) and my friends (Zahia, Yousra, Madiha, Fatima, Djahida, Manel...)*

***Zineb***

## **Abstract**

We have investigated a Schottky barrier solar cell based on p-type Cu(In,Ga)Se<sub>2</sub> (CIGS) material, using the Scaps-1D numerical simulation software for steady-state calculations. Internal parameters such as band diagram, electron and hole concentrations, and recombination rate were evaluated. External parameters such as current density-voltage ( $J - V$ ) and power-voltage ( $P - V$ ) characteristics were calculated. Photovoltaic output parameters, including short circuit current density ( $J_{sc}$ ), open circuit voltage ( $V_{oc}$ ), fill factor ( $FF$ ), maximum power ( $P_{max}$ ), and photovoltaic conversion efficiency ( $\eta$ ), were extracted. The investigation focused on changing the defect density ( $N_t$ ), thickness ( $d$ ), and doping concentration ( $N_A$ ) of the CIGS absorber layer. In terms of achieving the highest photovoltaic conversion efficiency ( $\eta$ ), increasing the doping concentration yielded 23.28%. Increasing the thickness of the p-type CIGS layer further improved efficiency to 25.22%. However, it is advisable to limit the defect density to avoid degradation, with a recommended value not exceeding  $10^{15} cm^{-3}$ . On the other hand, the photovoltaic output parameters of the cell show no dependency on the cathode work function ( $\phi_m$ ) changing in the range [4.1-4.7 eV]. These findings highlight the importance of optimizing parameters such as doping concentration, thickness, and defect density in order to achieve the highest photovoltaic conversion efficiency in Schottky barrier solar cells based on p-type CIGS material.

Keywords: CIGS; solar cell; Schottky barrier; numerical simulation

# Table of contents

<b>ACKNOWLEDGEMENT</b> .....	<b>I</b>
<b>Dedication</b> .....	<b>II</b>
<b>Abstract</b> .....	<b>III</b>
<b>Table of contents</b> .....	<b>IV</b>
<b>List of Figures</b> .....	<b>VI</b>
<b>List of tables</b> .....	<b>X</b>
<b>General introduction</b> .....	<b>1</b>
<b>References</b> .....	<b>4</b>
<b>CHAPTER I: Solar cells based on Cu (In, Ga) Se<sub>2</sub> (CIGS) material</b>	
<b>I.1.Introduction</b> .....	<b>7</b>
<b>I.2.Solar radiation</b> .....	<b>8</b>
<b>I.3 PN junction “base of the photovoltaic device”</b> .....	<b>10</b>
<b>I.4. Recombination phenomena</b> .....	<b>11</b>
<b>I.4.1 Radiative recombination</b> .....	<b>11</b>
<b>I.4.2 Shockley-Read-Hall (SRH) recombination</b> .....	<b>12</b>
<b>I.4.3 Auger recombination</b> .....	<b>12</b>
<b>I.5. Solar cell characterization</b> .....	<b>13</b>
<b>I.5.1 Equivalent circuit of a photovoltaic cell</b> .....	<b>13</b>
<b>I.5.2 Short-circuit current density (<math>J_{sc}</math>)</b> .....	<b>16</b>
<b>I.5.3 Open-circuit Voltage (<math>V_{oc}</math>)</b> .....	<b>16</b>
<b>I.5.4 Fill Factor (<math>FF</math>)</b> .....	<b>16</b>
<b>I.5.5 Power Conversion Efficiency (<math>\eta</math>)</b> .....	<b>17</b>
<b>I.5.6 Spectral response of a solar cell</b> .....	<b>18</b>
<b>I.5.7.External quantum Efficiency <math>EQE</math></b> .....	<b>18</b>
<b>I.5.8 Internal quantum Efficiency <math>IQE</math></b> .....	<b>18</b>
<b>I.6.Generations of solar cells</b> .....	<b>18</b>
<b>I.7. Thin-film photovoltaics</b> .....	<b>21</b>

<b>I.8. CIGS based solar cells .....</b>	<b>22</b>
<b>I.8.1 CIGS material properties.....</b>	<b>23</b>
<b>I.8.2. CIGS-based solar cells architecture.....</b>	<b>25</b>
<b>I.8.3. CIGS Cell Band Structure .....</b>	<b>26</b>
<b>I.9. Conclusion .....</b>	<b>27</b>
<b>References.....</b>	<b>29</b>
 <b>CHAPTER II: Schottky barrier solar cell based on CIGS material</b>	
<b>II.1 Introduction .....</b>	<b>36</b>
<b>II.2 Physics of the Schottky barrier solar cell. ....</b>	<b>36</b>
<b>II. 3 Charge transport in Schottky barrier solar cell.....</b>	<b>41</b>
<b>II.4. Overview of CIGS –based Schottky barrier solar cells .....</b>	<b>43</b>
<b>II.5 Conclusion.....</b>	<b>48</b>
<b>References.....</b>	<b>49</b>
 <b>CHAPTER III: Study of Schottky barrier solar cell based on CIGS material</b>	
<b>III.1 Introduction.....</b>	<b>52</b>
<b>III.2. SCAPS-1D: an overview.....</b>	<b>52</b>
<b>III. 3. Editing a solar cell structure via Scaps-1D.....</b>	<b>57</b>
<b>III.4. Description of the studied Schottky barrier solar cell based on CIGS material: .....</b>	<b>60</b>
<b>III.5. Results and discussion .....</b>	<b>63</b>
<b>III.6. Conclusion .....</b>	<b>81</b>
<b>References.....</b>	<b>84</b>
<b>General conclusion .....</b>	<b>88</b>

# List of Figures

## Chapter I

Figure number	Titles	Page number
I.1	Standards for measuring the spectrum of light energy emitted by the sun, concept of AM convention.	8
I.2	Solar spectra recorded under several conditions according to the AM convention. Source NREL solar spectrum. [13]	9
I.3	Principle of the solar cell operation	10
I.4	Mechanism of radiative recombination.	11
I.5	Shockley-Read-Hall (SRH) recombination mechanism	12
I.6	Auger recombination mechanism.	13
I.7	Equivalent circuit of a solar cell.	13
I.8	Representative $J(V)$ curve of a solar cell.	14
I.9	$I(V)$ characteristic of a p-n junction in the dark.	15
I.10	Record conversion efficiencies of different solar cell technologies in thin layer in cell and module. [28]	19
I.11	A chart showing the generations and chronological evolution solar cells [34].	20
I.12	Cell production by technology (in MW of DC current) [35].	21
I.13	Graph showing the progress in conversion efficiency in laboratory scale (squares), small modules (circles) and full-size modules (triangles) CIGS-based TFSC's [41].	23
I.14	a) Band gap as a function of lattice parameter of I-III-VI <sub>2</sub> semiconductors and II-VI semiconductors reprinted from Scheer [47]. b) Chalcopyrite structure of CuInSe <sub>2</sub> semiconductor reprinted from [48].	24
I.15	Basic structure of a Cu(In, Ga)Se <sub>2</sub> thin-film solar cell [45].	26

I. 16	Schematic representation of the expected band-alignment in a typical CIGS-based device at 0 V bias [55], for constant GGI, and hence constant bandgap ( $E_g \sim 1.2 eV$ ). The upper and lower black-lines indicate the conduction band edge ( $E_C$ ) and valence band edge ( $E_V$ ) respectively. The bandgap of the ZnO layer is assumed to be in the range $> 3 eV$ . ‘SCR’ refers to the Space Charge Region (depletion region), while ‘QNR’ refers to the ‘Quasi Neutral Region’, i.e. the bulk of the absorber layer where no internal electric field is present	27
-------	--	----

## Chapter II

Figure number	Titles	Page number
II.1	Energy band diagrams for a metal-p-type semiconductor contact when $\Phi_S > \Phi_M$ . Materials are shown in isolation (a) and after contact (b). All parameters are referenced to the vacuum level under the basis of ideal Schottky barrier theory [16].	37
II.2	a) Schottky barrier for an n-type semiconductor when $\Phi_M > \Phi_S$ . The Fermi levels equalize once that materials are in contact, which causes the bands to bend upwards and to create a barrier $\Phi_{bn}$ that electrons need to overcome to cross from the semiconductor to the metal, thus rectifying properties are achieved. b) When $\Phi_M > \Phi_S$ . for a p-type material, the bending of the bands does not prevent the motion of holes, and a contact with Ohmic instead of rectifying properties is created [16].	38
II.3	When $\Phi_M < \Phi_S$ bands are bent downwards and, a) Ohmic properties are achieved for n-type semiconductors whereas b) p-type semiconductors produce rectifying contacts due to the difficulty of holes to pass below the barrier $\Phi_{bp}$ . [16].	39
II.4	The representation of the generated electron-hole pair in Schottky barrier solar cell within: (a) an electrical circuit. (b) energy band structure showing the possible transport mechanisms ((1) -(5)).	42
II.5	Schematic diagram of :(a) CIGS-based Schottky barrier solar cell, (b) the corresponding band diagram under sunlight illumination and zero bias (short circuit condition).	47

### Chapter III

Figure number	Titles	Page number
III .1	The SCAPS start-up panel: The Action panel or main panel. The meaning of the blocks numbered 1 to 6 is explained in the text. [13].	55
III .2	Energy Bands Panel [13].	56
III. 3	Energy band panel after the calculations	56
III .4	Panel of I(V) characteristic curves in dark and light conditions. The solar cell output parameters are also displayed [13].	57
III .5	Solar cell definition panel	58
III.6	Layer properties panel.	58
III.7	Contact properties panel. [13].	59
III.8	Structure of the studied Schottky - barrier solar cell based on p-type CIGS material.	60
III.9	Band diagram of the Schottky barrier solar cell based on p-type CIGS material with Aluminum (Al) as the cathode metal ( $\phi_m = 4.1 eV$ ): (a) at thermal equilibrium, (b) at short circuit condition with AM 1.5G spectrum illumination.	64
III.10	Carrier density distributions along the Schottky barrier solar cell based on p-type CIGS material at thermal equilibrium, and at short circuit condition with AM 1.5G spectrum illumination	65
III.11	Simulated $J - V$ and $P - V$ characteristics of the Schottky barrier solar cell based on p-type CIGS material with Al as the cathode metal ( $\phi_m = 4.1 eV$ ), under the AM1.5G standard spectrum and $T = 300^{\circ}K$	66
III.12	Generation and recombination rate distributions through the Schottky barrier solar cell based on p-type CIGS material under the AM1.5G standard spectrum and $T = 300^{\circ}K$	66
III.13	Generation and recombination rate distributions through the Schottky barrier solar cell based on p-type CIGS material with the increase of the defect density	67

	$(N_t)$ within the range $[10^{10} - 10^{20} cm^{-3}]$ .	
III.14	Generation and recombination rate distributions through the Schottky barrier solar cell based on p-type CIGS material with the increase of the thickness ( $d$ ) within the range $[0.01 - 10 \mu m]$ .	68
III.15	Generation and recombination rate distributions through the Schottky barrier solar cell based on p-type CIGS material with the increase of the doping concentration ( $N_A$ ) within the range $[10^{10} - 5 \times 10^{17} cm^{-3}]$ .	68
III.16	Variation effect of the p-type CIGS layer defect density on : (a) $(J - V)$ characteristics and (b) the photovoltaic output parameters of the Schottky barrier solar cell .	70
III.17	Variation effect of the p-type CIGS layer thickness on: (a) $(J - V)$ characteristics and (b) the photovoltaic output parameters of the Schottky barrier solar cell .	72
III.18	Variation effect of the p-type CIGS layer doping concentration on : (a) $(J - V)$ characteristics and (b) the photovoltaic output parameters of the Schottky barrier solar cell .	75
III.19	Optical generation rate distribution along the Schottky barrier solar cell with the increase of the doping concentration ( $N_A$ ) within the range $[10^{10} - 5 \times 10^{17} cm^{-3}]$ .	77
III.20	Behaviour of : (a) $(J - V)$ characteristics and (b) the photovoltaic output parameters of the Schottky barrier solar cell with changing the cathode work function ( $\phi_m$ ) within the range $[4.1 - 4.7 eV]$ .	80

# List of tables

## Chapter I

Table number	Titles	Page number
I.1	Highest efficiencies of state of art solar cells based on different materials [32,33].	22

## Chapter III

Table number	Titles	Page number
III .1	Baseline parameters for modeling the Schottky barrier solar cell based on CIGS material at $T = 300 \text{ }^\circ\text{K}$ . [17, 18, 19, 20, 21, 22].	62
III .2	Variation effect of the p-type CIGS layer defect density on the photovoltaic output parameters of the Schottky barrier solar cell .	81
III .3	Variation effect of the p-type CIGS layer thickness on the photovoltaic output parameters of the Schottky barrier solar cell	73
III .4	Variation effect of the p-type CIGS layer doping concentration on the photovoltaic output parameters of the Schottky barrier solar cell .	76

# **General introduction**

## General introduction

The need for clean and renewable sources of energy is indeed increasing due to various geopolitical and environmental factors. Photovoltaics, along with other green technologies like wind, hydroelectric, solar thermal, and geothermal power generation, are recognized as viable solutions to meet the growing energy demand. Solar energy is particularly abundant, with the amount of energy available from the Sun at the Earth's surface far surpassing our current and future energy needs. The key challenge lies in designing efficient devices that can effectively convert sunlight into electricity while using sustainable and affordable materials. Additionally, it is important to develop fabrication processes that are cost-effective and scalable [1].

While crystalline silicon (c-Si) is widely used in photovoltaic solar cells, thin film technologies offer an alternative that can be cheaper and achieve comparable efficiencies. Thin film solar cells utilize direct energy band gap semiconductors, which have certain advantages over c-Si. One key advantage of thin film technologies is their ability to achieve similar sunlight absorption with only a few microns of material, compared to several hundred microns required by c-Si. This is because direct band gap materials allow for efficient absorption of sunlight in a smaller thickness. Three of the most successful thin film materials used in solar cells are: Cadmium Telluride (CdTe), hydrogenated Amorphous Silicon (a-Si:H) and Copper Indium Gallium Diselenide (Cu (In,Ga) Se<sub>2</sub>: CIGS) [2]. CIGS thin film solar cells have shown promise in terms of both efficiency and manufacturing scalability. CIGS is a direct band gap material that can be deposited as a thin film on flexible substrates. It is attractive due to its abundance and potential for low-cost manufacturing processes. It offers good light absorption properties [3,4] and has demonstrated high conversion efficiencies in laboratory settings [5-8].

A Schottky-barrier solar cell, also known as a metal-semiconductor (MS) solar cell, is a type of photovoltaic device that converts sunlight into electricity. It differs from traditional p-n junction solar cells by utilizing a metal-semiconductor interface; which creates a Schottky junction. The metal electrode acts as the top (front) contact, while the semiconductor material serves as the active layer responsible for absorbing light and generating charge carriers (electrons and holes). The Schottky junction forms a barrier to the flow of the majority charge carriers from the semiconductor material to the front contact. The Schottky junction plays a crucial role in the operation of the solar cell. It creates a built-in electric field that separates the photo-generated

charge carriers and drives them toward their respective electrodes. This separation is vital for the efficient extraction of carriers and reduces recombination losses, improving the overall performance of the solar cell [9-13].

Various materials have been used as the semiconductor in Schottky-barrier solar cells, including silicon (Si), gallium arsenide (GaAs), copper indium gallium selenide (CIGS), Indium Gallium Nitride (InGaN) and organic semiconductors. CIGS is an emerging thin-film semiconductor material that has shown promise for both traditional and Schottky-barrier solar cells [14-18]. It is important to note that the efficiency, cost, and application requirements of a solar cell technology depend on various factors, including the specific material, device architecture, and manufacturing processes employed. Ongoing research and technological advancements aim to address the challenges and improve the performance of Schottky-barrier solar cells, making them a promising alternative to traditional solar cell designs [13,19-25].

### **Objectives of the work:**

In this work, we will focus on the investigation of the Schottky barrier solar cell based on p-type  $\text{Cu}(\text{In,Ga})\text{Se}_2$  (CIGS) material, exposed to the AM1.5 G standard spectrum at ambient temperature (300°K). The solar cell consists of a p-type CIGS absorber layer with a front contact of Aluminum (Al) as cathode metal, and a back contact that acts as the anode. The work function ( $\phi_m$ ) of the cathode is 4.1 eV, lower than the electron affinity of the p-type CIGS material ( $\chi_{sc} = 4.8 \text{ eV}$ ). Consequently, the Al/p-type CIGS interface forms a Schottky barrier which blocks the flow of holes from the p-type CIGS layer toward the cathode; while enabling efficient collection of photogenerated electrons. The back contact forms an Ohmic contact, allowing easy passage of both electrons and holes for efficient carrier transport. In this investigation, we utilize the Scaps-1D numerical simulation software for steady-state calculations. Internal parameters such as band diagram, electron and hole concentrations, and recombination rate are evaluated. External parameters such as current density-voltage ( $J - V$ ) and power-voltage ( $P - V$ ) characteristics are calculated. The photovoltaic output parameters, including short circuit current density ( $J_{sc}$ ), open circuit voltage ( $V_{oc}$ ), fill factor ( $FF$ ), maximum power ( $P_{max}$ ), and photovoltaic conversion efficiency ( $\eta$ ), are extracted from the current density-voltage ( $J - V$ ) characteristics. The investigation will focus on varying parameters of the p-type CIGS absorber layer: defect density ( $N_t$ ) within the range  $[10^{10} - 10^{20} \text{ cm}^{-3}]$ , the thickness ( $d$ ) within the range  $[0.01-10\mu\text{m}]$ , and the doping concentration ( $N_A$ ) within the range  $[10^{10} - 5 \times 10^{17} \text{ cm}^{-3}]$ .

Furthermore, we will explore if there is an effect of changing the cathode work function ( $\phi_m$ ) in the range [4.1 – 4.7 eV] on the solar cell output parameters. To assess this effect, we will consider different cathode metals, including Al, Ta, Ti, Zn, Mo, W, and Cu, respectively.

Overall, the master thesis aims to provide a comprehensive understanding of photovoltaic energy, particularly focusing on CIGS-based Schottky barrier solar cells, and presents numerical simulations to investigate the performance of these solar cells under various parameters.

### **Thesis organization:**

The master thesis is structured into three main chapters, along with a general introduction and conclusion. Here is a breakdown of each chapter:

Chapter I: This chapter provides an introductory overview of the basic concepts in photovoltaic energy. It covers the fundamental properties and operation of solar cells based on PN junctions. Additionally, it focuses on copper indium gallium diselenide (Cu (In, Ga) Se<sub>2</sub>: CIGS) based solar cells, highlighting their important structural, electrical, and optical properties. CIGS is a semiconductor material that shows promise as an alternative to traditional silicon solar cells.

Chapter II: The main focus of this chapter is to provide an overview of CIGS-based Schottky barrier solar cells and the physics that limit the transport in such cells. The Schottky barrier solar cell is a type of solar cell that relies on a metal-semiconductor junction, known as a Schottky barrier, to generate electricity. This chapter explores the working principles and limitations of this type of solar cell.

Chapter III: This chapter is dedicated to the investigation of Schottky barrier solar cells based on p-type CIGS material using the numerical simulation software Scaps-1D. The research study aims to analyze the impact of varying parameters of the CIGS absorber layer on the performance of the solar cell. Specifically, the focus is on investigating the effects of changing the defect density ( $N_t$ ), thickness ( $d$ ), and doping concentration ( $N_A$ ) of the CIGS layer. Additionally, the study explores the influence of altering the cathode work function ( $\phi_m$ ) on the output parameters of the solar cell. The obtained results will be thoroughly discussed and analyzed in this chapter.

The general introduction sets the context for the research topic and provides an overview of the thesis. The general conclusion summarizes the key findings and discusses their implications.

## References

- [1] S. Huang, ‘Grand Challenges and Opportunities in Photovoltaic Materials and Devices’, *Frontiers in Photonics*, vol. 2, 2021, Accessed: Jun. 06, 2023. [Online]. Available: <https://www.frontiersin.org/articles/10.3389/fphot.2021.651766>
- [2] R. Aninat, ‘Study of Cu(In, Al)Se<sub>2</sub> thin films prepared by selenisation of sputtered metallic precursors for application in solar cells’, Ph.D thesis, Northumbria University, 2012. Accessed: Jun. 19, 2023. [Online]. Available: <https://nrl.northumbria.ac.uk/id/eprint/11373/>
- [3] J. J. Loferski, ‘Theoretical Considerations Governing the Choice of the Optimum Semiconductor for Photovoltaic Solar Energy Conversion’, *Journal of Applied Physics*, vol. 27, no. 7, pp. 777–784, May 2004, doi: 10.1063/1.1722483.
- [4] L. L. Kazmerski, F. R. White, and G. K. Morgan, ‘Thin-film CuInSe<sub>2</sub>/CdS heterojunction solar cells’, *Applied Physics Letters*, vol. 29, no. 4, pp. 268–270, Aug. 2008, doi: 10.1063/1.89041.
- [5] A. Kingma, ‘Electrical characterization of low temperature pulsed-electron-deposited Cu(In,Ga)Se<sub>2</sub> solar cells’, Ph.D thesis, Università di Parma. Dipartimento di Scienze chimiche, della vita e della sostenibilità ambientale, 2018. Accessed: Jun. 07, 2023. [Online]. Available: <https://www.repository.unipr.it/handle/1889/3671>
- [6] M. Powalla et al., ‘Advances in Cost-Efficient Thin-Film Photovoltaics Based on Cu(In,Ga)Se<sub>2</sub>’, *Engineering*, vol. 3, no. 4, pp. 445–451, Aug. 2017, doi: 10.1016/J.ENG.2017.04.015.
- [7] P. Jackson, R. Wuerz, D. Hariskos, E. Lotter, W. Witte, and M. Powalla, ‘Effects of heavy alkali elements in Cu(In,Ga)Se<sub>2</sub> solar cells with efficiencies up to 22.6%’, *physica status solidi (RRL) – Rapid Research Letters*, vol. 10, no. 8, pp. 583–586, 2016, doi: 10.1002/pssr.201600199.
- [8] M. A. Green, Y. Hishikawa, E. D. Dunlop, D. H. Levi, J. Hohl-Ebinger, and A. W. Y. Ho-Baillie, ‘Solar cell efficiency tables (version 51)’, *Progress in Photovoltaics: Research and Applications*, vol. 26, no. 1, pp. 3–12, 2018, doi: 10.1002/pip.2978.

- [9] R. T. (董梓則) Tung, ‘The physics and chemistry of the Schottky barrier height’, *Applied Physics Reviews*, vol. 1, no. 1, p. 011304, Jan. 2014, doi: 10.1063/1.4858400.
- [10] L. Fraas and L. Partain, ‘Solar Cells: A Brief History and Introduction’, in *Solar Cells and their Applications*, John Wiley & Sons, Ltd, 2010, pp. 1–15. doi: 10.1002/9780470636886.ch1.
- [11] P. T. Landsberg and C. Klumpke, ‘Theory of the Schottky Barrier Solar Cell’, *Proceedings of the Royal Society of London. Series A, Mathematical and Physical Sciences*, vol. 354, no. 1676, pp. 101–118, 1977.
- [12] S. Srivastava, N. K. Swami, and G. P. Srivastava, ‘Efficiency of Schottky barrier solar cells’, *physica status solidi (a)*, vol. 58, no. 2, pp. 343–348, 1980, doi: 10.1002/pssa.2210580203.
- [13] K. Chowdhury and R. Mandal, ‘Advancement of schottky barrier solar cells: a review’, in *contemporary issues in computing*, Volkson press, Jan. 2020, pp. 93–98. doi: 10.26480/cic.01.2020.93.98.
- [14] K.-J. Hsiao, J.-D. Liu, H.-H. Hsieh, and T.-S. Jiang, ‘Electrical impact of MoSe<sub>2</sub> on CIGS thin-film solar cells’, *Phys. Chem. Chem. Phys.*, vol. 15, no. 41, pp. 18174–18178, Oct. 2013, doi: 10.1039/C3CP53310G.
- [15] B. Theys et al., ‘Revisiting Schottky barriers for CIGS solar cells: Electrical characterization of the Al/Cu(InGa)Se<sub>2</sub> contact’, *physica status solidi (a)*, vol. 213, no. 9, pp. 2425–2430, 2016, doi: 10.1002/pssa.201533063.
- [16] Y. Osman, M. Fedawy, M. Abaza, and M. H. Aly, ‘Optimized CIGS based solar cell towards an efficient solar cell: impact of layers thickness and doping’, *Opt Quant Electron*, vol. 53, no. 5, p. 245, Apr. 2021, doi: 10.1007/s11082-021-02873-4.
- [17] N. Mufti et al., ‘Review of CIGS-based solar cells manufacturing by structural engineering’, *Solar Energy*, vol. 207, pp. 1146–1157, Sep. 2020, doi: 10.1016/j.solener.2020.07.065.
- [18] J. Ramanujam and U. P. Singh, ‘Copper indium gallium selenide based solar cells – a review’, *Energy Environ. Sci.*, vol. 10, no. 6, pp. 1306–1319, Jun. 2017, doi: 10.1039/C7EE00826K.

- [19] Y. Song, A. Osherov, V. Bulović, and J. Kong, ‘Graphene-Perovskite Schottky Barrier Solar Cells’, *Adv. Sustainable Syst.*, vol. 2, no. 4, p. 1700106, Apr. 2018, doi: 10.1002/adsu.201700106.
- [20] G. Fan et al., ‘Graphene/silicon nanowire Schottky junction for enhanced light harvesting’, *ACS Appl Mater Interfaces*, vol. 3, no. 3, pp. 721–725, Mar. 2011, doi: 10.1021/am1010354.
- [21] S. S. Li, ‘Theoretical analysis of a novel MPN gallium arsenide Schottky barrier solar cell’, *Solid State Electronics*, vol. 21, pp. 435–438, Feb. 1978, doi: 10.1016/0038-1101(78)90274-5.
- [22] A. Benslim, A. Meftah, M. Labed, A. Meftah, and N. Sengouga, ‘Study and optimization of InGaN Schottky solar cell performance’, *Optik*, vol. 247, p. 167984, Dec. 2021, doi: 10.1016/j.ijleo.2021.167984.
- [23] K. J. Singh, D. Chettri, T. J. Singh, T. Thingujam, and S. kumar Sarkar, ‘A performance optimization and analysis of graphene based schottky barrier GaAs solar cell’, *IOP Conf. Ser.: Mater. Sci. Eng.*, vol. 211, no. 1, p. 012024, Jun. 2017, doi: 10.1088/1757-899X/211/1/012024.
- [24] M. E. Edweeb, E. J. Charlson, and E. M. Charlson, ‘Sputtered Schottky barrier solar cells on p -type GaAs’, *Appl. Phys. Lett.*, vol. 43, no. 6, pp. 572–574, Sep. 1983, doi: 10.1063/1.94429.
- [25] J. K. Leggett, *Half Gone: Oil, Gas, Hot Air and the Global Energy Crisis*. Portobello Books, 2005.

# **CHAPTER I**

**Solar cells based on Cu (In, Ga) Se<sub>2</sub> (CIGS) material**

## I.1.Introduction

Global Energy demand is in increase continuously every year due to population growth and economic development. In order to fulfill the energy demand with time, roughly 30 TWh of energy is required by the end of 2050 [1, 2]. Today most of these energy demands are produced by burning fossil fuels such as coal, petroleum and natural gas. The peak supply of these energy from conventional sources has already been achieved recently or is about to be achieved within the next 20- 30 years [1, 2].

There is increasing need for clean, renewable sources of energy in today's geopolitical and environmental context. Photovoltaics, combined with other "green" technologies such as wind, hydroelectric, solar thermal and geothermal power generation, is now generally recognized to be a solution to the energy demand. The energy available from the Sun at the surface of the Earth is more than sufficient to provide for our present and future energy needs. The main challenge is to design devices that are efficient in converting the sunlight into electricity, made of sustainable and cheap elements, and that can be fabricated using low cost processes [3,4]

Ternary compounds of the group I-III-VI<sub>2</sub> of the chalcopyrite type are a class of semiconductors that have been extensively researched in recent years. These materials have the chemical formula ABC<sub>2</sub>, where A is a group I element (e.g., Cu), B is a group III element (e.g., In, Ga or Al), C is a group VI element (e.g., S, Se or Te) [5]. One of the key advantages of these materials is their chalcopyrite crystal structure, which gives them unique physical and chemical properties. The chalcopyrite structure has a relatively low symmetry, which can result in high carrier mobility and low defect densities. Additionally, these materials have a high stability, which makes them suitable for use in a variety of technological applications [6]. Another advantage of these materials is their high optical coefficient, which makes them useful in photovoltaic devices such as solar cells. The bandgap of chalcopyrite compounds is typically in the range of 1-2 eV, which makes them suitable for absorbing visible light and converting it into electrical energy [6,7]. In addition to their use in photovoltaics, chalcopyrite compounds have also been investigated for use in light-emitting diodes (LEDs) and photo-detectors. By controlling the composition and doping of these materials, researchers have been able to tailor their properties to specific applications [8].

Overall, the unique combination of physical and chemical properties exhibited by chalcopyrite compounds makes them an attractive material for a wide range of technological applications.

In this chapter we will provide an introductory overview of the basic concepts in photovoltaic energy. The properties of solar cells based on PN junctions and their mode of operation will be also presented. Thereafter, we will focus on the copper indium gallium diselenide (Cu (In, Ga) Se<sub>2</sub>: CIGS) based solar cells, and highlight the important structural, electrical and optical properties of the CIGS which is a semiconductor material that has emerged as a promising alternative to traditional silicon solar cells.

## I.2.Solar radiation

The sun is a nuclear fusion reactor that has been operating for 5 billion years, and through the process of converting hydrogen into helium, it emits huge amounts of energy into space (its power is estimated at  $63,500 \text{ kW} / \text{m}^2$ ). This radiation leaks out in all directions and travels through space at a constant speed of  $300,000 \text{ km}$  per second, called the speed of light. After traveling a distance of approximately 150 million kilometres, solar radiation reaches outside the Earth's atmosphere with a strength of about  $1350 \text{ W/m}^2$ , which is called the extra-atmospheric solar constant (Figure. I.1).

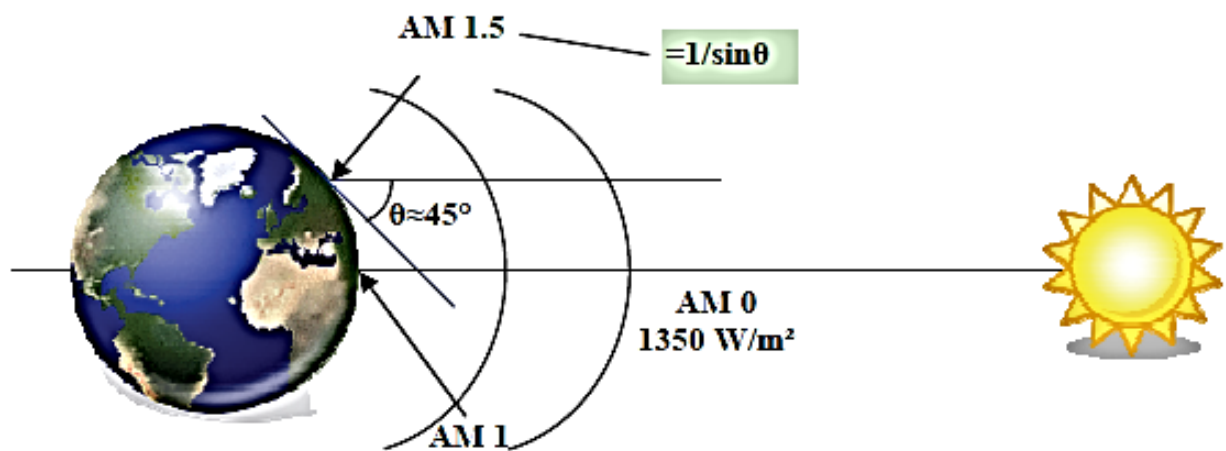


**Figure I.1:** Standards for measuring the spectrum of light energy emitted by the sun, concept of AM convention.

Current theories present solar radiation as particle emission [9,10]. This stream of particles, called photons, reaches the earth in different wavelengths ranging from UV ( $0.2 \mu\text{m}$ ) to far infrared ( $2.5 \mu\text{m}$ ). We use the AM concept of Air Mass in order to characterize the solar spectrum in terms of the emitted energy [11,12]. The total energy transmitted by solar radiation over the distance between the sun and the earth is of order  $1350 \text{ W/m}^2$  (AM0) in space outside Earth's atmosphere (Figure. I.1 and Figure I.2).

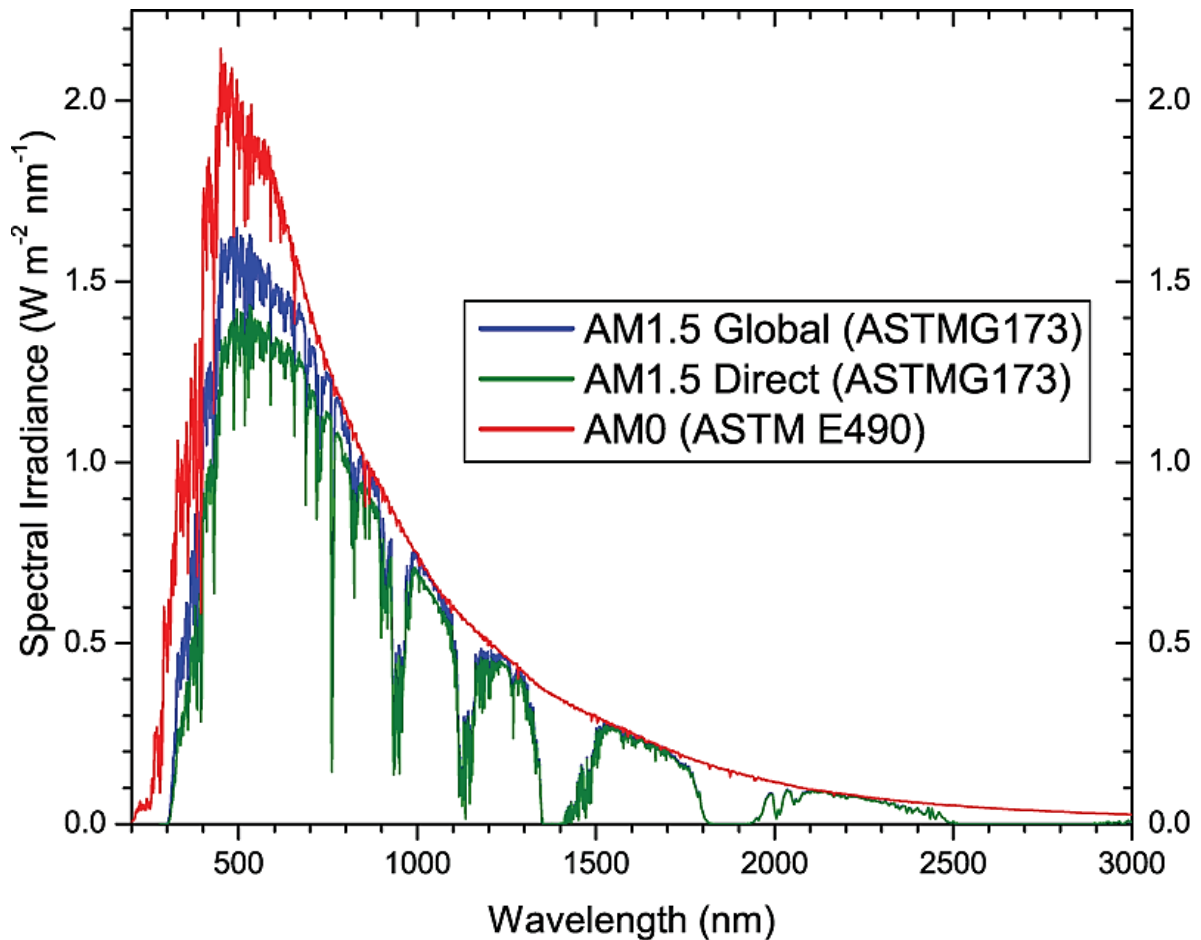


**Figure I.2:** Solar spectra recorded under several conditions according to the AM convention.

Source NREL solar spectrum. [13]

When Solar radiation passes through the atmosphere, it undergoes an attenuation and a modification of its spectrum, as a result of absorption and dispersion in gases, water and soil. Thus, the ozone layer absorbs part of the light spectrum from the sun, especially part of the ultraviolet radiation which is harmful to health. Direct sunlight radiation received at ground level (at an inclination of 90°) is up to  $1000 \text{ W/m}^2$  due to atmospheric absorption (AM1). This value changes according to the ray slope of light relative to the earth. The smaller the penetration angle  $\theta$ , the thicker the thickness atmosphere that the rays will have to cross will be large, resulting in a substantial loss of energy. For example, direct energy carried by solar radiation which arrives at an angle of 48° is about  $833 \text{ W/m}^2$  (AM1.5). To know the global radiation received on the ground, it is necessary to add to the latter the diffuse radiation. Diffuse radiation concerns all radiation whose trajectory between the sun and the observation point is not geometrically straight and which is dispersed or reflected by the atmosphere or the ground.

Considering this, we obtain a reference of the global spectrum noted AM1.5 with a power of  $1000W/m^2$ , Figure I.2 corresponds to our latitudes [13,14].

### I.3 PN junction “base of the photovoltaic device”

The solar cell is an electronic component capable of supplying energy, if properly lit. If the energy of the photons that reach the solar cell ( $h\nu$ ) is greater than the bandgap energy of the material, an electron-hole pair is generated. The electric field created between the two terminals of the PN junction allows the electron-hole pair to separate [15]. The operating principle of the solar cell is illustrated in Figure I.3.

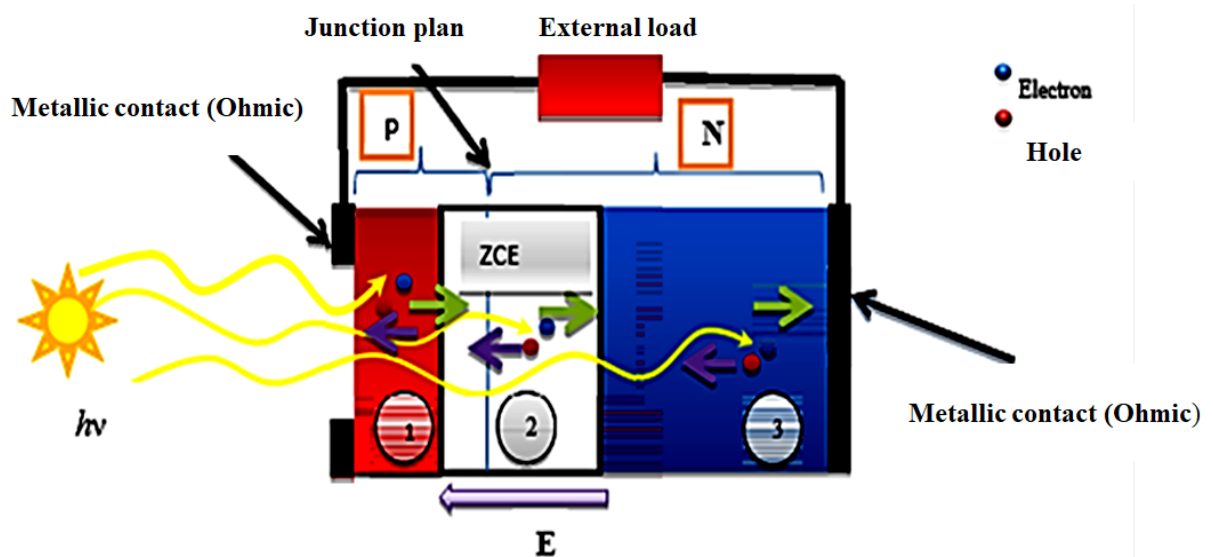


Figure I.3: Principle of the solar cell operation.

The incident photons create free carriers in each of the regions (1), (2) and (3) whose behaviour differs according to the place of their creation. The minority photocarriers diffuse in the electrically neutral P and N zones. Those which reach the space charge region are propelled by the electric field towards the region where they become the majority. These photocarriers therefore contribute to the scattering current, by creating a scattering photocurrent. In the space charge zone (Z.C.E or SCR), the electron-hole pairs, created by the photons, are dissociated by the electric field; the electron is propelled towards the N-type region and the hole towards the P-type region. These carriers give rise to a generation photo-current [16]. Thus, the energy conversion process in a solar cell can be summarized as follow [17]:

1. Absorption of photon energy from sunlight into the absorber or active layer of the solar cell.

2. Generation of charge carriers in the device by the process of electron excitation due to photo absorption.
3. Separation of charge carriers at the cell junction or interface.
4. Collection of charge carriers at the contacts.

## I.4. Recombination phenomena

The operation of a solar cell is based on the creation and separation of electron-hole pairs by absorption of light and under the action of an electric field. Nevertheless, there are always recombinations of these electron-hole pairs limiting the cell performance. In a semiconductor material, a given recombination mechanism is characterized by a recombination rate, representing the number of recombination per time unit and per volume unit. There are three main mechanisms: radiative recombination, Shockley-Read-Hall (SRH) recombination and Auger recombination. [18]

### I.4.1 Radiative recombination

Radiative recombination or band to band recombination (Figure I.4), corresponds to the transition of an electron from the conduction band to the valence band.

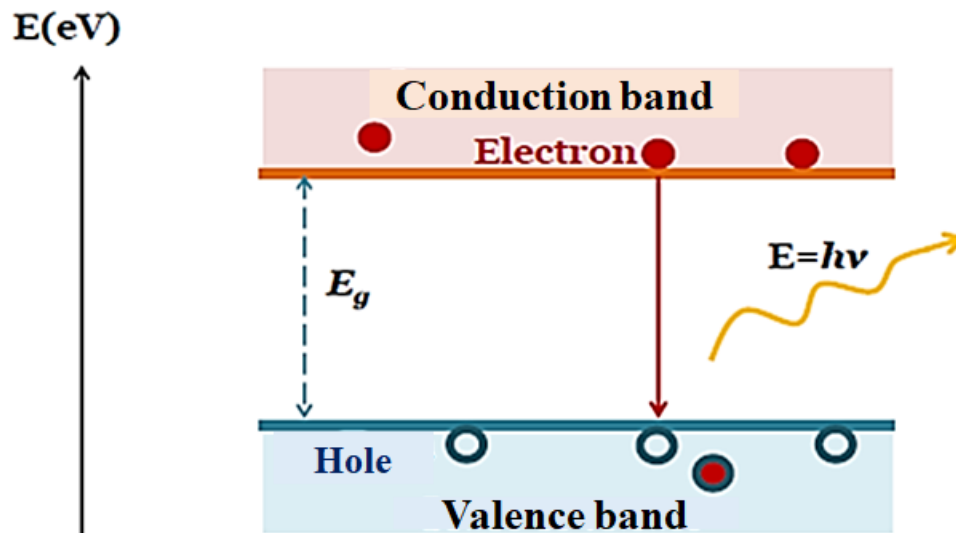


**Figure I.4:** Mechanism of radiative recombination.

It is accompanied by the issue of a photon with an energy close to that of the gap of the material (inverse process of the photogeneration) [19]. This type of recombination is a frequent process in

direct-gap semiconductors such as nitrides [20]. Note that it is the basis of photoluminescence and LEDs.

### I.4.2 Shockley-Read-Hall (SRH) recombination

The Shockley-Read-Hall (SRH) recombination mechanism is schematized in Figure I.5. This mechanism involves a localized defect in the band gap of the material which can be a recombinant center for free carriers [19]. This type of defects is predominant in nitride materials and this mechanism will therefore play an important role in the operation of solar cells based on these materials. [18]

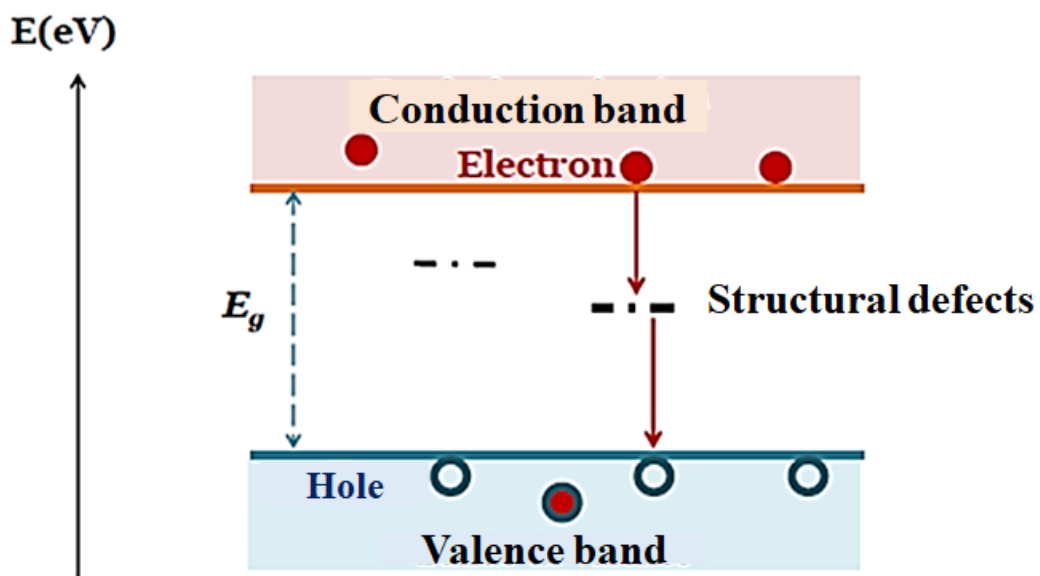


**Figure I.5:** Shockley-Read-Hall (SRH) recombination mechanism.

### I.4.3 Auger recombination

The Auger recombination mechanism is shown in Figure I.6. It is also band-to-band recombination, but unlike radiative recombination, the energy released is transmitted to a third carrier who finds himself excited in a level upper part of the conduction band. The third carrier can then thermalize by emitting one or more phonons. Note that this phenomenon also exists with holes in the valence band [18].

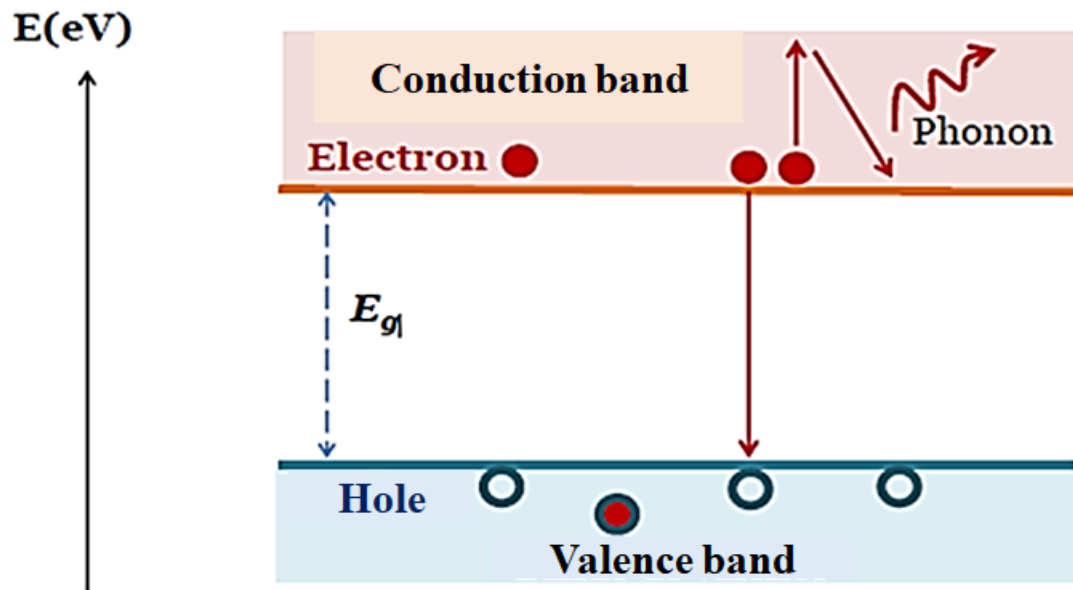


Figure I.6: Auger recombination mechanism.

## I.5. Solar cell characterization

### I.5.1 Equivalent circuit of a photovoltaic cell

A real solar cell can be schematized by Figure I.7. It proposes an electrical model of the photovoltaic cell.

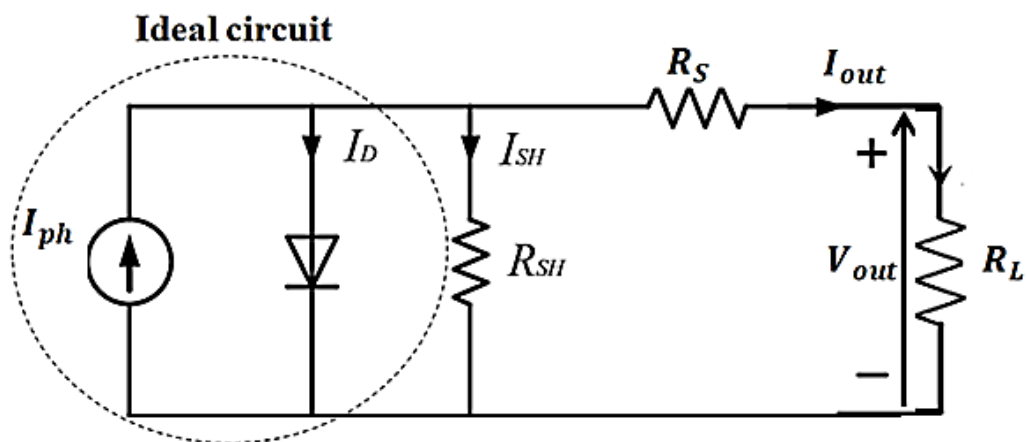
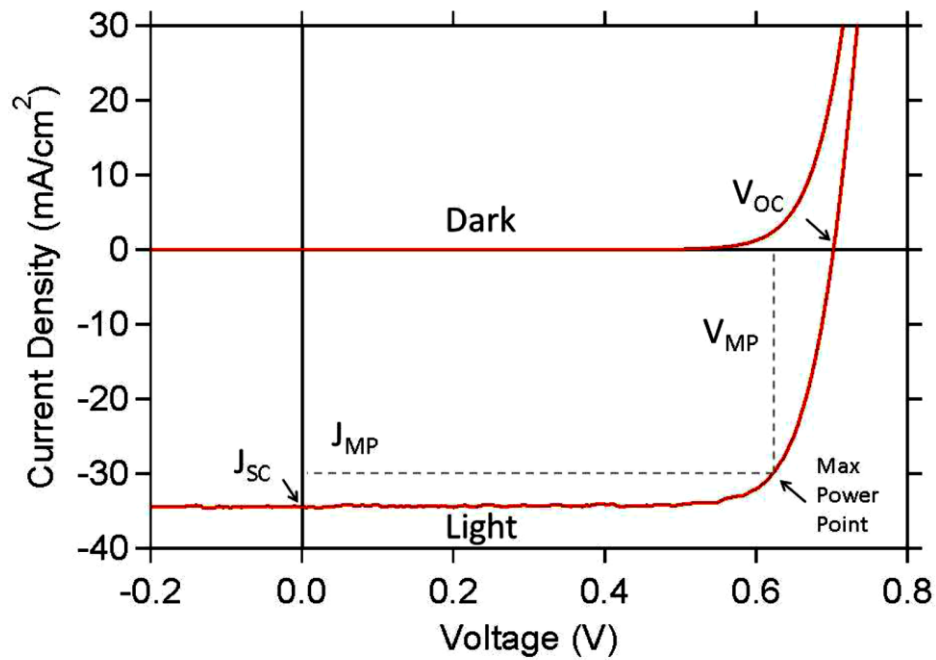


Figure I.7: Equivalent circuit of a solar cell.

We find there the generator current  $I_{ph}$ , corresponding to the photogenerated current opposed to the dark current  $I_{dark} = I_D$  of the forward biased diode, as well as resistors  $R_S$ ,  $R_{SH}$  and the load resistance  $R_L$ .  $R_S$ , represents, the resistance of the semiconductor, the contact resistance between the semiconductor and conductor, and the resistance of the contacts such as cell metallization,

interconnection or TCO layers [21]. This resistance should ideally be as low as possible to limit its influence on the cell current. This can be achieved by decreasing the resistivity of the used material.  $R_{sh}$ , the shunt (parallel) resistor translates the presence of a leakage current through the emitter caused by a fault. This is the case when diffusion from high temperature metal contacts pierces the emitter. It can also be due to a short circuit on the edges of the cell. This resistance should tend to infinity in order to maximize the current delivered to the external load [21]. Figure I.8 shows a typical set of the current density-voltage ( $J(V)$ ) curves in the dark and at standard illumination.



**Figure I.8:** Representative  $J(V)$  curve of a solar cell.

The  $J(V)$  curve can shift towards negative current density values due to the effect of light. By illuminating the cell, the light generated current  $I_{ph}$  is subtracted to the dark current flowing into the diode ( $I_{dark} = I_D$ ), so that the total current flowing between the device terminals ( $I$ ) becomes:

$$I = I_{ph} - I_D \quad \text{Eq. I.1}$$

In the dark condition, the current-voltage ( $I_D(V)$ ) characteristic of an ideal diode is governed by Shockley's equation [22]:

$$I_D(V) = I_0 \left( \exp\left(\frac{qV}{Ak_B T}\right) - 1 \right) \quad \text{Eq.I.2}$$

Where  $I_0$  is the saturation current,  $A$  the ideality factor,  $k_B$  is the Boltzmann constant,  $T$  the temperature in degrees Kelvin and  $q$  the charge of the electron.

The dark  $I_D(V)$  curve is presented in Figure I.9.

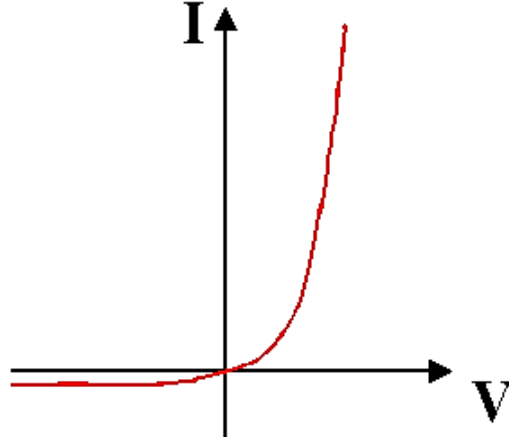


**Figure I.9:**  $I_D(V)$  characteristic of a p-n junction in the dark.

To account for realistic losses [23,24], the diode recombination, the series ( $R_s$ ), and parallel, or shunt ( $R_{sh}$ ) resistances are introduced, and the dark current-voltage ( $I_D(V)$ ) characteristic of the real diode becomes:

$$I_D(V) = I_0 \left( \exp \left( \frac{q(V-IR_s)}{Ak_B T} \right) - 1 \right) + \left( \frac{V-IR_s}{R_{sh}} \right) \quad \text{Eq.I.3}$$

Under illumination, the produced current ( $I$ ) through the external circuit is [23,24]:

$$I(V) = I_{ph} - I_D(V) \cong I_{sc} - \left[ I_0 \left( \exp \left( \frac{q(V+IR_s)}{Ak_B T} \right) - 1 \right) + \left( \frac{V+IR_s}{R_{sh}} \right) \right] \quad \text{Eq.I.4}$$

The current  $I$  is generally related to the surface and the current density  $J$  is expressed as ( $mA/cm^2$ ). The illuminated curve occurring in the fourth quadrant, indicates that the cell is delivering power to the load. In the laboratory, this load is often a power supply capable of acting as a current sink. The current directions in Eq.I.4 represent the illuminated configuration, and we use the + sign in the ( $V + IR_s$ ) terms. If the cell is placed in the dark, the  $I_{ph}$  (or  $I_{sc}$ ) term disappears, the power supply must supply current to the cell, and the current through  $R_s$  changes direction, so the – sign is appropriate in the ( $V - IR_s$ ) terms of Eq.I.3 .

$I(V)$  (or  $J(V)$ ) curves provide most of the following performance parameters: short-circuit current ( $I_{sc}$ ) or current density ( $J_{sc}$ ), which is the current for 0V applied voltage; open-circuit

voltage ( $V_{oc}$ ), which represents the voltage for no current passing through the solar cell; fill factor ( $FF$ ), which indicates how close, in percentage, the solar cell is from its maximum potential power considering the  $V_{oc}$  and  $J_{sc}$ , and light to power conversion efficiency ( $\eta$ ) which relates to the solar cell conversion efficiency.

### I.5.2 Short-circuit current density ( $J_{sc}$ )

The short-circuit current density,  $J_{sc}$ , is the current through the solar cells when  $V = 0$ , which is a similar condition as the two electrodes of the cell being short-circuited together. Because  $V = 0$ , and power is the product of current and voltage, no power is generated at this point but  $J_{sc}$  marks the onset of power generation.  $J_{sc}$  of a solar cell depends on the incident photon flux density on the cell, which is determined by the spectrum of the incident light. The optimum current that the solar cell can deliver strongly depends on the optical properties such as absorption in the absorber layer and total reflection of the solar cell. [24]

### I.5.3 Open-circuit Voltage ( $V_{oc}$ )

The open-circuit voltage,  $V_{oc}$ , is the voltage at which no current flows across the solar cell, which is the same as the device being open-circuited. This is the maximum voltage that a cell can deliver. Since  $J = 0$  there is no power produced at this point but it marks the boundary for voltages at which power can be produced. The  $V_{oc}$  corresponds to the amount of forward bias voltage at which the dark current compensates the photo-current in the solar cell. The  $V_{oc}$  can be calculated from an equation given below by assuming that the net current is zero.

$$V_{oc} = \frac{Ak_B T}{q} \ln\left(\frac{J_{ph}}{J_0} + 1\right) \quad \text{Eq.I.5}$$

Where  $\frac{k_B T}{q}$  is the thermal voltage,  $J_{ph}$  is the photocurrent density,  $J_0$  is the dark saturation current and  $A$  is the ideality factor.

### I.5.4 Fill Factor ( $FF$ )

The fill factor ( $FF$ ) is defined as the ratio of the maximum power ( $P_{max} = J_{MP} \times V_{MP}$ ) generated by a solar cell to the product of  $V_{oc}$  and  $J_{sc}$ .

$$FF = \frac{P_{MP}}{J_{sc} \cdot V_{oc}} = \frac{J_{MP} \cdot V_{MP}}{J_{sc} \cdot V_{oc}} \quad \text{Eq.I.6}$$

It is an indication of how close  $J_{MP}$  and  $V_{MP}$  come to the boundaries of power generation of  $J_{SC}$  and  $V_{OC}$ . It is also an indication of the sharpness of the  $J(V)$  curve that connects  $J_{SC}$  and  $V_{OC}$ . High  $FF$  is always desired since this is the indication of higher maximum power but the diode-like behavior of solar cells results in  $FF$  always being less than one. It can easily be shown from geometrical considerations that for a linear relationship between  $I$  and  $V$ , type  $V = R.I$  (implying that the device behaves like a simple resistor),  $FF = 1/4$ . The fill factor of high efficiency CIGS devices produced today are typically in the range 70-80% (81.2% in the 19.9% CIGS device reported in [25]). High  $J_{SC}$ ,  $V_{OC}$  and  $FF$  are required to obtain high efficiency ( $\eta$ ). Both  $J_0$  and  $J_{SC}$  depend on the energy band gap ( $E_g$ ), therefore  $J(V)$  can be expected to depend on  $E_g$  too. More precisely; when  $E_g$  increases,  $J_{SC}$  decreases, since less photons have enough energy to be absorbed, and  $J_0$  increases, since more carriers are available at the electrodes for recombination.  $E_g$  is then the main factor limiting  $V_{OC}$  [4], but  $R_{sh}$  also has an important impact, since recombinations reduce the open circuit voltage. In the ideal case,  $I_{SC}$  depends linearly on the area of the device that is illuminated, and is also affected by  $R_s$ . The diode ideality factor ( $A$ ), which can help determine whether SRH recombination are predominantly taking place in the SCR, or in the bulk or the contacts, is also a valuable parameter [4].

### 1.5.5 Power Conversion Efficiency ( $\eta$ )

The most commonly used parameters to compare the performance of a solar cell is the power conversion efficiency (PCE or  $\eta$ ) which is defined as the ratio of the output energy from the solar cells to input energy from the sun. The efficiency of a solar cell is determined as:

$$\eta\% = \frac{P_{max}}{P_{in}} \times 100\% = \left( \frac{J_{mp}V_{mp}}{P_{in}} \right) \times 100\% = \left( \frac{V_{oc}J_{sc}FF}{P_{in}} \right) \times 100\% \quad \text{Eq.I.7}$$

The above equation clearly shows that  $FF$ ,  $J_{SC}$ , and  $V_{OC}$  all have direct effects on  $\eta$ . The efficiency of the solar cells is also very dependent on the power and spectrum of the incident light source and the temperature of the solar cell, since the solar cells do not absorb and convert photons to electrons at all wavelengths with the same efficiency. So all the conditions under which the conversion efficiency of the cell is measured should be carefully controlled in order to compare various solar cells. Even though the solar spectrum at the earth's surface varies with location, cloud coverage, and other factors, the AM 1.5 G spectrum is the most commonly used

standard spectrum for measuring and comparing the performance of photovoltaic devices. The record efficiency of CIGSe-based solar cells is 20.3% [26].

### I.5.6 Spectral response of a solar cell

The spectral response  $RS$  of a photovoltaic cell is the ratio between the current of short-circuit ( $I_{sc}$ ) generated by the cell and the incident light power ( $P_{in}$ ), depending on the different wavelengths forming the incident radiation. The spectral response  $RS$  is given by the following relation [27]:

$$RS = \frac{I_{sc}(\lambda)}{P_{in}(\lambda)} (A/Watt) \quad \text{Eq.I.8}$$

### I.5.7. External quantum Efficiency ( $EQE$ )

The external quantum efficiency ( $EQE$ ) of the cell is the ratio of the number of carriers generated on the number of incident photons for each wavelength ( $\lambda$ ), it is related to the spectral response by [27]:

$$EQE(\lambda) = RS(\lambda) \cdot \frac{h.c}{e.\lambda} \quad \text{Eq.I.9}$$

### I.5.8 Internal quantum Efficiency ( $IQE$ )

The internal quantum efficiency  $IQE$  of the cell is the ratio of the number of carriers generated on the number of photons penetrating into the material, it is related to the efficiency external quantum ( $EQE$ ) by the equation

$$IQE(\lambda) = \frac{EQE(\lambda)}{1-R(\lambda)} \quad \text{Eq I.10}$$

Where  $R(\lambda)$  represents the reflection coefficient for the wavelength ( $\lambda$ ).

## I.6. Generations of solar cells

The field of solar cells is generally divided into four generations:

➤ The first generation includes solar panels based on crystalline silicon. Developed since 60 years, the silicon-based solar panel industry today presents a certain technological maturity with the highest efficiencies (24.7% in the laboratory) and a market share of around 80% of the current photovoltaic market. [28,29]

➤ The second generation of solar cells was developed from the 80s with the objective of reducing costs by relying on the use of thin layers. Using only a few microns of material, the researchers succeeded to find an alternative to the very expensive manufacture of inherent silicon ingots in the first-generation solar panels manufacture. The technologies based on this approach use Cu(In, Ga)Se<sub>2</sub>, CdTe and amorphous (a-Si) semiconductors with a very high absorption coefficient. Cu(In, Ga)Se<sub>2</sub> (CIGSe) based solar cells are thin film solar cells which show efficiencies around 20.3% in the laboratory [30],[31] as shown in Figure I.10. [28]. Some literatures [32,33] report an efficiency of 22.6% for the CIGS –based solar cells.

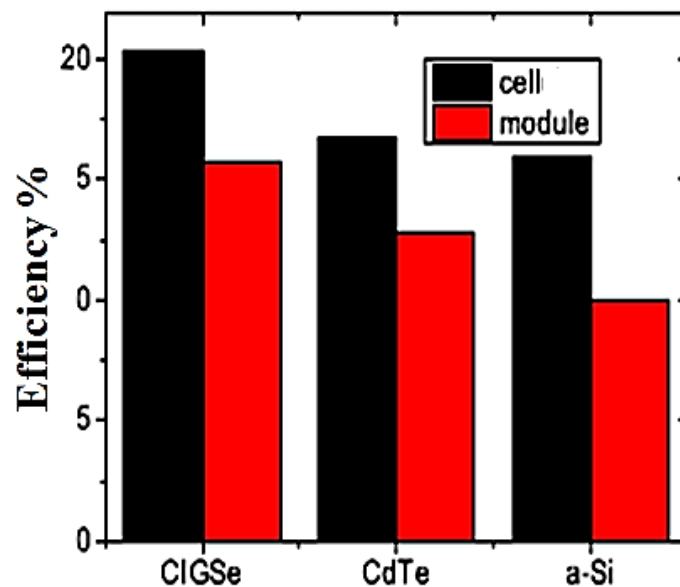


**Figure I.10:** Record conversion efficiencies of different solar cell technologies in thin layer in cell and module. [28]

➤ The third generation brings together all the new approaches proposed and developed over the past few years. This generation is focused on reducing the costs of manufacturing by proposing new approaches (organic solar cells, cells of Graetzel...). It also searches for exceed the current limits of efficiencies by using original concepts such as multijunction solar cells, intermediary gap solar cells or the use of hot carriers. The majority of third generation systems are currently under development and target more or less long term applications. [28]

➤ Fourth-generation Solar Cells: these are solar cells which are also called organic-inorganics because, they combine the flexibility of polymer thin films with the stability of inorganic nanostructured layers with a view targeted at maintaining the low cost of thin film photovoltaic, improving charge transport (carrier lifetime), enhancement in energy harvesting cross section of the solar cell and improved optical coupling by increasing the optical path length especially

when metal nanoparticles (mNP) are incorporated within the layers of a perovskite solar cell (PSC) [34]. An example of a fourth generation solar cell is a perovskite solar cell (PSC) that has incorporated within its layers carbon nanotubes (CNT), metal nanoparticles (mNP), nano hybrid materials or graphene [34]. Furthermore, it has been established that, the incorporation of inorganic materials within active materials like PSC, has greatly improved the carrier lifetime of solar cell devices [28].

Other types of junctions that cannot be classed within any generation are [28]:

1. Semiconductor insulator junctions.
2. Metal insulator semiconductor junction.
3. Metal-semiconductor or Schottky junctions, which are primarily the type of junction adopted in this research work for the solar cell study.

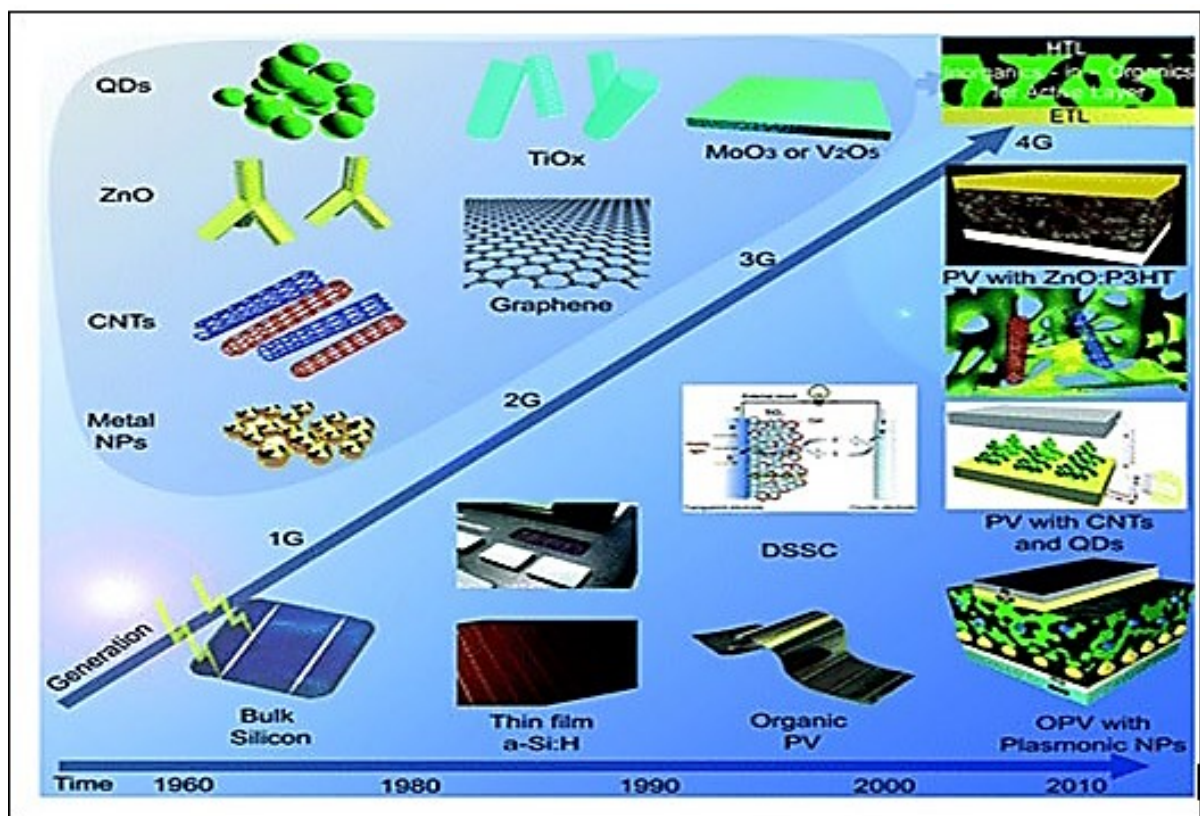


**Figure I.11:** A chart showing the generations and chronological evolution solar cells [34].

### I.7. Thin-film photovoltaics

Most photovoltaic solar cells are made using crystalline silicon (c-Si), much cheaper devices can be made using thin film technologies based on the use of direct energy band gap semiconductors. c-Si, with its indirect energy band gap, requires thicknesses of several hundreds of microns to absorb most of the sunlight. Also, the photogenerated carriers need to diffuse this distance back to the junction without being lost by recombination, which can only be achieved by purifying the silicon to a high level and growing crystals free from defects. In thin films, on the other hand, their direct band gap allow a similar absorption of the sunlight with only a few microns of material, and the carriers are generated very close to or within the junction, minimizing the need for a long minority carrier diffusion length. Thin films can therefore be made cheaper and of comparable efficiencies to c-Si. The most successful thin film materials used are cadmium telluride (CdTe), hydrogenated amorphous Si (a-Si), and copper indium gallium diselenide (CIGS). Figure I.12 shows the market share of the different produced technologies [4].

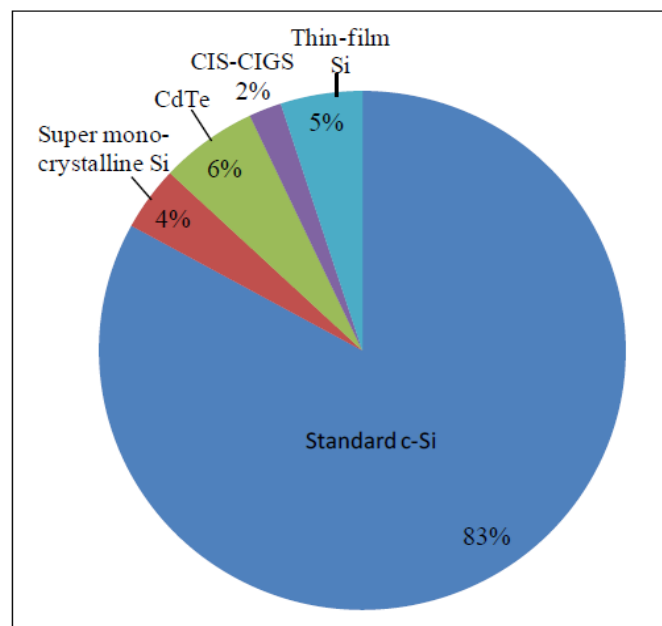


**Figure I.12:** Cell production by technology (in MW of DC current) [35].

The state of art efficiencies extracted for solar cells based on several crystalline and amorphous photo reactive materials are summarized in Table.I.1 [32,33].

**Table.I.1:** Highest efficiencies of state of art solar cells based on different materials [32,33].

<b>Technology</b>	<b>Efficiency</b>
Crystalline Si	26.3%
Multi-Crystalline Si	21.3%
Amorphous Si	10.2%
CIGS	22.6%
CdTe	22.1%
Perovskite Cells	19.7%
Dye-sensitized Cells	11.9%
Organic Cells	11.1%

### **I.8. CIGS based solar cells**

The quaternary semiconductor Cu (In, Ga)Se<sub>2</sub> (CIGS) is one of the most promising materials for Thin Film Solar Cells (TFSC's). It has a direct bandgap in the ideal energy range for solar energy conversion (1.04-1.68 eV), which results in an absorption coefficient of  $\sim 10^5 \text{ cm}^{-1}$ , sufficient to absorb most incident light within a few  $\mu\text{m}$ 's [36,37]. The possibility to apply CIGS for photovoltaic was already realized in the early 1970's, when the first solar cells based on bulk single crystal CuInSe<sub>2</sub> (CIS) quickly reached conversion efficiencies exceeding 10% [38,39]. The first thin-film devices followed shortly after and had initial efficiencies limited to  $\sim 5\text{-}6\%$  [37], but owing to much research and development currently with CIGS the 20% efficiency record has been exceeded by various groups. The progress in CIGS-based devices over the past 30 years is shown in Figure I.13 [40,41].

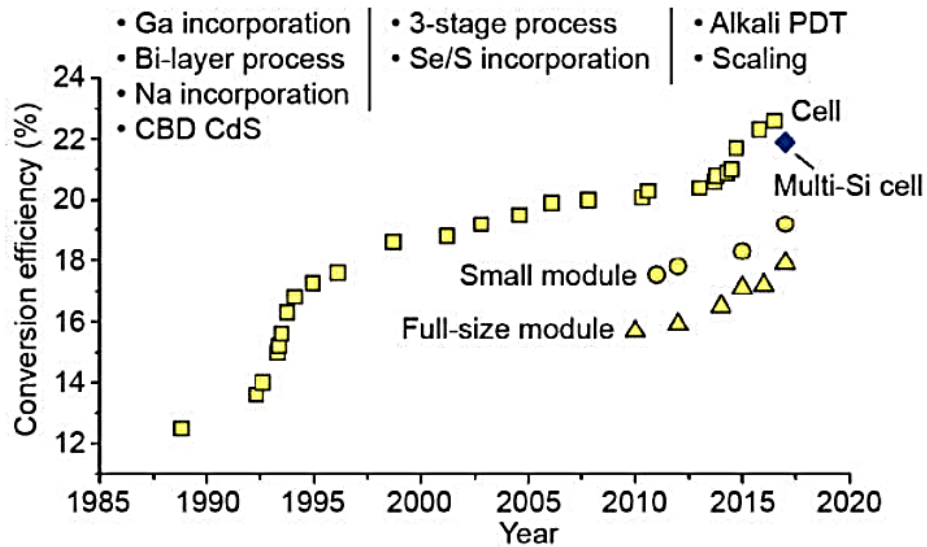


**Figure I.13:** Graph showing the progress in conversion efficiency in laboratory scale (squares), small modules (circles) and full-size modules (triangles) CIGS-based TFSC's [41].

On the laboratory scale, the verified efficiency record is currently at 22.6% [42,43], which already exceeds the current record efficiency of 22.0% on the same scale devices based on multicrystalline Si. Transferring the high efficiencies of CIGS lab-scale cells to the modular scale has been a challenge due to issues in scaling up the most successful deposition techniques. Nevertheless, the 19.2% efficiency record currently reached on CIGS modules is only slightly lower than the 19.9% record for comparable Poly-Si modules and proves CIGS technology can be highly competitive with conventional c-Si. Significant cost reduction in CIGS TFSC's are to be expected once further upscaling of production is achieved [40,41].

### I.8.1 CIGS material properties

Polycrystalline Cu ( $In_{1-x}, Ga_x$ )Se<sub>2</sub> (CIGS) is a II-III-VI<sub>2</sub> is a nonstoichiometric compound with intrinsic p-type semiconducting properties. CIGS is composed by four elements: copper, indium, gallium and selenium. CIGS shows a typical [44] chalcopyrite structure deriving from the group IV class of tetrahedrally bonded semiconductors (Figure I.14), similar to the zinc-blende (ZnS) one, according to the Grimm-Sommerfeld rule [45]. The lattice is a body-centered tetragonal such that each Cu (Group I) or In, Ga (Group III) has 4 bonds with Se (Group VI). On the other hand, Se atom has 2 bonds each with Cu and In (or Ga). Group III elements (ex: Ga) added to the lattice in place of In increase the bandgap at the cost of added stress to the lattice. In the lattice,

the unit cell aspect ratio,  $c/a$ , is close to 2. Deviations can arise due to the different strengths of Cu-Se, In-Se and Ga-Se bonds [33,46].

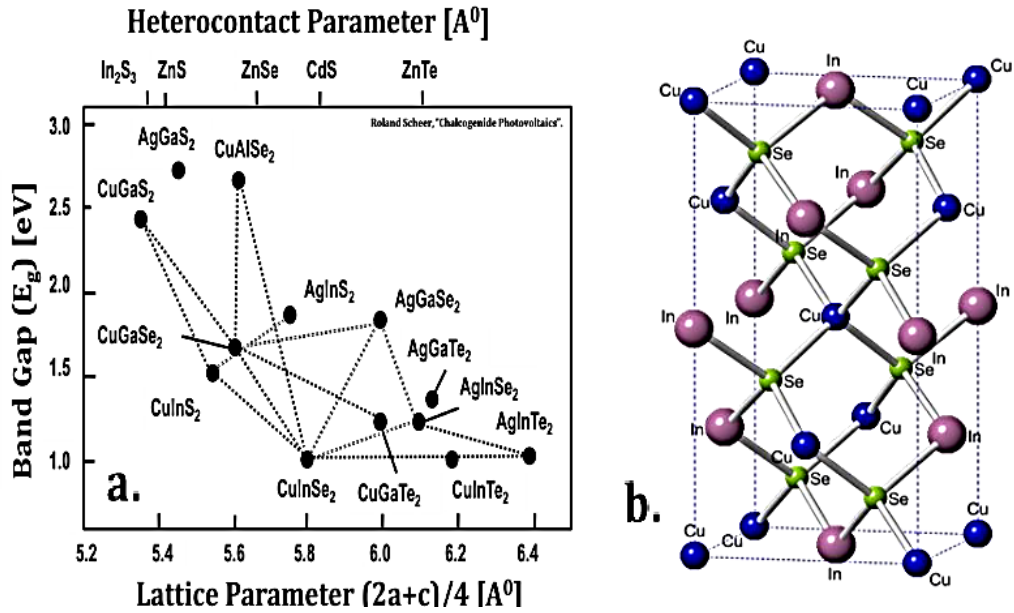


**Figure I.14:** a) Band gap as a function of lattice parameter of I-III-VI<sub>2</sub> semiconductors and II-VI semiconductors reprinted from Scheer [47]. b) Chalcopyrite structure of CuInSe<sub>2</sub> semiconductor reprinted from [48].

Different compounds can be obtained by varying the stoichiometry in the chemical formula  $Cu(In_{1-x}, Ga_x)Se_2$  from 0 (pure (copper indium selenide, CIS) to 1 (pure copper gallium selenide, CGS). [45].

One consequence of this structure variation is the variation of the CIGS band-gap as a function of the Ga content. From CuInSe<sub>2</sub> to CuGaSe<sub>2</sub>, the band-gap varies from approximately 1.04 eV to 1.68 eV [49]. When the composition  $x = [Ga]/([Ga] + [In])$  is introduced, the band-gap energy ( $E_g$ ), as a function of  $x$ , can be expressed by the following empirical formula [33]:

$$E_g(x) = (1 - x)E_g(CIS) + xE_g(CGS) - bx(1 - x) \quad \text{Eq.I.11}$$

Where the band gap of CuInSe<sub>2</sub> ( $E_g(CIS)$ ) is 1.04 eV, the band gap of CuGaSe<sub>2</sub> ( $E_g(CGS)$ ) is 1.68 eV; and  $b$  is the bowing parameter that depends on the growth. The most reproducible values of  $b$  are around 0.15-0.24 eV [50].

The most important variables in CIGS composition are the relative Cu-content, expressed as  $[Cu]/([Ga] + [In])$  or CGI, and the relative Ga-content, expressed previously as  $x = [Ga]/([Ga] + [In])$  or GGI. Variation of the CGI leads to variations in the phase and conductivity type of CIGS. For good absorber layer quality, the bulk conductivity needs to be P-type which is achieved for CGI  $\sim 0.9$ , i.e. slightly Cu-poor compared to stoichiometric composition. Variation of the GGI leads to variations in the bandgap, where GGI = 0 corresponds to  $\sim 1.04$  eV and GGI = 1 corresponds to  $\sim 1.68$  eV. The best device efficiencies have been reached using GGI  $\sim 0.3$ , corresponding to a bandgap of  $\sim 1.2$  eV. Although this is slightly lower than the theoretically ideal bandgap of  $\sim 1.4$  eV for conversion of solar light, increasing the GGI beyond  $\sim 0.3$  leads to only limited increase in  $V_{oc}$  and reduced device performance, most likely due to increased interface recombination [40,49-51].

Finally, it is worth noting that the chalcopyrite phase field is increased by the addition of Ga or Na [51]. As a result, the Na inclusion in the CuInSe<sub>2</sub> structure causes a replacement of InCu antisite defects by Na atoms, thus reducing the density of compensating donors [49]. The calculated effect of Na inclusion is therefore consistent with the increase of compositional range in which single-phase chalcopyrite exists and shows an higher conductivity, as experimentally observed. The high absorption coefficient ( $\alpha > 10^5 \text{ cm}^{-1}$ ) and the p-type behavior obtained when CIGS is grown in an excess of selenium (with a hole concentration of  $10^{16} - 10^{17} \text{ cm}^{-3}$  and a record in charge carrier mobility of  $200 \text{ cm}^2/\text{Vs}$ ), make CIGS films very promising as absorber layers in thin film solar cells, so that conversion efficiencies exceeding 20% were demonstrated in laboratory device prototypes [41,45].

### **I.8.2. CIGS-based solar cells architecture**

The basic structure of a Cu(In, Ga)Se<sub>2</sub> thin-film solar cell is depicted in Figure I.15. The most commonly used substrate is soda-lime glass, 1-3 mm thick, covered by a thin molybdenum film (300 nm-1 $\mu\text{m}$  thick) acting as the backside ohmic contact. The Na content in soda-lime has been shown to be useful for enhancing the solar cell performances, as it diffuses through the Mo film and increases open circuit voltage [52], as well as p-type conductivity and average grain size [53]. The heterojunction is constituted by a p-CIGS layer (thickness ranging between 1.5 and 2.5  $\mu\text{m}$ ) and a transparent conducting oxide (TCO, usually Al-doped ZnO), buffered by a thin layer of CdS (or ZnS, ZnMgO) and a layer of undoped ZnO. As remarked above, CIGS is a p-type semiconductor with a carrier concentration of about  $10^{16} \text{ cm}^{-3}$  [54], while Al-doped ZnO is a n-type semiconductor with a carrier concentration of  $10^{20} \text{ cm}^{-3}$  [54].

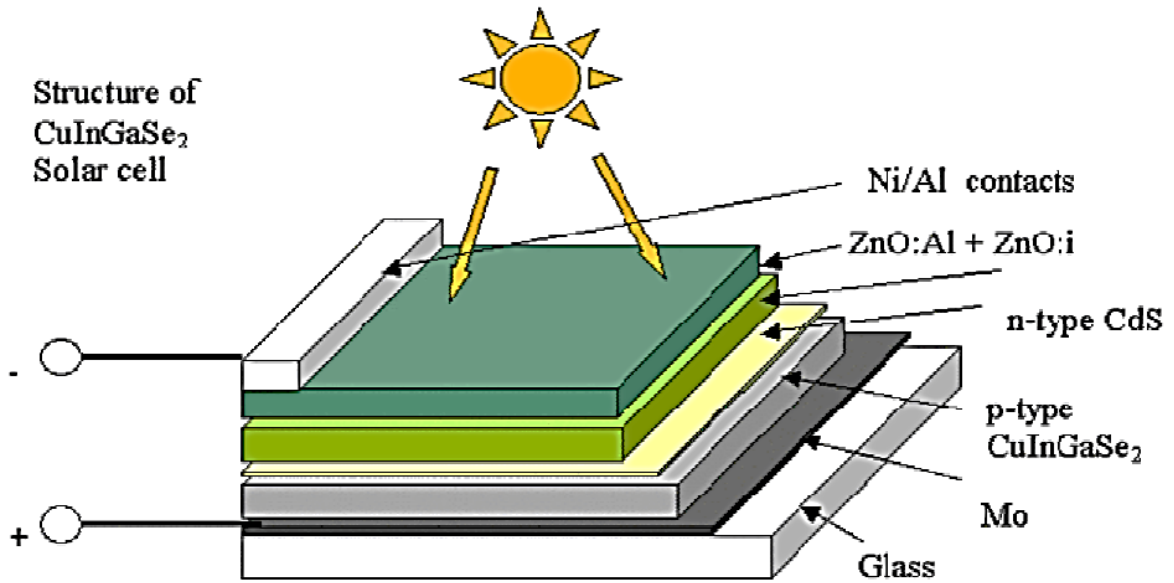


**Figure I.15:** Basic structure of a Cu(In, Ga)Se<sub>2</sub> thin-film solar cell [45].

This asymmetric doping causes the space-charge region to extend much more inside the CIGS film than into the ZnO layer. The front contact is generally composed by Al or alternate nichel (Ni)/Al layers. Finally, an antireflecting coating (100-200 nm thick layer of MgF<sub>2</sub>) aimed at avoiding light losses due to the semiconductor-air interface [45].

### I.8.3. CIGS Cell Band Structure

The band structure of a CIGS-based photovoltaic cell is shown in Figure I.16 [55]. After absorption of the light radiation, the creation of the electron-hole pairs takes place within the absorber material. The molybdenum rear contact collects the holes. The formation of a MoSe<sub>2</sub> layer at the CIGS/Mo interface constitutes the ohmic contact between the absorber and the back contact. It generates a band curvature for efficiently collecting the holes and pushing the electrons back to the upper electrode. In order to avoid volume and interface recombinations, it is necessary to remove the electronic junction of the physical junction (CdS/CIGS) rich in defects. This is why the p-n junction must be pushed back (buried) into the CIGS volume. To do this, in a standard manner, a surface inversion is performed by generating a gallium gradient on the surface of the absorber.

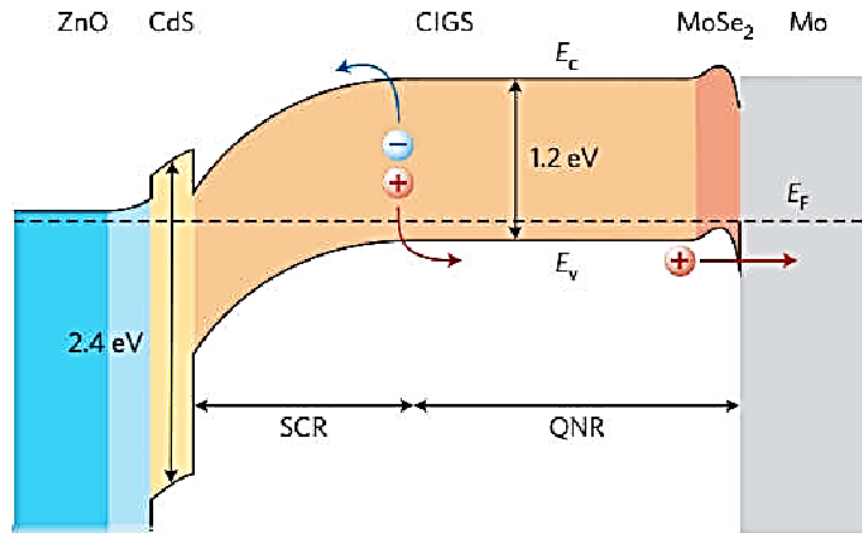


**Figure I. 16:** Schematic representation of the expected band-alignment in a typical CIGS-based device at 0 V bias [55], for constant GGI, and hence constant bandgap ( $E_g \sim 1.2$  eV). The upper and lower black-lines indicate the conduction band edge ( $E_C$ ) and valence band edge ( $E_V$ ) respectively. The bandgap of the ZnO layer is assumed to be in the range  $> 3$  eV. ‘SCR’ refers to the Space Charge Region (depletion region), while ‘QNR’ refers to the ‘Quasi Neutral Region’, i.e. the bulk of the absorber layer where no internal electric field is present.

Depending on the quantity of gallium, the CIGS can be a p-type or n-type semiconductor. The junction between the CdS and the CIGS thus constitutes an energy barrier at the conduction band level. This barrier is favorable to the proper functioning of the cell because it increases the inversion of the absorber at the surface with the creation of an n-type zone. The front contact in ZnO then collects the electrons [56].

## I.9. Conclusion

In this chapter, we gave an overview on Photovoltaics (PV) which is the technology that converts sunlight directly into electricity using solar cells. Solar cells are the fundamental building blocks of PV systems and are typically made from semiconductor materials. Solar cells can be categorized into different generations based on the materials used and the manufacturing processes involved. The properties of CIGS materials make them attractive for solar cell applications. They have a high absorption coefficient, which means they can absorb a large amount of light even with a thin layer. This allows for the use of less material, reducing costs. CIGS materials also exhibit excellent thermal stability and are relatively tolerant to variations in

composition, making them suitable for large-scale production. Overall, CIGS-based solar cells offer a promising alternative to traditional silicon-based solar cells, with the potential for improved efficiency and cost-effectiveness. Ongoing research and development in thin film technologies, including CIGS, aim to further enhance their performance and increase their market share in the renewable energy sector.

## References

- [1] J. K. Leggett, *Half Gone: Oil, Gas, Hot Air and the Global Energy Crisis*. Portobello Books, 2005.
- [2] K. Aryal, 'High Efficiency Ultrathin CIGS Solar Cells', Ph.D thesis, Electrical & Computer Engineering, Old Dominion University, Jul. 2015, doi: 10.25777/dsrd-mh49. [https://digitalcommons.odu.edu/ece\\_etds/48](https://digitalcommons.odu.edu/ece_etds/48)
- [3] S. Huang, 'Grand Challenges and Opportunities in Photovoltaic Materials and Devices', *Frontiers in Photonics*, vol. 2, 2021, Accessed: Jun. 06, 2023. [Online]. Available: <https://www.frontiersin.org/articles/10.3389/fphot.2021.651766>
- [4] R. Aninat, 'Study of Cu(In, Al)Se<sub>2</sub> thin films prepared by selenisation of sputtered metallic precursors for application in solar cells', Ph.D thesis, Northumbria University, 2012. Accessed: Jun. 19, 2023. [Online]. Available: <https://nrl.northumbria.ac.uk/id/eprint/11373/>
- [5] R. Rani and R. Velavan, Preparation and characterisation of certain ii vi i iii vi<sub>2</sub> semiconductor thin films and transparent conducting oxides, *Malaya Journal of Matematik*, Vol. S, No. 2, 3911-3915, 2020, doi: 10.26637/MJM0S20/1008
- [6] R. Woods-Robinson et al., 'Wide Band Gap Chalcogenide Semiconductors', *Chem Rev*, vol. 120, no. 9, pp. 4007–4055, May 2020, doi: 10.1021/acs.chemrev.9b00600.
- [7] K.-C. Hsu, Y.-S. Fu, P.-Y. Lin, I.-T. Tang, and J.-D. Liao, 'Fabrication and Characterization of CuInSe<sub>2</sub> Thin Film Applicable for a Solar Energy Light Absorption Material via a Low Temperature Solid State Reaction', *International Journal of Photoenergy*, vol. 2013, Jan. 2013, doi: 10.1155/2013/156964.
- [8] R. C. Smith, 'Device applications of the ternary semiconducting compounds', *J. Phys. Colloques*, vol. 36, no. C3, pp. C3-99, Sep. 1975, doi: 10.1051/jphyscol:1975318.
- [9] B. Flèche , D. Delagnes, *Energie solaire photovoltaïque* . June 2007. Accessed: Jun. 06, 2023. [Online]. Available: [http://doc-developpement-durable.org/file/Energie/Solaire-photovolta%C3%AFque/Energie\\_solaire\\_photovoltaique.pdf](http://doc-developpement-durable.org/file/Energie/Solaire-photovolta%C3%AFque/Energie_solaire_photovoltaique.pdf)

- [10] Y. Marouf, 'Etude et simulation des cellules solaires multi-jonctions à base de matériaux semi-conducteurs III-V.', Ph.D thesis, Université Mohamed Khider - Biskra, 2019. Accessed: Jun. 06, 2023. [Online]. Available: <http://archives.univ-biskra.dz:80/handle/123456789/24554>
- [11] Solar Spectra'. <https://www.nrel.gov/grid/solar-resource/spectra.html> (accessed Jun. 06, 2023).
- [12] C. Riordan and R. Hulstron, 'What is an air mass 1.5 spectrum? (solar cell performance calculations)', in IEEE Conference on Photovoltaic Specialists, May 1990, pp. 1085–1088 vol.2. doi: 10.1109/PVSC.1990.111784.
- [13] Reference Air Mass 1.5 Spectra'. <https://www.nrel.gov/grid/solar-resource/spectra-am1.5.html> (accessed Jun. 06, 2023).
- [14] S. Petibon, 'Nouvelles architectures distribuées de gestion et de conversion de l'énergie pour les applications photovoltaïques', Ph.D thesis, Toulouse 3, 2009. Accessed: Jun. 06, 2023. [Online]. Available: <https://www.theses.fr/2009TOU30004>
- [15] A. Mahfoud, Modélisation des cellules solaires tandem à couches minces et à haut rendement. Ph.D thesis, Sétif: Université Ferhat Abbas faculté de technologie département d'électronique, 2018. [Online]. Available: <http://dspace.univ-setif.dz:8888/jspui/bitstream/123456789/1785/1/THESE%20ABDERREZEK%20MAHFOUD.pdf>
- [16] H. Mathieu and H. Fanet, Physique des semiconducteurs et des composants électroniques - 6ème édition: Cours et exercices corrigés. Dunod, 2009.
- [17] A. Stephen, 'Optimisation of charge carrier mobility and lifetime in silicon nanowire solar cells growth by Plasma Enhanced Chemical Vapour Deposition (PECVD) technique at low temperatures', Ph.D. thesis, De Montfort University, 2020. Accessed: Jun. 06, 2023. [Online]. Available: <https://hdl.handle.net/2086/20988>
- [18] A. Adaine, 'Optimisation numérique de cellules solaires à très haut rendement à base d'InGaN', Ph.D thesis, Université de Lorraine, 2018. Accessed: Jun. 06, 2023. [Online]. Available: <https://theses.hal.science/tel-01870260>
- [19] N. Richet, Les cellules photovoltaïques en silicium : théorie et fabrication, 1 vols, no. 1. in Quinte Sciences, no. 1. [Les Ulis]: EDP Sciences, 2016.

- [20] J.-L. Coutaz, *Optoélectronique terahertz*. EDP sciences, 2012.
- [21] A. N. Corpus Mendoza, ‘Influence of the p-type layer on the performance and stability of thin film silicon solar cells’, Ph.D thesis, University of Sheffield, 2017. Accessed: Jun. 06, 2023. [Online]. Available: <https://etheses.whiterose.ac.uk/16581/>
- [22] R. F. Pierret, *Semiconductor Device Fundamentals*. Addison-Wesley, 1996.
- [23] M. Wolf and H. Rauschenbach, ‘Series resistance effects on solar cell measurements’, *Advanced Energy Conversion*, vol. 3, no. 2, pp. 455–479, Apr. 1963, doi: 10.1016/0365-1789(63)90063-8.
- [24] A. Sabadus, V. Mihailetchi, and M. Paulescu, ‘Parameters extraction for the one-diode model of a solar cell’, presented at the TIM17 Physics conference, Timisoara, Romania, 2017, p. 040005. doi: 10.1063/1.5017444.
- [25] I. Repins et al., ‘19.9%-efficient ZnO/CdS/CuInGaSe<sub>2</sub> solar cell with 81.2% fill factor’, *Prog. Photovolt: Res. Appl.*, vol. 16, no. 3, pp. 235–239, May 2008, doi: 10.1002/pip.822.
- [26] P. Jackson et al., ‘New world record efficiency for Cu(In,Ga)Se<sub>2</sub> thin-film solar cells beyond 20%’, *Progress in Photovoltaics: Research and Applications*, vol. 19, no. 7, pp. 894–897, 2011, doi: 10.1002/pip.1078.
- [27] H. J. Hovel and B. O. Seraphin, ‘Semiconductors and Semimetals, Vol. 11: Solar Cells’, *Physics Today*, vol. 29, no. 11, pp. 65–68, Nov. 1976, doi: 10.1063/1.3024511.
- [28] E. Leonard, ‘Cellules solaires à base de couche mince de Cu(In,Ga)Se<sub>2</sub> submicrométrique : optimisation des performances par ingénierie optique et électronique’, Ph.D thesis, Université de Nantes, 2013.
- [29] Global market outlook for photovoltaics 2013-2017’, Global CCS Institute. <https://www.globalccsinstitute.com/resources/publications-reports-research/global-market-outlook-for-photovoltaics-2013-2017/> (accessed Jun. 07, 2023).
- [30] M. A. Green, K. Emery, Y. Hishikawa, W. Warta, and E. D. Dunlop, ‘Solar cell efficiency tables (version 39)’, *Progress in Photovoltaics: Research and Applications*, vol. 20, no. 1, pp. 12–20, 2012, doi: 10.1002/pip.2163.

- [31] A. Chirilă et al., ‘Highly efficient Cu(In,Ga)Se<sub>2</sub> solar cells grown on flexible polymer films’, *Nat Mater*, vol. 10, no. 11, pp. 857–861, Sep. 2011, doi: 10.1038/nmat3122
- [32] M. A. Green et al., ‘Solar cell efficiency tables (version 49)’, *Progress in Photovoltaics: Research and Applications*, vol. 25, no. 1, pp. 3–13, 2017, doi: 10.1002/pip.2855.
- [33] M. J. Sibakoti, Performance Limitations in Wide Bandgap CIGS-Based Solar Cells, Ph.D thesis, University of Minnesota, 2017, Available: [https://conservancy.umn.edu/bitstream/handle/11299/200258/Sibakoti\\_umn\\_0130E\\_18337.pdf](https://conservancy.umn.edu/bitstream/handle/11299/200258/Sibakoti_umn_0130E_18337.pdf)
- [34] K. D. G. I. Jayawardena, L. J. Rozanski, C. A. Mills, M. J. Beliatis, N. A. Nismy, and S. R. P. Silva, “‘Inorganics-in-Organics’”: recent developments and outlook for 4G polymer solar cells’, *Nanoscale*, vol. 5, no. 18, pp. 8411–8427, Aug. 2013, doi: 10.1039/C3NR02733C.
- [35] PV News Annual Data Collection Results: 2010 Cell, Module Production Explodes Past 20 GW’. <https://www.greentechmedia.com/articles/read/pv-news-annual-data-collection-results-cell-and-module-production-explode-p> (accessed Jun. 07, 2023).
- [36] J. J. Loferski, ‘Theoretical Considerations Governing the Choice of the Optimum Semiconductor for Photovoltaic Solar Energy Conversion’, *Journal of Applied Physics*, vol. 27, no. 7, pp. 777–784, May 2004, doi: 10.1063/1.1722483.
- [37] L. L. Kazmerski, F. R. White, and G. K. Morgan, ‘Thin-film CuInSe<sub>2</sub>/CdS heterojunction solar cells’, *Applied Physics Letters*, vol. 29, no. 4, pp. 268–270, Aug. 2008, doi: 10.1063/1.89041.
- [38] S. Wagner, J. L. Shay, B. Tell, and H. M. Kasper, ‘Green electroluminescence from CdS–CuGaS<sub>2</sub> heterodiodes’, *Appl. Phys. Lett.*, vol. 22, no. 8, pp. 351–353, Apr. 1973, doi: 10.1063/1.1654669.
- [39] J. L. Shay, S. Wagner, and H. M. Kasper, ‘Efficient CuInSe<sub>2</sub> /CdS solar cells’, *Appl. Phys. Lett.*, vol. 27, no. 2, pp. 89–90, Jul. 1975, doi: 10.1063/1.88372.
- [40] A. Kingma, ‘Electrical characterization of low temperature pulsed-electron-deposited Cu(In,Ga)Se<sub>2</sub> solar cells’, Ph.D thesis, Università di Parma. Dipartimento di Scienze chimiche, della vita e della sostenibilità ambientale, 2018. Accessed: Jun. 07, 2023. [Online]. Available: <https://www.repository.unipr.it/handle/1889/3671>

- [41] M. Powalla et al., 'Advances in Cost-Efficient Thin-Film Photovoltaics Based on Cu(In,Ga)Se<sub>2</sub>', *Engineering*, vol. 3, no. 4, pp. 445–451, Aug. 2017, doi: 10.1016/J.ENG.2017.04.015.
- [42] P. Jackson, R. Wuerz, D. Hariskos, E. Lotter, W. Witte, and M. Powalla, 'Effects of heavy alkali elements in Cu(In,Ga)Se<sub>2</sub> solar cells with efficiencies up to 22.6%', *physica status solidi (RRL) – Rapid Research Letters*, vol. 10, no. 8, pp. 583–586, 2016, doi: 10.1002/pssr.201600199.
- [43] M. A. Green, Y. Hishikawa, E. D. Dunlop, D. H. Levi, J. Hohl-Ebinger, and A. W. Y. Ho-Baillie, 'Solar cell efficiency tables (version 51)', *Progress in Photovoltaics: Research and Applications*, vol. 26, no. 1, pp. 3–12, 2018, doi: 10.1002/pip.2978.
- [44] M. Chandramohan, S. Velumani, and T. Venkatachalam, 'Band structure calculations of Cu(In<sub>1-x</sub>Ga<sub>x</sub>)Se<sub>2</sub>', *Materials Science and Engineering: B*, vol. 174, no. 1, pp. 200–204, Oct. 2010, doi: 10.1016/j.mseb.2010.03.043.
- [45] M. Calicchio, 'Technological processes for CIGS based solar cells', Ph.D thesis, Università degli studi di Parma .Dipartimento di Fisica e Scienze della Terra "Macedonio Melloni, 2013. Accessed: Jun. 07, 2023. [Online]. Available: <https://www.repository.unipr.it/handle/1889/2144>
- [46] S. Siebentritt, M. Igalson, C. Persson, and S. Lany, 'The electronic structure of chalcopyrites-bands, point defects and grain boundaries', *Prog. Photovolt: Res. Appl.*, vol. 18, no. 6, pp. 390–410, Sep. 2010, doi: 10.1002/pip.936.
- [47] S. R. Kodigala, *CIGS based thin film solar cells*, vol. 35. Academic Press, 2011.
- [48] T. Gödecke, T. Haalboom, and F. Ernst, 'Phase equilibria of Cu-In-Se. I. Stable states and non-equilibrium states of the In<sub>2</sub>Se<sub>3</sub>-Cu<sub>2</sub>Se subsystem', *Zeitschrift Fur Metallkunde*, 2000, Accessed: Jun. 07, 2023. [Online]. Available: <https://www.semanticscholar.org/paper/Phase-equilibria-of-Cu-In-Se.-I.-Stable-states-and-G%C3%B6decke-Haalboom/e4745ec1c10d782c30369ee3fb7f1a99a553f3fc>
- [49] S.-H. Wei, S. B. Zhang, and A. Zunger, 'Effects of Ga addition to CuInSe<sub>2</sub> on its electronic, structural, and defect properties', *Applied Physics Letters*, vol. 72, no. 24, pp. 3199–3201, Jun. 1998, doi: 10.1063/1.121548

- [50] B. Tell, J. L. Shay, and H. M. Kasper, 'Room-Temperature Electrical Properties of Ten I-III-VI<sub>2</sub> Semiconductors', *Journal of Applied Physics*, vol. 43, no. 5, pp. 2469–2470, May 1972, doi: 10.1063/1.1661532.
- [51] R. Herberholz, V. Nadenau, U. Rühle, C. Köble, H. W. Schock, and B. Dimmler, 'Prospects of wide-gap chalcopyrites for thin film photovoltaic modules', *Solar Energy Materials and Solar Cells*, vol. 49, no. 1, pp. 227–237, Dec. 1997, doi: 10.1016/S0927-0248(97)00199-2.
- [52] J. Hedstrom et al., 'ZnO/CdS/Cu(In,Ga)Se<sub>2</sub> thin film solar cells with improved performance', *Conference Record of the Twenty Third IEEE Photovoltaic Specialists Conference - 1993 (Cat. No.93CH3283-9)*, pp. 364–371, 1993, doi: 10.1109/PVSC.1993.347154
- [53] A. Naveed et al., 'A Highly Reversible Zn Anode with Intrinsically Safe Organic Electrolyte for Long-Cycle-Life Batteries', *Advanced Materials*, vol. 31, no. 36, p. 1900668, 2019, doi: 10.1002/adma.201900668.
- [54] F. Pattini, 'Growth of oxide thin films for energy devices by Pulsed Electron Deposition', Ph.D thesis, Università degli studi di Parma .Dipartimento di Fisica, 2009. Accessed: Jun. 19, 2023. [Online]. Available: <https://www.repository.unipr.it/handle/1889/1001>
- [55] A. Chirilă et al., 'Highly efficient Cu(In,Ga)Se<sub>2</sub> solar cells grown on flexible polymer films', *Nat Mater*, vol. 10, no. 11, pp. 857–861, Sep. 2011, doi: 10.1038/nmat3122.
- [56] B. Salhi, 'The Photovoltaic Cell Based on CIGS: Principles and Technologies', *Materials*, vol. 15, no. 5, Art. no. 5, Jan. 2022, doi: 10.3390/ma15051908..

# CHAPTER II

**Schottky barrier solar cell based on CIGS material**

## II.1 Introduction

A Schottky-barrier solar cell, also known as a metal-semiconductor (MS) solar cell is a type of photovoltaic device that converts sunlight into electricity. It is named after the Schottky barrier, which is the energy barrier formed at the interface between a metal and a semiconductor. In a Schottky-barrier solar cell, a metal electrode is in contact with a semiconductor material, forming a Schottky junction. The metal electrode acts as the top contact, while the semiconductor material serves as the active layer that absorbs light and generates charge carriers (electrons and holes). The Schottky junction forms a barrier to the flow of charge carriers, creating a built-in electric field that separates the photo-generated carriers and drives them towards their respective electrodes. Unlike traditional p-n junction solar cells, which rely on a p-n junction formed within a single semiconductor material, Schottky-barrier solar cells utilize the Schottky barrier for charge separation. The metal used in the Schottky contact typically has a lower work function than the semiconductor material (if it is p-type doped), resulting in a rectifying behavior at the junction. This rectification allows the efficient extraction of photo-generated carriers and reduces recombination losses [1-5]. The advantages of Schottky-barrier solar cells include their potential for high efficiency, as they can offer excellent charge carrier separation and collection. They are particularly suitable for applications that require low-cost and lightweight solar devices, such as portable electronics or space applications. However, they generally have lower open-circuit voltage compared to p-n junction solar cells and can be sensitive to temperature variations [6-9]. Various materials have been used as the semiconductor in Schottky-barrier solar cells, including silicon (Si), gallium arsenide (GaAs), copper indium gallium selenide (CIGS), Indium Gallium Nitride (InGaN) and organic semiconductors. The choice of materials depends on factors such as desired efficiency, cost, and application requirements. Overall, Schottky-barrier solar cells are an interesting alternative to traditional p-n junction solar cells, offering unique advantages and potential for further development in photovoltaic technology. [5,6,10-15]. Chapter II focuses on providing an overview of CIGS-based Schottky barrier solar cells and discussing the physics that limit the transport in such cells.

## II.2 Physics of the Schottky barrier solar cell.

The difference between the work functions of a metal ( $\Phi_M$ ) and a semiconductor ( $\Phi_S$ ), and the misalignment of the energy bands of the semiconductor with the work function of the metal can generate a barrier with rectifying properties on a metal-semiconductor contact. Figure II.1 shows

the formation of a barrier height for a metal/p-type semiconductor interface according to ideal Schottky barrier theory [16].

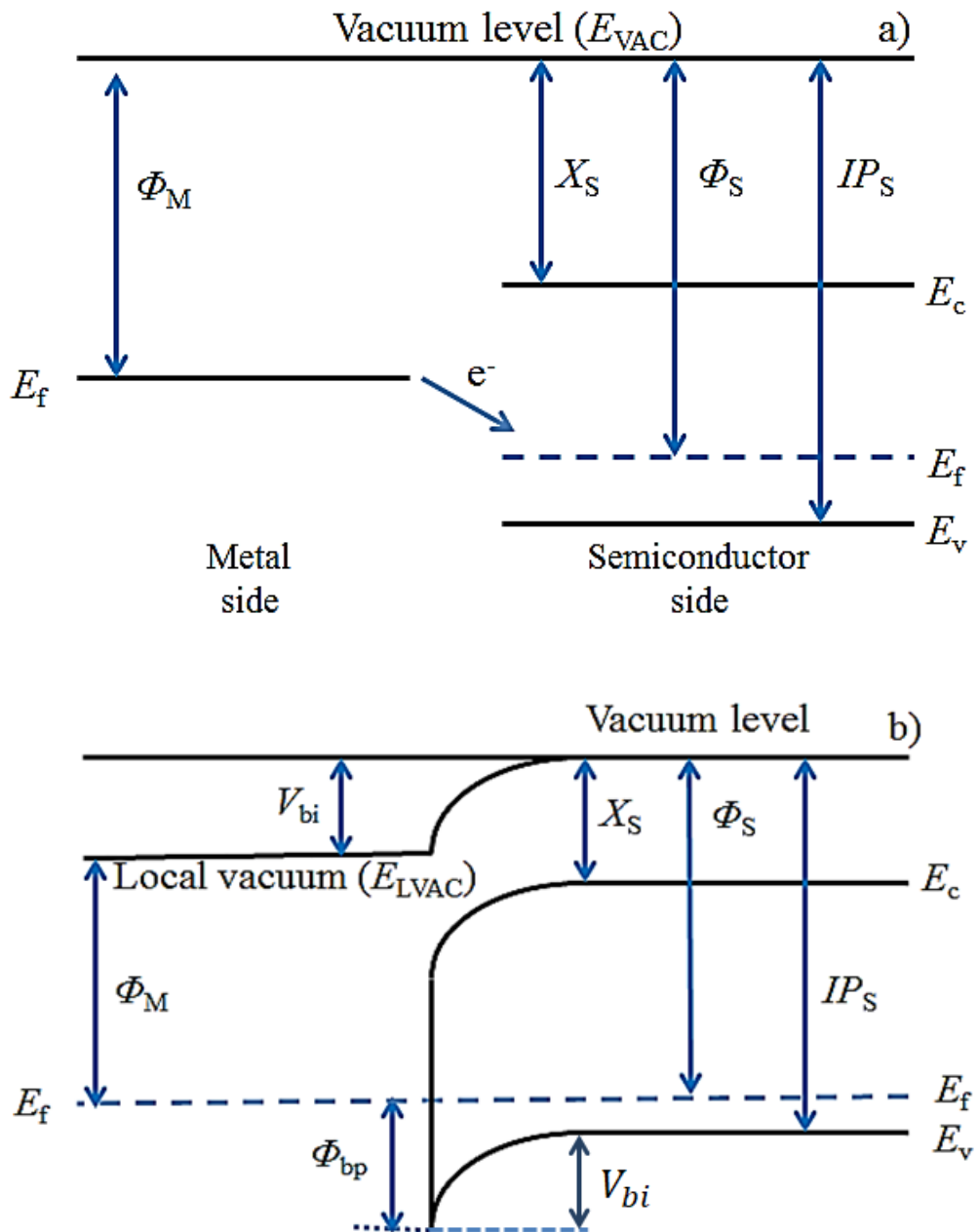


**Figure II.1:** Energy band diagrams for a metal-p-type semiconductor contact when  $\Phi_S > \Phi_M$ . Materials are shown in isolation (a) and after contact (b). All parameters are referenced to the vacuum level under the basis of ideal Schottky barrier theory [16].

The energy band diagram for both materials in isolation is shown in Figure. II.1a). Here, the most important properties such as work function of the metal  $\Phi_M$ , and electron affinity  $X_S$ , ionization potential  $IP_S$ , and work function  $\Phi_S$  of the semiconductor, are all referenced to the

vacuum level  $E_{VAC}$  [17,18]. Since  $\Phi_S > \Phi_M$  in this example, there is an electron charge transfer from the metal to the semiconductor which equalizes the Fermi levels once both materials are brought into contact. This causes a built-in potential  $V_{bi}$  and a local vacuum level  $E_{LVAC}$  to appear as a consequence of the charge transfer. A Schottky barrier height  $\Phi_{bp}$  is also created, which represents a potential barrier that holes in the p-type semiconductor must overcome to transit to the metal side [17,18]. The value of  $\Phi_{bp}$  for an ideal contact is represented by the Schottky-Mott approximation in Eq. II.1 [16]:

$$\Phi_{bp} = IP_S - \Phi_M = (X_S + E_g) - \Phi_M = qV_{bi} + (E_f - E_v) \quad \text{Eq.II.1}$$

Figure. II.2 shows the case when  $\Phi_S < \Phi_M$ , where a flow of electrons from the semiconductor into the metal equalizes the Fermi levels and produces a depletion region in the semiconductor [16].

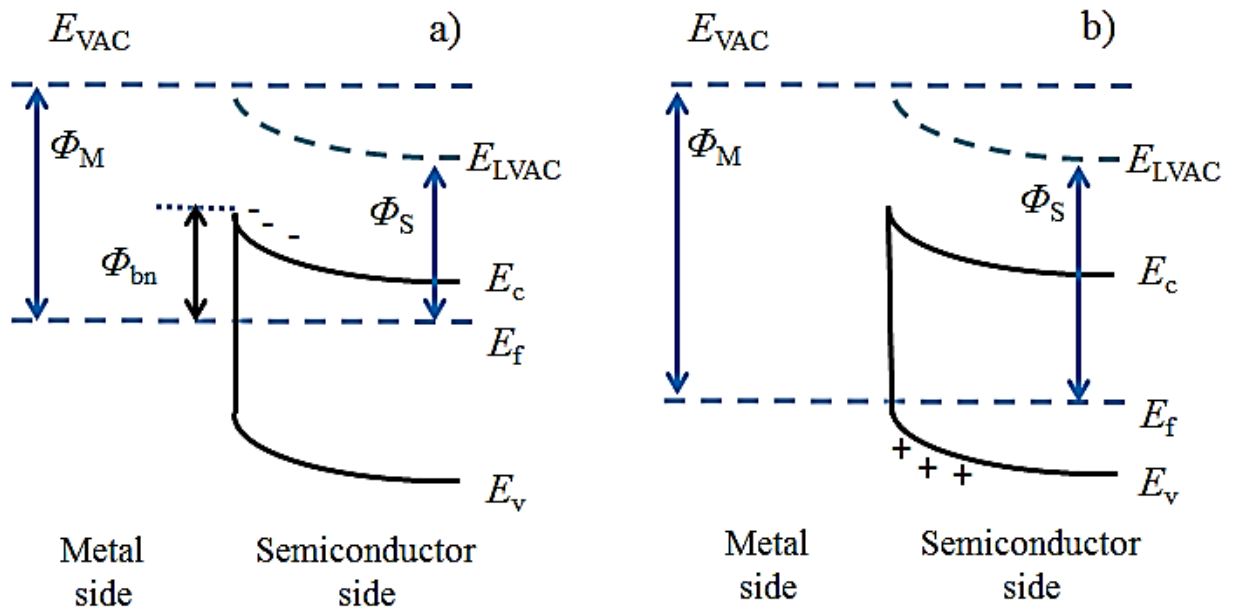


**Figure II.2.** a) Schottky barrier for an n-type semiconductor when  $\Phi_M > \Phi_S$ . The Fermi levels equalize once that materials are in contact, which causes the bands to bend upwards and to create a barrier  $\Phi_{bn}$  that electrons need to overcome to cross from the semiconductor to the metal, thus rectifying properties are achieved. b) When  $\Phi_M > \Phi_S$ . for a p-type material, the bending of the bands does not prevent the motion of holes, and a contact with Ohmic instead of rectifying properties is created [16].

This bends the bands upwards as shown in Figure II.2a) for n-type semiconductors. Here, the electrons need to overcome the barrier  $\Phi_{bn}$  to be able to pass from the semiconductor into the

metal, which results in rectifying properties. For the case of a p-type semiconductor, the bending of the band does not stop the flow of holes, thus the contact becomes Ohmic as shown in Figure II.2b) [17,19]. On the other hand, the bands bend downwards when  $\Phi_M < \Phi_S$ . For this case, an Ohmic behaviour is achieved for n-type materials, since the flow of electrons does not find a barrier as shown in Figure. II.3 a), whereas a rectifying contact is created for p-type material, where holes find difficulties to pass underneath the barrier, as shown in Figure. II.3 b). Generally, the case  $\Phi_M > \Phi_S$  is true for most of the metal/n-type semiconductor contacts, whereas  $\Phi_M < \Phi_S$  is true for most of the metal/p-type semiconductor contacts therefore, the majority of the metal-semiconductor contacts produce Schottky contacts [17,19].

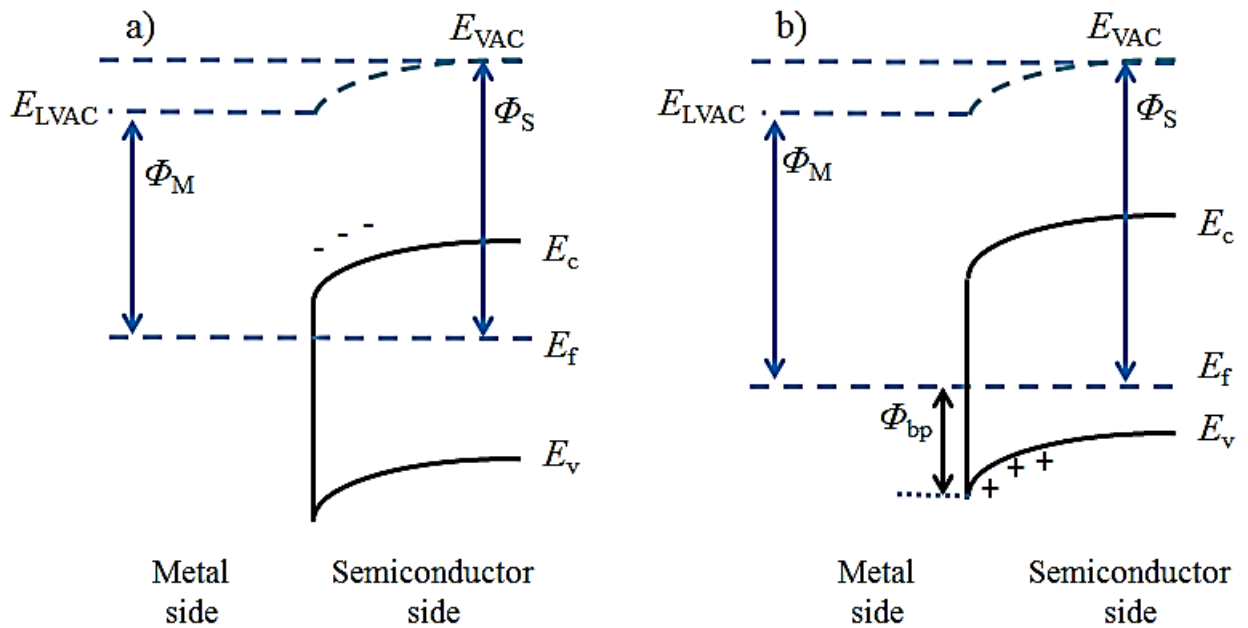


**Figure II.3:** When  $\Phi_M < \Phi_S$  bands are bent downwards and, a) Ohmic properties are achieved for n-type semiconductors whereas b) p-type semiconductors produce rectifying contacts due to the difficulty of holes to pass below the barrier  $\Phi_{bp}$ . [16].

When  $\Phi_S > \Phi_M$  for the p-type material, a hole, at the semiconductor surface, can be thermionically emitted into the metal if its energy is above the barrier height ( $\Phi_{bp}$ ) and the thermionically emitted hole density is:

$$p_{th} = N_V \exp\left(-\frac{\Phi_{bp}}{k_B T}\right) \quad \text{Eq.II.2}$$

where  $N_V$  is the effective density of states at the valence band Edge ( $E_V$ ).

At thermal equilibrium, the current density is balanced by two equal and opposite flows of carriers, and thus there is zero net current. Holes in the semiconductor (sc) tend to flow (or emit) into the metal (m), and there is an opposing balanced flow of holes from metal into the semiconductor. These current components ( $J_{sc \rightarrow m}$  and  $J_{m \rightarrow sc}$  respectively) are proportional to the density of holes at the boundary:

$$|J_{sc \rightarrow m}| = |J_{m \rightarrow sc}| \propto p_{th} \quad \text{Eq.II.3}$$

Or

$$|J_{sc \rightarrow m}| = |J_{m \rightarrow sc}| = C_1 N_V \exp\left(-\frac{\Phi_{bp}}{k_B T}\right) \quad \text{Eq.II.4}$$

where  $J_{sc \rightarrow m}$  is the current density from the semiconductor to the metal,  $J_{m \rightarrow sc}$  is the current density from the metal to the semiconductor, and  $C_1$  is a proportionality constant.

When a forward bias ( $V$ ) is applied to the contact, the built-in potential ( $V_{bi}$ ) across the barrier is reduced to  $(V_{bi} - V)$ , and the hole density at the surface increases to:

$$p_{th} = N_V \exp\left(-\frac{(\Phi_{bp} - qV)}{k_B T}\right) \quad \text{Eq.II.5}$$

The current density ( $J_{sc \rightarrow m}$ ) that results from the hole flow out of the semiconductor is therefore altered by the same  $p_{th}$  factor. The flux of holes from the metal to the semiconductor, however, remains the same because the barrier ( $\Phi_{bp}$ ) remains at its equilibrium value. The net current under forward bias is then:

$$J = (J_{sc \rightarrow m}) - (J_{m \rightarrow sc}) = C_1 N_V \exp\left(-\frac{(\Phi_{bp} - qV)}{k_B T}\right) - C_1 N_V \exp\left(-\frac{\Phi_{bp}}{k_B T}\right)$$

$$J = C_1 N_V \exp\left(-\frac{\Phi_{bp}}{k_B T}\right) \left[ \exp\left(\frac{qV}{k_B T}\right) - 1 \right] \quad \text{Eq.II.6}$$

With the same argument for the reverse-bias condition, the expression for the net current is identical to Eq.II.6 except that ( $V$ ) is replaced by  $(-V)$ . The coefficient  $C_1 N_V$  is found to be equal to  $A^* T^2$ , where  $A^*$  is called the effective Richardson constant (in units of  $A/(K^2 cm^2)$ ) and  $T$  is the absolute temperature. The value of  $A^*$  depends on the effective mass.

The current-voltage characteristic of a metal-semiconductor contact under thermionic emission condition is then:

$$J(V) = J_0 \left( \exp\left(\frac{qV}{k_B T}\right) - 1 \right) \quad \text{Eq.II.7}$$

$$J_0 = A^* T^2 \exp\left(-\frac{\Phi_{bp}}{k_B T}\right) \quad \text{Eq.II.8}$$

Where  $J_0$  is the saturation current density and the applied voltage  $V$  is positive for forward bias and negative for reverse bias.

### II. 3 Charge transport in Schottky barrier solar cell

When the sunlight shines on a Schottky junction solar cell, only photons with greater energy than the semiconductor band gap ( $E_g$ ) are able to release a valence electron and thus electron–hole pairs are generated. The established electric field inside the junction region works on separating these pairs by drifting the holes toward the semiconductor and electrons toward the metal [20] as shown in Figure II. 4. However, these charges provide a forward bias polarization of the Schottky junction so that part of the photogenerated charges cause an internal current through the forward bias Schottky junction (diode current ( $I_D$ )). Hence, only a part of the generated charges contributes to the external current ( $I$ ). Therefore,

$$I = I_{ph} - I_D \quad \text{Eq.II.9}$$

where  $I_{ph} \cong I_{sc}$  represent the photogenerated current and the short-circuit current, respectively.

When the Schottky-barrier-type structure is designed as a photovoltaic device, it is operated in the fourth quadrant of the  $I(V)$  plot. Consequently it is convenient to express the produced current ( $I$ ) through the external circuit when a voltage ( $V$ ) is developed. Taking into account the series ( $R_s$ ) and shunt ( $R_{sh}$ ) resistances and the ideality factor ( $A$ ), the equation that provides the current ( $I$ ) as a function of the voltage ( $V$ ) (in the load resistance) is given by [20]:

$$I(V) = I_{ph} - I_D(V) \cong I_{sc} - \left[ I_0 \left( \exp\left(\frac{q(V+IR_s)}{Ak_B T}\right) - 1 \right) + \left(\frac{V+IR_s}{R_{sh}}\right) \right] \quad \text{Eq.II.10}$$

The dark saturation current,  $I_0$ , is the major factor influencing the value of  $FF$  and  $V_{oc}$  [21].

Figure II.4 (b) illustrates the possible transport mechanisms in Schottky barrier solar cells. This includes: (1) depletion layer (SCR) recombination-generation, (2) thermionic emission over the barrier, (3) field emission or tunnelling through the barrier, (4) thermionic field emission and (5) drift-diffusion in space-charge region ( $x < W$ ) and in the quasi-neutral region ( $x > W$ ).

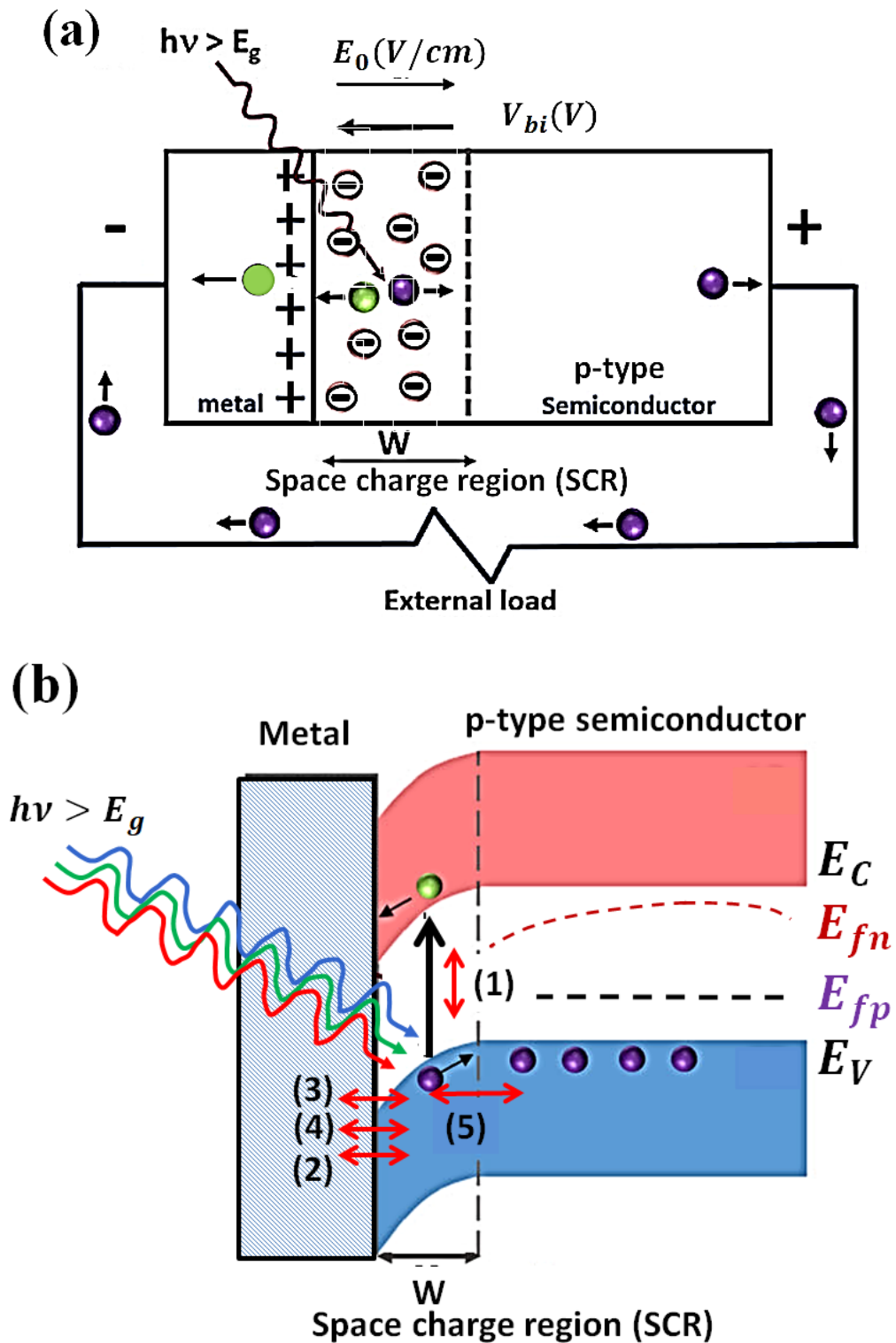


**Figure II.4:** The representation of the generated electron-hole pair in Schottky barrier solar cell within: (a) an electrical circuit. (b) energy band structure showing the possible transport mechanisms ((1) -(5)).

If the dominant transport of the forward-biased Schottky junction is the thermionic emission. In this case, the dark saturation current is given by:

$$I_0 = SA^*T^2 \exp\left(\frac{-\phi_B}{k_B T}\right) \quad \text{Eq.II.11}$$

Where  $S$  is the effective area of contact in  $cm^2$ ,  $(A^*)$  is effective Richardson's constant in  $A\ cm^{-2}\ ^\circ K^{-2}$ ,  $T$  is the absolute temperature in  $^\circ K$  and  $(\phi_B)$  is the Schottky barrier height in  $eV$ .

The open circuit voltage  $V_{OC}$  can be deduced by setting  $I(V_{oc}) = 0$ , if  $(R_s)$  and  $(R_{sh})$  are neglected, then :

$$V_{oc} \cong A \left[ \left( \frac{k_B T}{q} \right) \ln \left( \frac{I_{sc}}{SA^*T^2} \right) + \frac{\phi_B}{q} \right] \quad \text{Eq.II.12}$$

It is important to state, that the greater the value of  $\phi_B$ , the lower the value of  $I_0$ , and consequently, the lower is the  $I_D$  value [20]. The diode structure shown on figure II.4 would produce a minority carrier solar cell with the dark current ( $I_D$ ) approaching the ideal value limited by the drift-diffusion mechanisms [22] and characteristics equivalent to that of n-p junction solar cell would result

## II.4. Overview of CIGS –based Schottky barrier solar cells

A CIGS Schottky barrier solar cell is a type of thin-film solar cell that uses a metal-semiconductor junction to convert sunlight into electricity. CIGS stands for copper indium gallium diselenide, which is the semiconductor material used for the absorber layer. The metal layer is usually aluminum or molybdenum. The CIGS-Mo (or CIGS-Al) interface is a Schottky barrier to holes, which means that it blocks the flow of positive charges from the CIGS layer to the metal layer. This helps to create a voltage difference between the two layers and generate electric current when light is absorbed by the CIGS layer [15,23].

The efficiency of CIGS Schottky barrier solar cells depends on several factors, such as the bandgap and thickness of the CIGS layer, the type and quality of the metal contact, and the presence of defects and interface states. According to some recent studies, the highest efficiency reported for CIGS solar cells is 27.652% [24], which is achieved by optimizing the thickness and doping of the CIGS layer and adding an electron back reflector layer. The main challenges for improving the efficiency of CIGS Schottky barrier solar cells are to reduce the recombination

losses at the metal-semiconductor interface and to increase the open circuit voltage and fill factor of the device.

A Schottky junction solar cell based on p-type Cu(In, Ga)Se<sub>2</sub> (CIGS) material operates based on the principles of photovoltaic effect and the formation of a Schottky barrier at the junction between the CIGS layer and a metal contact. Here's a brief explanation of the physics involved:

1. Schottky barrier formation: At the junction between the CIGS layer and the metal contact, a Schottky barrier is formed. This barrier arises due to the difference in work function between the CIGS material and the metal contact. The metal contact is typically chosen to be a low work function material like molybdenum (Mo) or Aluminum (Al). This barrier creates a potential energy step that affects the flow of charge carriers (electrons and holes) across the interface. In a CIGS-based Schottky barrier solar cell, the metal contact typically acts as the cathode (negative electrode), while the CIGS layer functions as the anode (positive electrode).
2. Absorption of photons: When photons from sunlight strike the CIGS layer, they can be absorbed by the material. The bandgap of CIGS is tuned to absorb a significant portion of the solar spectrum.
3. Generation of electron-hole pairs: The absorbed photons excite electrons from the valence band to the conduction band, leaving behind holes in the valence band. This process generates electron-hole pairs, creating a population of free electrons and holes within the CIGS layer.
4. Charge separation: Due to the built-in electric field at the junction between the CIGS layer and the metal contact, the generated electrons and holes are separated. The electrons are attracted to the metal contact, while the holes remain within the CIGS layer.
5. Collection of electrons: The Schottky barrier at the interface allows the electrons to flow from the CIGS layer into the metal contact, creating a photocurrent. This flow of electrons constitutes the electrical output of the solar cell.
6. Recombination and losses: To ensure efficient device performance, it is essential to minimize recombination losses within the CIGS layer and at the metal contact interfaces. Strategies such as passivation layers and surface treatments are employed to reduce recombination and improve the overall device efficiency.

It is important to note that the detailed physics and device characteristics of a Schottky junction solar cell based on p-type CIGS material can be quite complex and involve additional considerations, including material composition, device structure, and optimization of interfaces. This simplified explanation provides an overview of the key principles involved.

Some of the advantages of CIGS Schottky barrier solar cells are [8,24-28]:

- They have a high absorption coefficient and a tunable bandgap, which means they can absorb more sunlight and adjust to different wavelengths with less material.
- They have a low thermal budget and a simple structure, which means they can be fabricated at lower temperatures and costs than conventional solar cells.
- They have a high open circuit voltage and a low contact resistance, which means they can produce more power and reduce losses at the metal-semiconductor interface.
- They have a better resistance to heat than silicon-based solar cells, which improves their performance and stability at high temperatures.
- They do not contain the toxic element cadmium, which is present in some other thin-film solar cells such as CdTe.
- They can be produced on flexible substrates, which enables more applications and integration possibilities.
- They can be combined with perovskite as a top cell in a tandem configuration, which can increase the power conversion efficiency and energy yield significantly.

Some of the disadvantages of CIGS Schottky barrier solar cells are [25,26]:

- They have a low fill factor and a high ideality factor, which means they have a low output current and a high recombination rate at the junction.
- They have a low stability and a high sensitivity to environmental factors, such as moisture, oxygen, and temperature, which can degrade their performance over time
- They have a limited availability and a high toxicity of some of the materials used, such as indium, gallium, and selenium, which can pose challenges for mass production and disposal.

The fill factor and the ideality factor of CIGS Schottky barrier solar cells can be improved by various methods, such as [23,24]:

- Adding an electron back reflector layer (EBR) at the back contact to minimize the recombination of carriers and increase the output current.
- Optimizing the thickness and doping of the CIGS layer to enhance the absorption and carrier collection.
- Improving the quality and uniformity of the metal contact to reduce the contact resistance and interface states.
- Using a graded bandgap structure for the CIGS layer to match the solar spectrum and reduce the thermalization losses.

The stability and sensitivity of CIGS Schottky barrier solar cells can be enhanced by various methods, such as [23,25,28]:

- Adding an insulator layer between the metal and the CIGS layer to prevent direct contact and reduce the degradation caused by moisture, oxygen, and temperature.
- Using a transparent conducting oxide (TCO) layer instead of a metal layer to improve the transparency and conductivity of the contact and reduce the reflection losses.
- Applying a surface treatment to the CIGS layer to remove impurities, passivate defects, and improve the surface morphology and structure orientation.
- Incorporating a buffer layer between the CIGS layer and the TCO layer to improve the band alignment and reduce the interface recombination.

In the following, we provide a brief description of the specified Schottky barrier solar cell based on Cu(In,Ga)Se<sub>2</sub> (CIGS) material that we will study in this work. Figure II.5 (a) displays the schematic diagram of the CIGS-based Schottky solar cell and the corresponding band diagram is shown in Figure II.5 (b) under sunlight illumination (short circuit condition). The base layer is p-type CIGS with band gap energy  $E_g \cong 1.15 \text{ eV}$ . This latter corresponds to a  $Ga/(In + Ga)$  ratio of  $x \cong 0.25$  which is recommended for high performance CIGS solar cells [29].

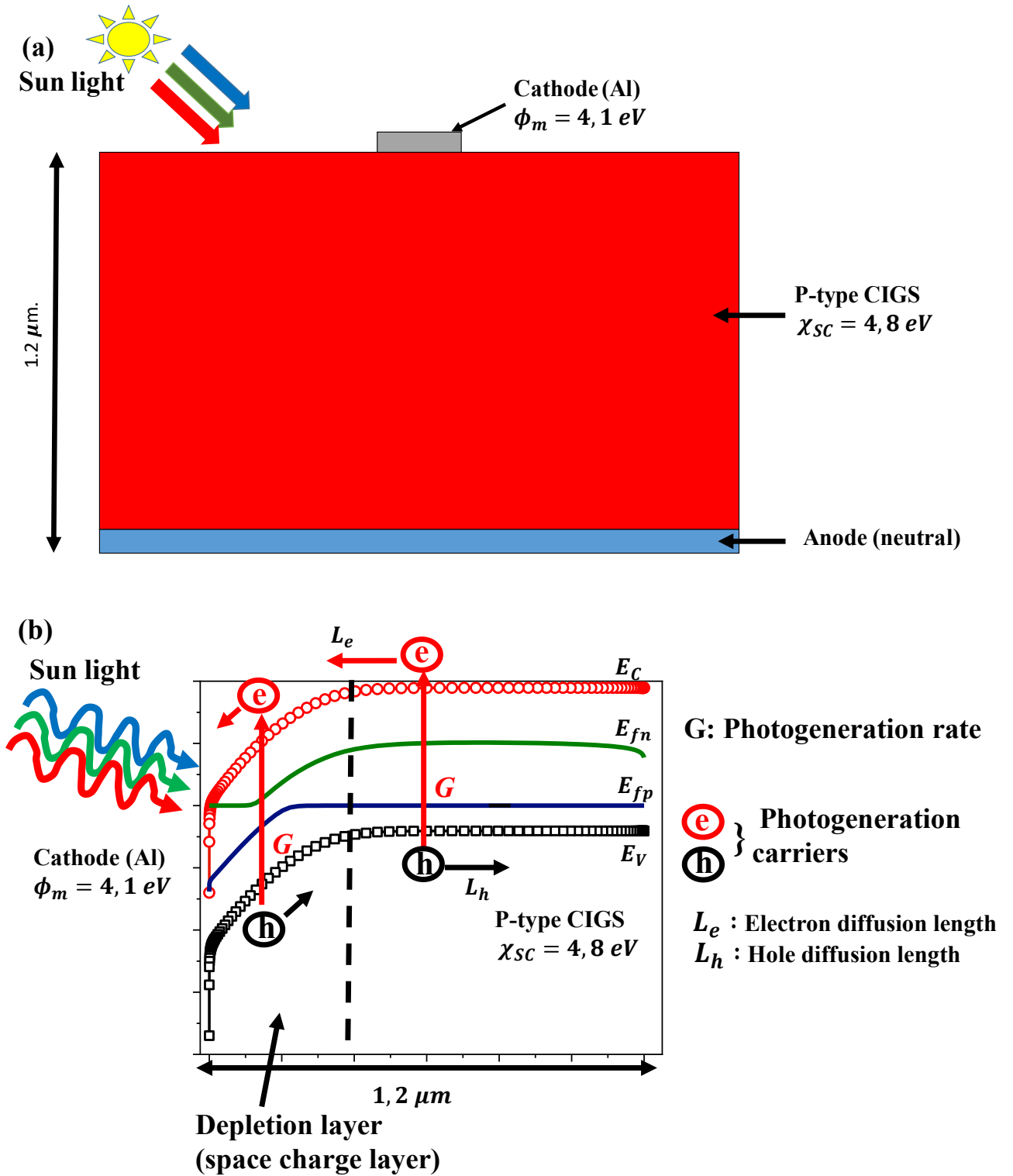


Figure II.5: Schematic diagram of (a) CIGS-based Schottky barrier solar cell, (b) the corresponding band diagram under sunlight illumination and zero bias (short circuit condition).

The Schottky barrier at the metal/semiconductor interface is obtained by making the cathode metal (which is situated on the top of the cell) from Aluminum (Al). With such a choice; the cathode work function ( $\phi_m = 4.1 \text{ eV}$ ) is lower than the electron affinity of the p-type CIGS material ( $\chi_{sc} = 4.8 \text{ eV}$ ). However, the anode is defined to be neutral (Ohmic contact). The bands of CIGS at the Al/ p-type CIGS) interface bend downward at zero bias (Figure II.5 (b)). Once optical absorption occurs in the Schottky solar cell, electron-hole pairs (EHP) are photogenerated in the device and charge separation occurs, at the Schottky interface, by the built-in field of the depletion region, resulting in a photovoltage between the metallic cathode and the bulk of the p-type CIGS material. The sweeping effect drifts the minority carriers (electrons e) into the top metal contact; and the majority carriers (holes h) into the neutral p-type region; where they have to reach the collection electrode (anode) by diffusion. Incident photon illumination creates electron-hole pairs in the depletion region, as well as in the neutral region of the p-type CIGS material. For the latter, however, only those electrons, within the diffusion length from the edge of the depletion region, have a chance to diffuse to the depletion region, and only those holes, within the diffusion length from the edge of the bottom collection electrode, have a chance to diffuse to the anode electrode. The carriers sweeping effect in the depletion region, and the carrier diffusion in the neutral region, produce the photo-generated current which flows in the opposite direction of the forward dark current as mentioned in the previous section.

## II.5 Conclusion

Cu (In, Ga)Se<sub>2</sub> (CIGS) is a semiconductor material that has gained significant attention in photovoltaic research due to its high absorption coefficient and suitable bandgap for solar energy conversion. In CIGS-based solar cells, one of the device structures that can be employed is the Schottky barrier solar cell. This type of solar cell relies on the formation of a Schottky barrier at the interface between a metal contact and the CIGS absorber layer. The Schottky barrier solar cell architecture offers certain advantages, such as simplicity and potential for low-cost fabrication. However, it also poses some challenges that limit the efficiency and performance of the device. Efforts are made to optimize and improve the performance of CIGS-based Schottky barrier solar cells. Various techniques, including interface engineering, surface passivation, and material modification, are employed to reduce the recombination at the metal-semiconductor interface and enhance carrier collection. The main focus of this chapter was to provide an overview of CIGS-based Schottky barrier solar cells and the physics that limit the transport in such cells.

## References

- [1] R. T. (董梓則) Tung, 'The physics and chemistry of the Schottky barrier height', *Applied Physics Reviews*, vol. 1, no. 1, p. 011304, Jan. 2014, doi: 10.1063/1.4858400.
- [2] L. D. Partain and L. M. Fraas, *Solar Cells and Their Applications*. John Wiley & Sons, 2010.
- [3] P. T. Landsberg and C. Klimpke, 'Theory of the Schottky Barrier Solar Cell', *Proceedings of the Royal Society of London. Series A, Mathematical and Physical Sciences*, vol. 354, no. 1676, pp. 101–118, 1977.
- [4] S. Srivastava, N. K. Swami, and G. P. Srivastava, 'Efficiency of Schottky barrier solar cells', *physica status solidi (a)*, vol. 58, no. 2, pp. 343–348, 1980, doi: 10.1002/pssa.2210580203
- [5] K. Chowdhury and R. Mandal, 'Advancement of schottky barrier solar cells: a review', in *contemporary issues in computing*, volkson press, Jan. 2020, pp. 93–98. doi: 10.26480/cic.01.2020.93.98.
- [6] Y. Song, A. Osherov, V. Bulović, and J. Kong, 'Graphene-Perovskite Schottky Barrier Solar Cells', *Adv. Sustainable Syst.*, vol. 2, no. 4, p. 1700106, Apr. 2018, doi: 10.1002/adsu.201700106.
- [7] M. Shanmugam, T. Bansal, C. A. Durcan, and B. Yu, 'Schottky-barrier solar cell based on layered semiconductor tungsten disulfide nanofilm', *Applied Physics Letters*, vol. 101, no. 26, p. 263902, Dec. 2012, doi: 10.1063/1.4773525
- [8] K. Dasgupta, K. Chowdhury, A. Mondal, S. Ray, and U. Gangopadhyay, 'Advancement and Challenges for Schottky Barrier MIS/SIS Solar Cells: A Review', *Trans Indian Natl. Acad. Eng.*, vol. 7, no. 1, pp. 13–28, Mar. 2022, doi: 10.1007/s41403-021-00263-6
- [9] M. Farhat, S. Kais, and F. H. Alharbi, 'Plasmonically Enhanced Schottky Photovoltaic Devices', *Sci Rep*, vol. 7, no. 1, p. 14253, Oct. 2017, doi: 10.1038/s41598-017-14528-0.
- [10] G. Fan et al., 'Graphene/silicon nanowire Schottky junction for enhanced light harvesting', *ACS Appl Mater Interfaces*, vol. 3, no. 3, pp. 721–725, Mar. 2011, doi: 10.1021/am1010354.
- [11] S. S. Li, 'Theoretical analysis of a novel MPN gallium arsenide Schottky barrier solar cell', *Solid State Electronics*, vol. 21, pp. 435–438, Feb. 1978, doi: 10.1016/0038-1101(78)90274-5.

- [12] A. Benslim, A. Meftah, M. Labeled, A. Meftah, and N. Sengouga, 'Study and optimization of InGaN Schottky solar cell performance', *Optik*, vol. 247, p. 167984, Dec. 2021, doi: 10.1016/j.ijleo.2021.167984
- [13] K. J. Singh, D. Chettri, T. J. Singh, T. Thingujam, and S. kumar Sarkar, 'A performance optimization and analysis of graphene based schottky barrier GaAs solar cell', *IOP Conf. Ser.: Mater. Sci. Eng.*, vol. 211, no. 1, p. 012024, Jun. 2017, doi: 10.1088/1757-899X/211/1/012024.
- [14] Mousa E. Edweeb, E. J. Charlson, E. M. Charlson; Sputtered Schottky barrier solar cells on p-type GaAs. *Appl. Phys. Lett.* 15 September 1983; 43 (6): 572–574. <https://doi.org/10.1063/1.94429>.
- [15] K.-J. Hsiao, J.-D. Liu, H.-H. Hsieh, and T.-S. Jiang, 'Electrical impact of MoSe<sub>2</sub> on CIGS thin-film solar cells', *Phys. Chem. Chem. Phys.*, vol. 15, no. 41, pp. 18174–18178, Oct. 2013, doi: 10.1039/C3CP53310G
- [16] A. N. Corpus Mendoza, 'Influence of the p-type layer on the performance and stability of thin film silicon solar cells', Ph.D thesis, University of Sheffield, 2017. Accessed: Jun. 06, 2023. [Online]. Available: <https://theses.whiterose.ac.uk/16581/>
- [17] G. W. Pierce, 'Crystal Rectifiers for Electric Currents and Electric Oscillations. Part I. Carborundum', *Phys. Rev. (Series D)*, vol. 25, no. 1, pp. 31–60, Jul. 1907, doi: 10.1103/PhysRevSeriesI.25.31.
- [18] J. A. Spies et al., 'pin double-heterojunction thin-film solar cell p-layer assessment', *Solar Energy Materials and Solar Cells*, vol. 93, no. 8, pp. 1296–1308, Aug. 2009, doi: 10.1016/j.solmat.2009.01.024.
- [19] E. H. Rhoderick, 'Metal-semiconductor contacts', *IEE Proceedings I (Solid-State and Electron Devices)*, vol. 129, no. 1, pp. 1–14, Feb. 1982, doi: 10.1049/ip-i-1.1982.0001.
- [20] A. J. Wirth-Lima, P. P. Alves-Sousa, and W. Bezerra-Fraga, 'n-Graphene/p-Silicon-based Schottky junction solar cell, with very high power conversion efficiency', *SN Appl. Sci.*, vol. 2, no. 2, p. 246, Feb. 2020, doi: 10.1007/s42452-020-2056-1.
- [21] D. L. Pulfrey, 'MIS solar cells: A review', *IEEE Transactions on Electron Devices*, vol. 25, pp. 1308–1317, Nov. 1978, doi: 10.1109/T-ED.1978.19271.

- [22] H. C. Card and E. H. Rhoderick, 'Studies of tunnel MOS diodes I. Interface effects in silicon Schottky diodes', *J. Phys. D: Appl. Phys.*, vol. 4, no. 10, p. 1589, Oct. 1971, doi: 10.1088/0022-3727/4/10/319.
- [23] B. Theys et al., 'Revisiting Schottky barriers for CIGS solar cells: Electrical characterization of the Al/Cu(InGa)Se<sub>2</sub> contact', *physica status solidi (a)*, vol. 213, no. 9, pp. 2425–2430, 2016, doi: 10.1002/pssa.201533063.
- [24] Y. Osman, M. Fedawy, M. Abaza, and M. H. Aly, 'Optimized CIGS based solar cell towards an efficient solar cell: impact of layers thickness and doping', *Opt Quant Electron*, vol. 53, no. 5, p. 245, May 2021, doi: 10.1007/s11082-021-02873-4.
- [25] N. Mufti et al., 'Review of CIGS-based solar cells manufacturing by structural engineering', *Solar Energy*, vol. 207, pp. 1146–1157, Sep. 2020, doi: 10.1016/j.solener.2020.07.065.
- [26] J. Ramanujam and U. P. Singh, 'Copper indium gallium selenide based solar cells – a review', *Energy Environ. Sci.*, vol. 10, no. 6, pp. 1306–1319, Jun. 2017, doi: 10.1039/C7EE00826K.
- [27] E. T. Efaz et al., 'A review of primary technologies of thin-film solar cells', *Eng. Res. Express*, vol. 3, no. 3, p. 032001, Sep. 2021, doi: 10.1088/2631-8695/ac2353.
- [28] M. Jošt et al., 'Perovskite/CIGS Tandem Solar Cells: From Certified 24.2% toward 30% and Beyond', *ACS Energy Lett.*, vol. 7, no. 4, pp. 1298–1307, Apr. 2022, doi: 10.1021/acsenerylett.2c00274.
- [29] K. Aryal, 'High Efficiency Ultrathin CIGS Solar Cells', Ph.D thesis, Electrical & Computer Engineering, Old Dominion University, Jul. 2015, doi: 10.25777/dsr-d-mh49. [https://digitalcommons.odu.edu/ece\\_etds/48](https://digitalcommons.odu.edu/ece_etds/48)

# **CHAPTER III**

**Study of Schottky barrier solar cell based on CIGS material**

### III.1 Introduction

In this chapter, we will investigate the Schottky barrier solar cell based on p-type Cu(In, Ga)Se<sub>2</sub> (CIGS) material, exposed to the AM1.5 G standard spectrum at ambient temperature (300°K). The cathode metal, which serves as the front contact of the cell, is Aluminum (Al) with a work function ( $\phi_m$ ) of 4.1 eV, lower than the electron affinity of the p-type CIGS material ( $\chi_{sc} = 4.8 \text{ eV}$ ). This configuration forms a Schottky barrier for holes. The anode at the back of the cell is defined to be neutral (Ohmic contact). To conduct the investigation, we will utilize the numerical simulation software Scaps-1D. This software allows us to perform steady-state calculations of various internal parameters of the solar cell, including the band diagram, electron and hole concentrations, and recombination rate. Additionally, it enables the calculation of external parameters such as current density-voltage ( $J - V$ ) and power-voltage ( $P - V$ ) characteristics. These calculations will allow us to extract important photovoltaic output parameters, namely the short circuit current density  $J_{sc}$ , the open circuit voltage  $V_{oc}$ , the fill factor  $FF$ , the maximum power  $P_{max}$  provided by the cell and the photovoltaic conversion efficiency  $\eta$ . Our investigation will focus on varying the parameters of the CIGS absorber layer, specifically the defect density ( $N_t$ ) within the range  $[10^{10} - 10^{20} \text{ cm}^{-3}]$ , the thickness ( $d$ ) within the range  $[0.01-10\mu\text{m}]$ , and the doping concentration ( $N_A$ ) within the range  $[10^{10} - 5 \times 10^{17} \text{ cm}^{-3}]$ . Furthermore, we will explore if there is an effect of changing the cathode work function ( $\phi_m$ ) in the range  $[4.1 - 4.7 \text{ eV}]$  on the solar cell output parameters. To assess this effect, we will consider different cathode metals, including Al, Ta, Ti, Zn, Mo, W, and Cu, respectively.

### III.2. SCAPS-1D: an overview

The numerical simulation is a powerful tool that leads to a comprehensive understanding of solar cells, identifying the main parameters that affect their performance and designing new experimental production structures. Many simulation programs have been used for the CIGS solar cells, such as SILVACO ATLAS [1], AMPS [2], and SCAPS [3-5]. SCAPS-1D (Solar Cell Capacitance Simulator one Dimension) is a one-dimensional solar cell simulation software developed at the University of Gent in Belgium by Marc Burgelman and his colleagues [6]. Its primary purpose is to simulate the electrical characteristics of photonic devices, particularly thin film solar cells. Initially, SCAPS was developed specifically for simulating CuInSe<sub>2</sub> and CdTe cell structures. However, subsequent versions have expanded its capabilities to make it

applicable for the simulation of the electrical characteristics, performance, and spectral response of several crystallines and thin film–based photovoltaic cells, such as perovskite, CZTS, Si, GaAs, amorphous silicon (a-Si:H), micro-morphed silicon ( $\mu\text{-Si:H/a-Si:H}$ ) and CIGS solar cells [7]. One of its advantages is that the SCAPS simulation results agreed well with the corresponding experimental results, such as perovskite, CZTS, Si, CdTe, and CIGS solar cells [4,8-11]. With SCAPS, we can simulate solar cell structures that consist of multiple layers, including up to seven intermediate layers, as well as front and rear contacts. The software allows for the specification of various doping profiles within the layers and provides the ability to define energy distributions of donor or acceptor levels within the volume and at the interfaces. SCAPS also allows for the simulation of different light spectra by specifying the energy distribution of incident photons. SCAPS offers flexibility in introducing parameters with graduated variations, depending on the composition and depth of the solar cell. This allows exploring different material compositions, layer thicknesses, and doping profiles to understand their impact on the electrical characteristics and performance of the solar cell. Overall, SCAPS-1D provides researchers and engineers with a powerful tool for simulating and analyzing the behavior of various types of solar cells, aiding in the design and optimization of photonic devices for improved performance and efficiency. SCAPS simulates the energy diagrams in steady states and calculates the electron–hole recombination profile with the charge carrier transport in one dimension by solving the fundamental semiconductor equations. These equations are Poisson’s equations that connect the electrostatic potential to the charge (Eq. III.1) and the continuity equations for electrons and holes (Eq. III.2 and III.3) [7,12]:

$$\frac{d^2}{dx^2} \psi(x) = \frac{q}{\epsilon_0 \epsilon_r} (p(x) - n(x) + N_D - N_A + \rho_p - \rho_n) \quad \text{Eq. III.1}$$

Where  $\psi$  is electrostatic potential,  $q$  is electrical charge,  $\epsilon_r$  is relative permittivity and  $\epsilon_0$  is the vacuum permittivity,  $p$  and  $n$  are free hole and electron concentrations,  $N_D$  is charged impurities of donor and  $N_A$  is acceptor type,  $\rho_p$  and  $\rho_n$  are holes and electrons distribution in defect states, respectively. The continuity equations for electrons and holes are:

$$\frac{1}{q} \left( \frac{dJ_n}{dx} \right) + G - R = 0 \quad \text{Eq. III.2}$$

$$-\frac{1}{q} \left( \frac{dJ_p}{dx} \right) + G - R = 0 \quad \text{Eq. III.3}$$

Where  $J_n$  and  $J_p$  are electron and hole current densities,  $R$  is the recombination rate, and  $G$  is the generation rate.

Carrier transport in semiconductors occurs by drift and diffusion and can be expressed by the equations

$$J_n = qD_n \frac{dn}{dx} - q\mu_n n \frac{d\psi}{dx} \quad \text{Eq. III.4}$$

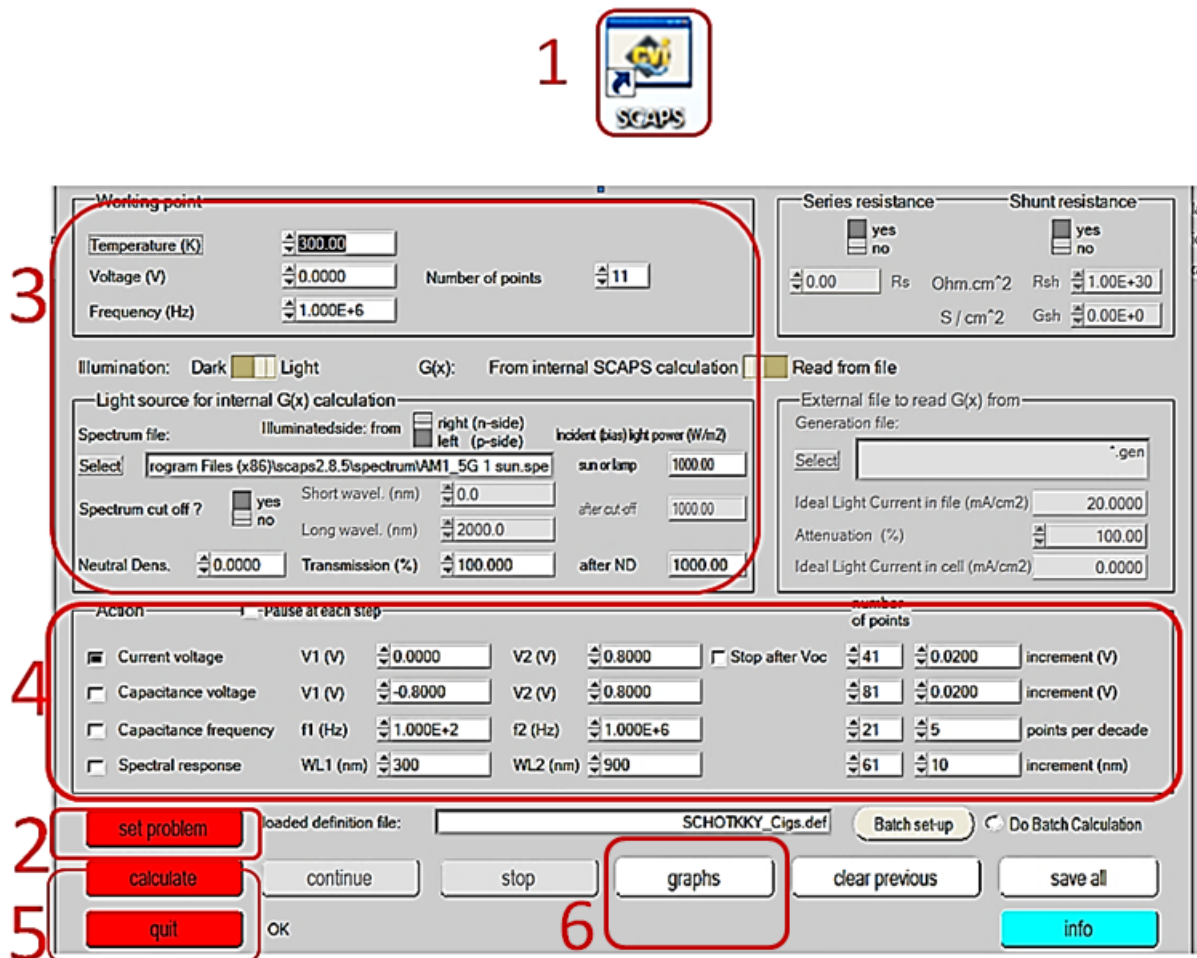
$$J_p = -qD_p \frac{dp}{dx} - q\mu_p p \frac{d\psi}{dx} \quad \text{Eq. III.5}$$

Where  $D_n$  and  $D_p$  are electron and hole diffusion coefficients,  $\mu_n$  and  $\mu_p$  are electron and hole mobilities.

SCAPS is a Windows-oriented program, developed with Lab Windows/CVI of National Instruments. We use here the LW/CVI terminology of a 'Panel' (names used in other softwares are: a window, a page, a pop-up...). SCAPS opens with the 'Action Panel' [13]. There are dedicated panels for the basic actions (Figure III.1) [13]:

1. Run SCAPS.
2. Definition of the problem including the geometry, the materials and all properties of the investigated solar cell.
3. Indication of the circumstances in which we want to do the simulation, i.e. specification of the working point. This means stating the parameters which are not varied in a measurement simulation, and which are relevant to that measurement such as the temperature  $T$ , the voltage  $V$ , the frequency  $f$  and the dark or light conditions. A one sun (equal to  $1000 \text{ W/m}^2$ ) illumination with the 'air mass 1.5, global' (AM1.5 G) spectrum is the default, but we have a large choice of monochromatic light and spectra for the specialized simulations.
4. Indication of what we will calculate, i.e. which measurement we will simulate. We can select one or more of the following measurements: current-voltage ( $I - V$ ), capacitance - voltage ( $C - V$ ), capacitance - frequency ( $C - f$ ) and the spectral response (quantum efficiency:  $QE(\lambda)$ ).
5. Starting the calculations. The Energy Bands Panel opens (Figure III.2), and the calculations start. At the bottom of the Panel, we see a status line, e.g. "iv from 0.000 to 0.550 V:  $V = 0.550 \text{ V}$ ", showing us how the simulation proceeds. Meanwhile, SCAPS stands us a free movie how the conduction and valence bands, the Fermi levels and the whole caboodle are evolving.

6. Display of the simulated curves. After the calculations, SCAPS switches to the Energy band panel (Figure III.3). We can now look to the band diagrams, carrier densities, current densities, at the last bias point (ex:  $V = 0.8$  Volt). We can output, save and plot the results (buttons save graphs, save data, show data and plot). We can also display and save additional curves such as those of the generation- recombination rate profiles and  $I - V$  characteristics (buttons Gen-Rec and I-V). Figure III.4 shows for example the panel of  $I(V)$  characteristic curves in dark and light conditions. The solar cell output parameters are, also, displayed.



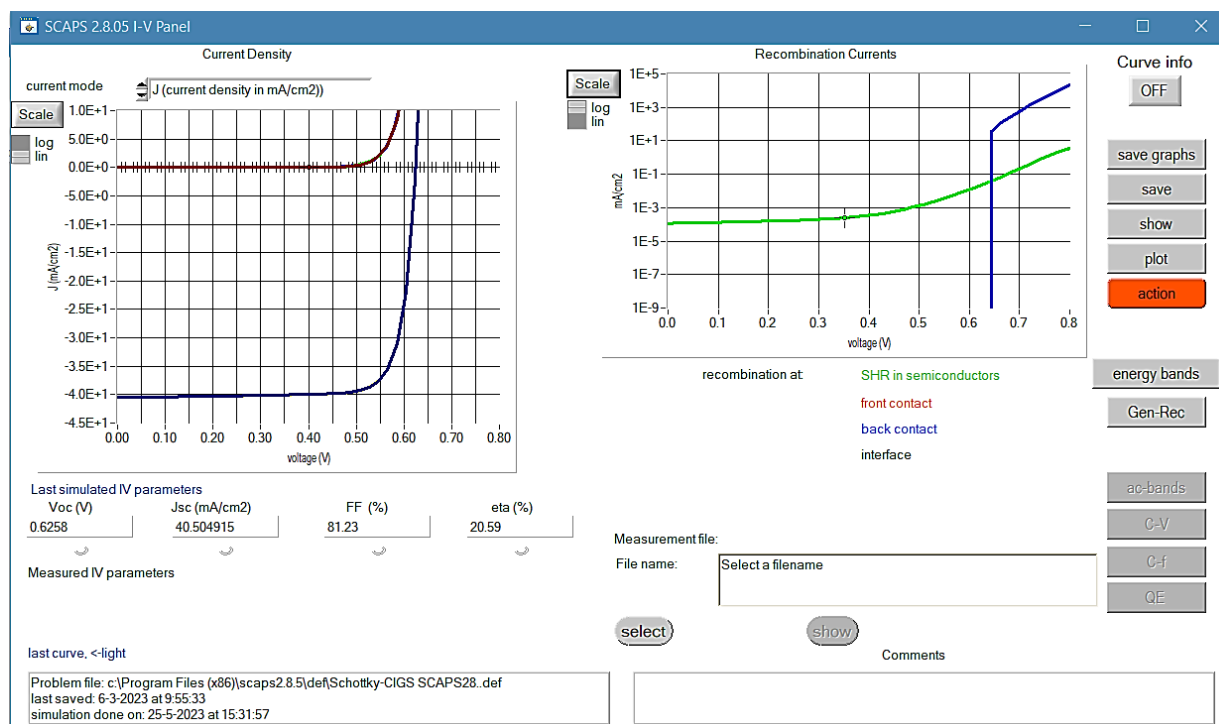
**Figure III 1:** The SCAPS start-up panel: The Action panel or main panel. The meaning of the blocks numbered 1 to 6 is explained in the text. [13].



Figure III.2: Energy Bands Panel [13].



Figure III.3: Energy band panel after the calculations.



**Figure III.4:** Panel of  $I(V)$  characteristic curves in dark and light conditions. The solar cell output parameters are also displayed [13].

### III. 3. Editing a solar cell structure via Scaps-1D

When clicking the ‘Set Problem’-button on the action panel, the ‘Solar cell definition’-panel is displayed. This panel allows to create/edit solar cell structures and to save those to or load from definition files. These definition files are standard ASCII-files with extension ‘\*.def’. Layer-, contact-, and interface properties can be edited by clicking on the appropriate box as shown in Figure III.5. The light illuminated side can be chosen at the right or left contact.

Layers can be added by clicking ‘add layer’. They are introduced one by one, with their optical and electrical properties (Figure. III.6). SCAPS absorption files are ASCII-files (simple text files) with the extension ‘\*.abs’, and they reside by default in the [SCAPS]\absorption subdirectory. If a line in this file can be interpreted as starting with at least two numeric values, the first value is interpreted as the wavelength  $\lambda$  (in nm) and the second as the absorption coefficient  $\alpha$  (in 1/m).

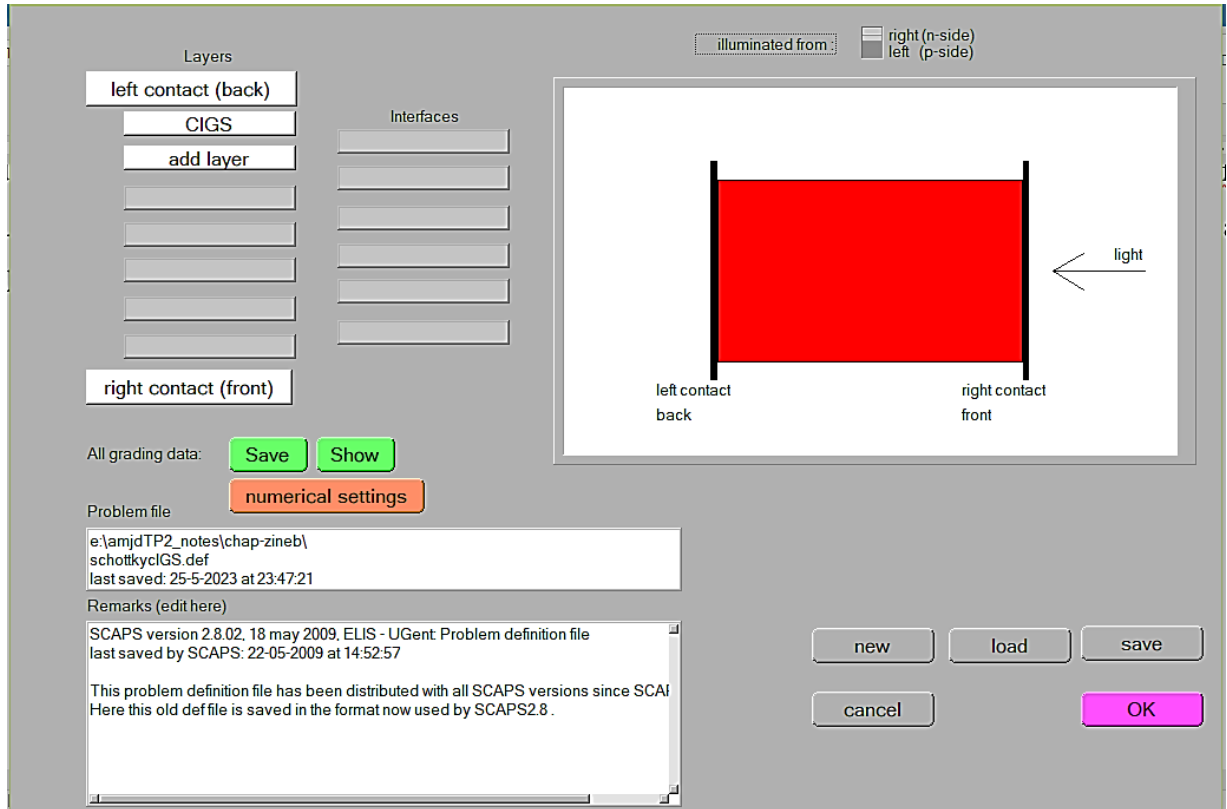


Figure III.5: Solar cell definition panel.

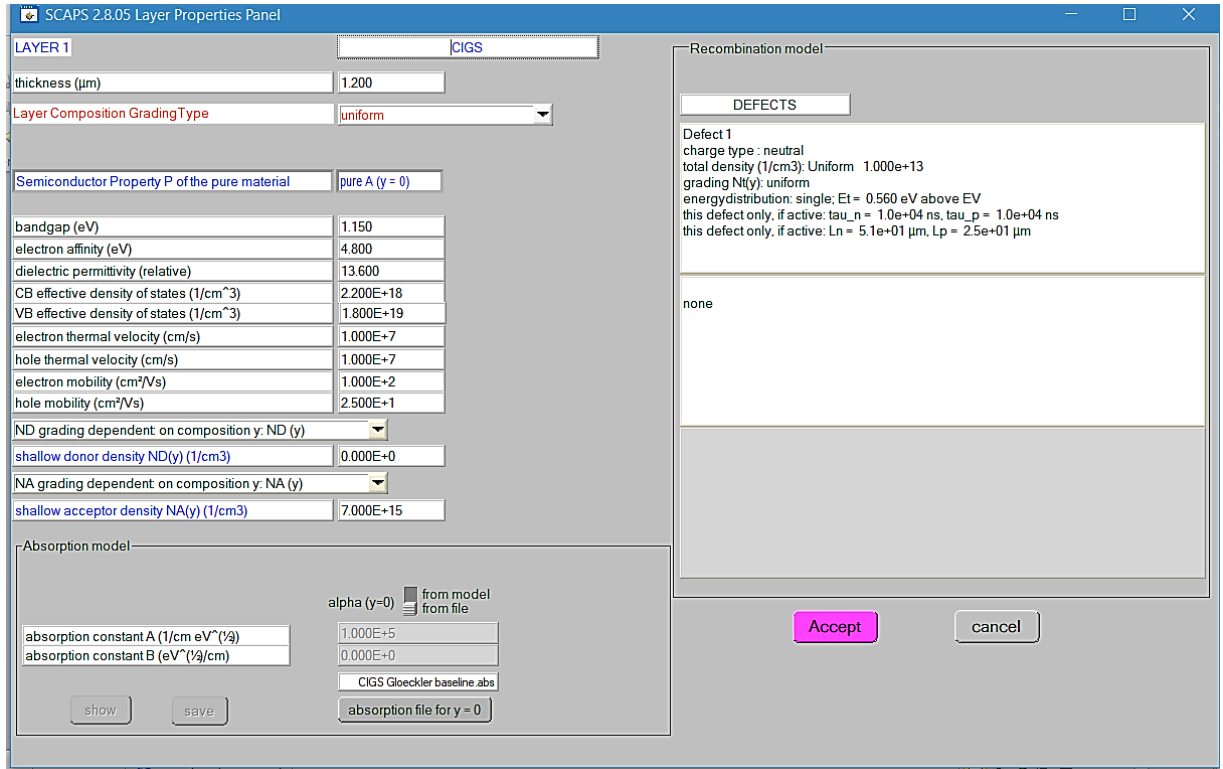
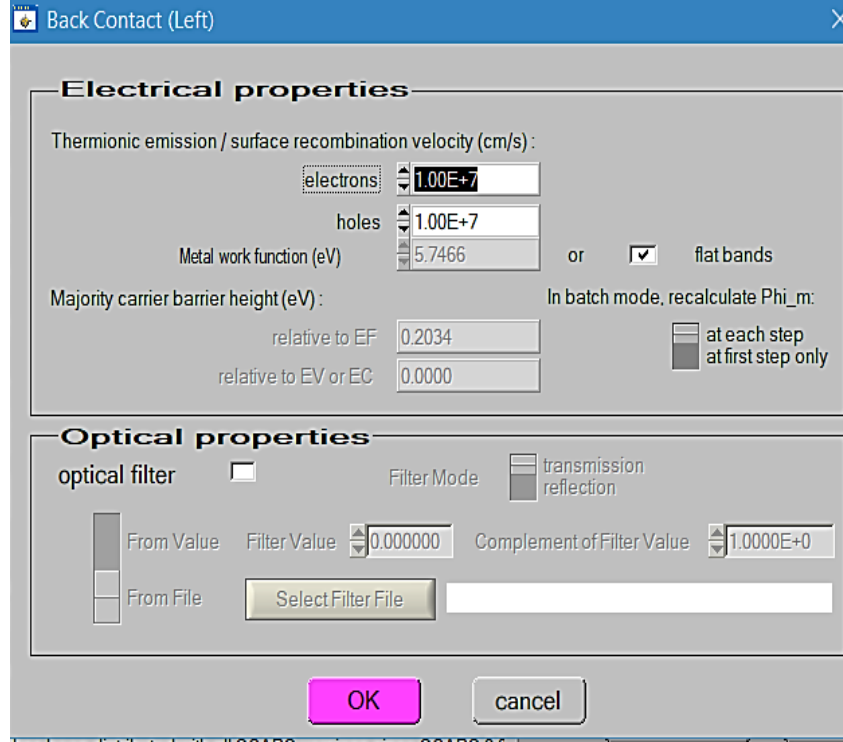


Figure III.6: Layer properties panel.

The contact properties can be set by either clicking the front or back contact button on the cell definition panel, which opens the ‘contact properties panel’ as shown on Figure III.7. The surface recombination velocities and the metal work function  $\phi_m$  (for majority carriers) can be input.



**Figure III.7:** Contact properties panel. [13].

However, we can also choose the option “flat bands”. In this case, SCAPS calculates for every temperature the metal work function  $\phi_m$  in such a way that flat-band conditions prevail. When the layer adjacent to the contact is n-type Eq.III.6 is used, when it is p-type Eq.III.7 is used, when it can be considered to be intrinsic Eq.III.8 is used [13].

$$\phi_m = \chi_{sc} + k_B T \ln \left( \frac{N_C}{N_D - N_A} \right) \quad \text{Eq.III.6}$$

$$\phi_m = \chi_{sc} + E_g - k_B T \ln \left( \frac{N_C}{N_A - N_D} \right) \quad \text{Eq.III.7}$$

$$\phi_m = \chi_{sc} + k_B T \ln \left( \frac{N_C}{n_i} \right) \quad \text{Eq.III.8}$$

Where  $\chi_{sc}$  is the electron affinity of the semiconductor layer,  $(N_D - N_A)$  is the net doping in n-type semiconductor,  $(N_A - N_D)$  is the net doping in p-type semiconductor,  $n_i$  is the intrinsic concentration and  $N_C$  the effective density of state ( $cm^{-3}$ ) at  $E_C$ .

At the contacts a (wavelength dependent) reflection/transmission  $R(\lambda)$  or  $T(\lambda)$  can be set. These can be set either as a constant value (wavelength independent) or as a filter file.

#### III.4. Description of the studied Schottky barrier solar cell based on CIGS material:

Figure III.8 shows the structure of the studied Schottky - barrier solar cell based on p-type CIGS material. The right contact is illuminated and acts as the front contact. This latter is chosen to be the cathode and is made of Aluminum (Al) with a work function ( $\phi_m$ ) of 4.1 eV. The work function of Aluminum is lower than the electron affinity of the CIGS absorber layer ( $\chi_{sc}$ ), which is 4.8 eV. Consequently, the Schottky contact condition is fulfilled at the front contact.

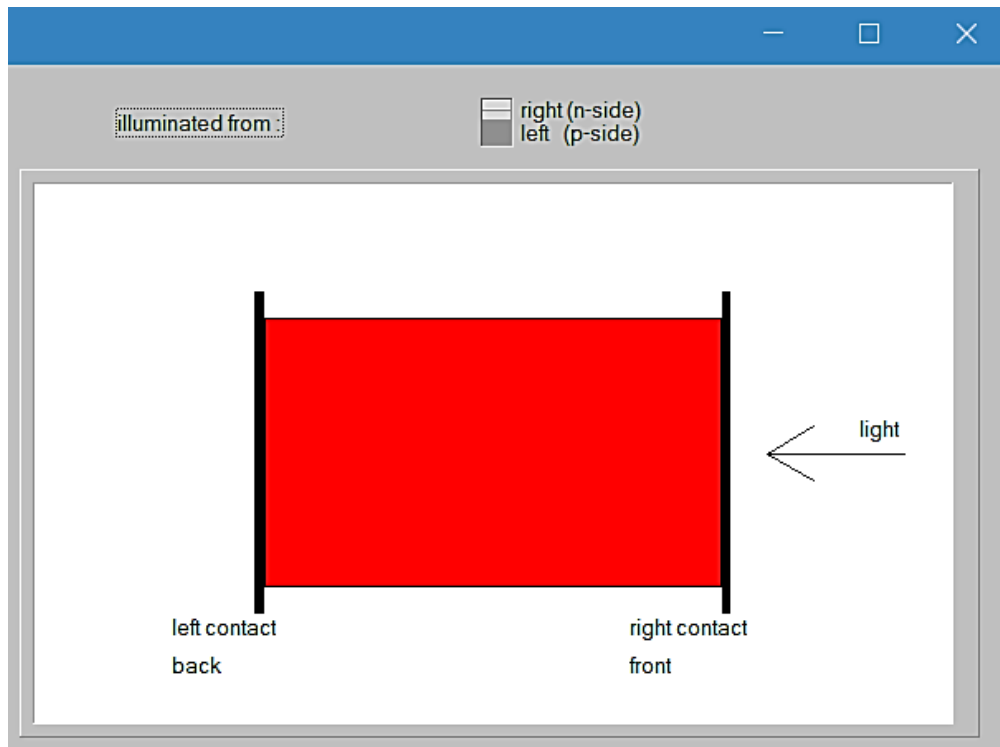


**Figure III.8:** Structure of the studied Schottky - barrier solar cell based on p-type CIGS material.

The purpose of using a Schottky contact at the front contact is to create a barrier that allows selective carrier collection. In this case, the lower work function of Aluminum compared to the electron affinity of CIGS leads to a barrier for holes, allowing efficient collection of photogenerated electrons while blocking the flow of holes from the p-type CIGS layer to the front contact [14,15]. On the other hand, the left (back) contact, which acts as the anode, is defined to be neutral and forms an Ohmic contact. The Ohmic contact allows both electrons and holes to pass through easily without any significant barrier. The flat bands condition is chosen

for the back contact, which means that the energy bands align with the Fermi level of the material. This condition ensures efficient carrier transport without hindrance. To account for surface recombination, surface recombination velocities ( $S_n$  and  $S_p$ ) are specified. The values given are  $S_n = S_p = 10^7 \text{ cm/s}$  [13]. These velocities represent the rates at which electrons and holes recombine at the surface of the material. This structure aims to maximize the collection of photogenerated electrons at the front contact while allowing easy passage of both electrons and holes at the back contact, facilitating efficient carrier transport in the studied CIGS solar cell [16].

The numerical simulation is performed using the software tool Scaps-1D. The simulation aims to calculate the basic characteristics of the solar cell under steady-state conditions, considering the input parameters specified in Table III.1. The material properties that are used are extracted from some known and reliable studies [2,7,15,17-22].

As mentioned in section III.2, Scaps-1D, solves the one-dimensional equations, including Poisson's equation, transport equations, and continuity equations for electrons and holes. These equations describe the behavior of the semiconductor material, taking into account the Shockley-Read-Hall recombination model. By numerically solving these equations, Scaps-1D calculates various characteristics of the solar cell, such as the band diagram, generation and recombination rates, carrier densities, and cell currents [23,24]. These results provide insights into the performance and behavior of the solar cell. During the simulation, the solar cell is subjected to the AM1.5G solar spectrum, which represents the standard solar spectrum for terrestrial applications, and has an incident power density of  $100 \text{ mW/cm}^2$ . The simulation assumes room temperature conditions ( $300^\circ\text{K}$ ).

To accurately model the absorption properties of the CIGS material, the Scaps library provides the CIGS absorption file data ( $\alpha(\lambda)$ ) [17]. This data represents the wavelength-dependent absorption coefficient, which determines the material's ability to absorb light at different wavelengths. The photovoltaic parameters are simulated without considering the influences of the series and shunt resistance.

By utilizing the Scaps-1D simulation tool and incorporating the relevant parameters and inputs (Table III.1), the study aims to obtain a comprehensive understanding of the solar cell's behavior, performance, and key characteristics under the specified conditions.

**Table III 1.** Baseline parameters for modeling the Schottky barrier solar cell based on CIGS material at  $T = 300 \text{ }^\circ\text{K}$ . [2,7,15,17-22].

Parameters	Value
Solar cell thickness, $d$ ( $\mu\text{m}$ )	1.2 then varied within the range [0.01-10 $\mu\text{m}$ ]
Energy band gap, $E_g$ (eV)	1.15
Relative dielectric permittivity, $\epsilon_r$	13.6
Electron affinity, $\chi_{sc}$ (eV)	4.8
Effective density of state at $E_C$ , $N_C$ ( $\text{cm}^{-3}$ )	$2.2 \times 10^{18}$
Effective density of state at $E_V$ , $N_V$ ( $\text{cm}^{-3}$ )	$1.8 \times 10^{19}$
Electron thermal velocity( $\text{cm/s}$ )	$10^7$
Hole thermal velocity( $\text{cm/s}$ )	$10^7$
Electron mobility, $\mu_n$ ( $\text{cm}^2\text{V}^{-1}\text{s}^{-1}$ )	100
Hole mobility, $\mu_p$ ( $\text{cm}^2\text{V}^{-1}\text{s}^{-1}$ )	25
Doping concentration $N_A$ ( $\text{cm}^{-3}$ ) in p-type CIGS layer	$7 \times 10^{15}$ then varied within the range [ $10^{10} - 5 \times 10^{17} \text{cm}^{-3}$ ].
Defect density $N_t$ ( $\text{cm}^{-3}$ ) in p-type CIGS layer	$10^{13}$ then varied within the range [ $10^{10} - 10^{20} \text{cm}^{-3}$ ].
Defect type	Neutral
Electron capture cross section ( $\text{cm}^2$ )	$10^{-15}$
Hole capture cross section ( $\text{cm}^2$ )	$10^{-15}$

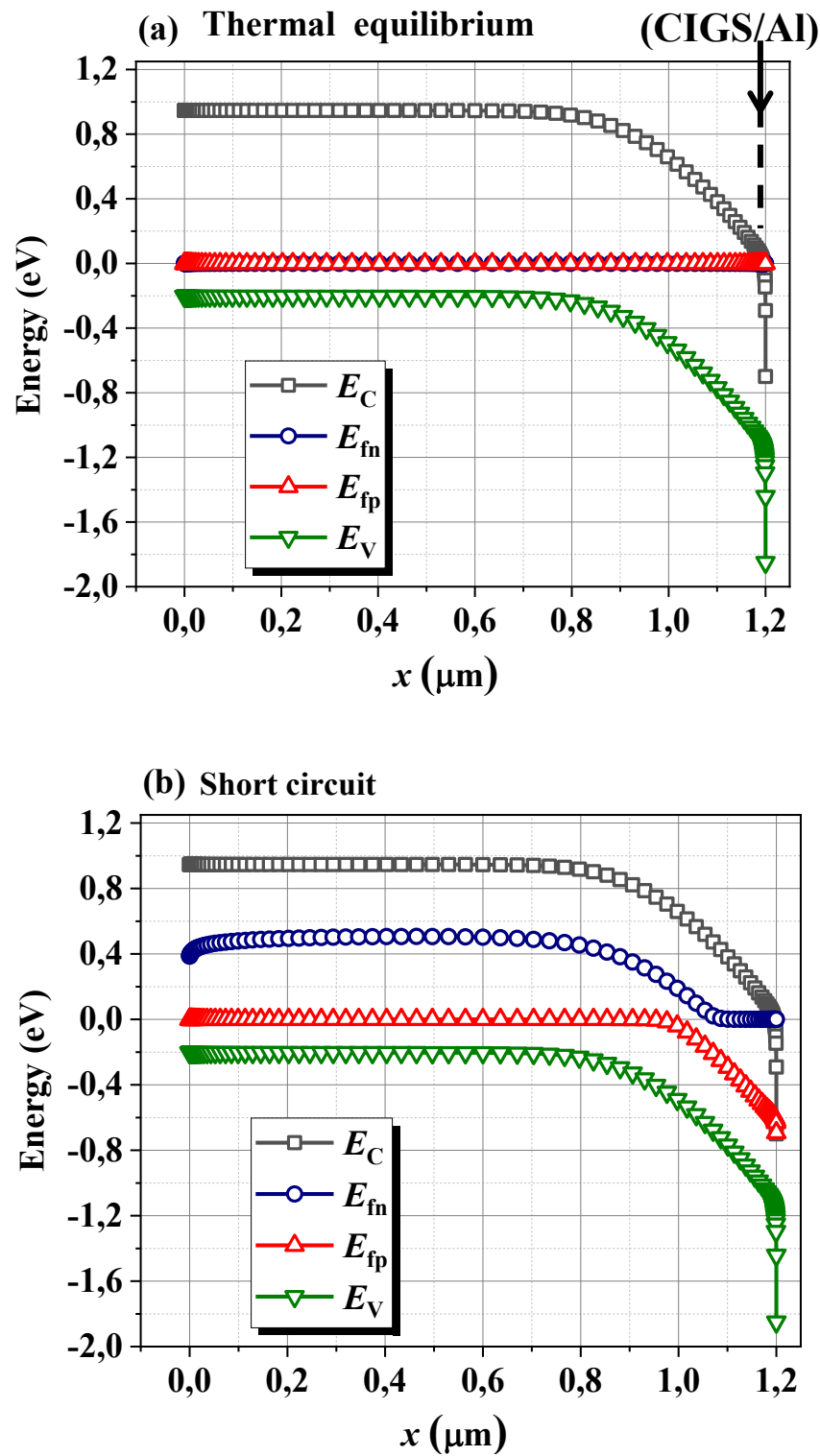
Defect energetic distribution	Single
Defect energy level $E_t$ (eV)	$E_V + 0.56$
Electron life time, $\tau_n$ (s)	$10^{-5}$
Hole life time, $\tau_p$ (s)	$10^{-5}$
Electron diffusion length, $L_n$ ( $\mu m$ )	51
Hole diffusion length, $L_p$ ( $\mu m$ )	25
Cathode work function ( $\phi_m$ (eV))	4.1 (Al) then varied in the range [4.1 – 4.7 eV]

### III.5. Results and discussion

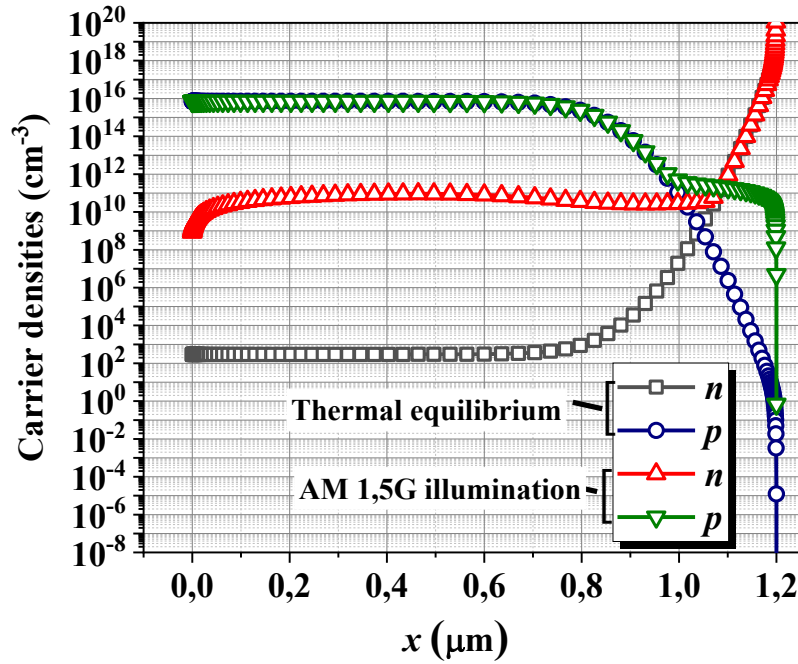
Figure III.9 shows, the band diagram of the Schottky barrier solar cell based on p-type CIGS material with Aluminum (Al) as the cathode metal ( $\phi_m = 4.1$  eV). The corresponding Schottky barrier height  $\phi_{bp}$  for holes is :

$$\phi_{bp} = (\chi_{sc} + E_g) - \phi_m = 1.85 \text{ eV} \quad \text{Eq.III.9}$$

The cell thickness is  $= 1.2 \mu m$ , the doping concentration of the p-type CIGS layer is  $N_A = 7 \times 10^{15} \text{ cm}^{-3}$  and the defect density  $N_t = 10^{13} \text{ cm}^{-3}$ . Case (a) of Figure III.9 corresponds to the thermal equilibrium; case (b) corresponds to the short – circuit condition with AM1.5G spectrum illumination. The bands of the CIGS layer at the (Al/ CIGS) interface bend downward. Relatively to the thermal equilibrium, the splitting of the quasi-Fermi levels, at short-circuit condition, shows an increase, by photo-generation, of the hole carrier density in the depletion region near the Schottky contact ((Al/ CIGS) interface). However, the electron carrier density increases in the remaining part of the depletion region and in the quasi-neutral region of the p-type CIGS layer. This is clearly showed by Figure III.10 which displays, the carrier density distributions along the Schottky barrier solar cell based on p-type CIGS material, at thermal equilibrium and short-circuit condition with the AM 1.5G spectrum illumination.



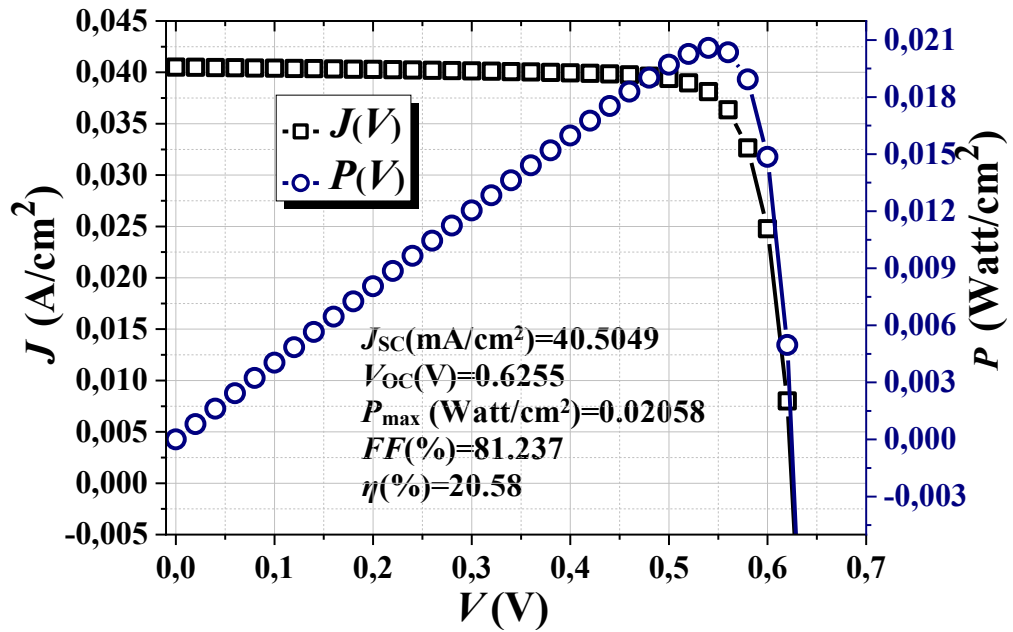
**Figure III. 9:** Band diagram of the Schottky barrier solar cell based on p-type CIGS material with Aluminum (Al) as the cathode metal ( $\phi_m = 4.1 \text{ eV}$ ): (a) at thermal equilibrium, (b) at short circuit condition with AM 1.5G spectrum illumination.



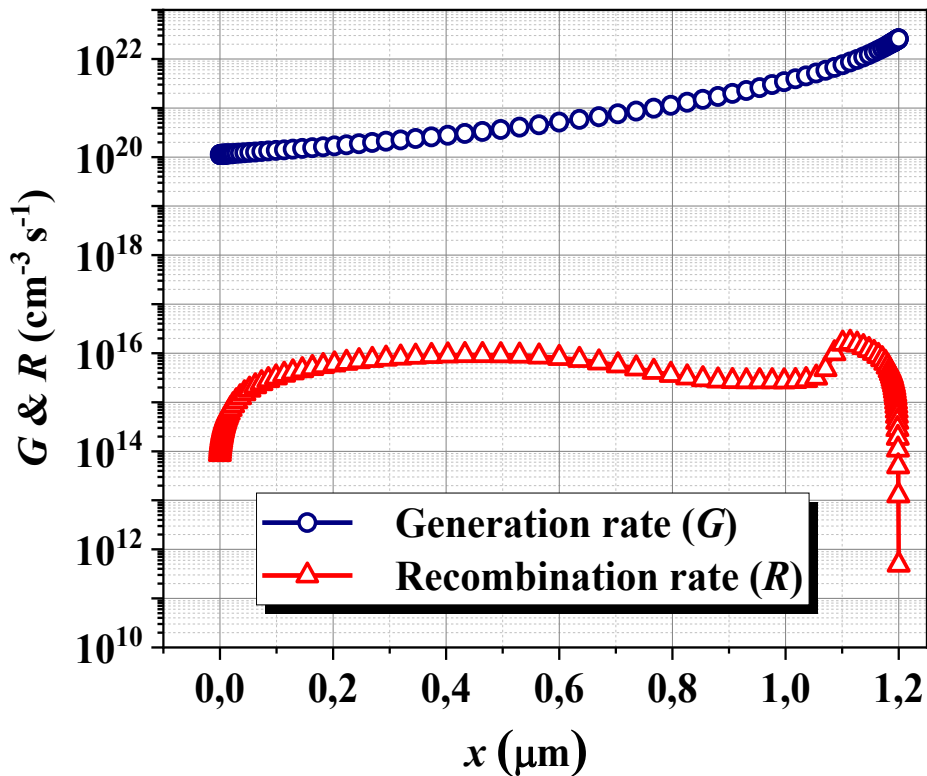
**Figure III.10:** Carrier density distributions along the Schottky barrier solar cell based on p-type CIGS material at thermal equilibrium, and at short circuit condition with AM 1.5G spectrum illumination.

Figure III.11 presents the simulated current density – voltage ( $J - V$ ) and the provided power – voltage ( $P - V$ ) characteristics. The photovoltaic output parameters of the cell are  $J_{sc} = 40.50 \text{ mA/cm}^2$ ,  $V_{oc} = 0.6255 \text{ V}$ ,  $P_{max} = 0.02058 \text{ W/cm}^2$ ,  $FF = 81.23\%$  and the conversion efficiency  $\eta = 20.58\%$ . This latter is close to some recent works [25,26]; which reported a conversion efficiency of 20.49 % [25] and 20.7% [26] respectively. This suggests that our simulation results align well with other works and validate the accuracy of the simulation software and modeling approach. Having similar output parameters to reported works is a positive outcome, as it indicates that our p-type CIGS Schottky barrier solar cell is performing well and achieving competitive efficiency levels.

Figure III.12 shows the generation and recombination rates through the solar cell under the AM1.5G standard spectrum and  $T = 300^\circ\text{K}$ . In the Schottky barrier solar cell based on p-type CIGS material with aluminum (Al) as the cathode metal, the recombination rate is primarily limited by the minority carrier densities (Figure III.10). Specifically, the recombination rate is influenced by the hole carrier density in the depletion region near the p-type CIGS/Al interface and by the electron carrier density in the remaining part of the depletion region and the quasi-neutral region of the p-type CIGS layer.



**Figure III.11:** Simulated  $J - V$  and  $P - V$  characteristics of the Schottky barrier solar cell based on p-type CIGS material with Al as the cathode metal ( $\phi_m = 4.1 \text{ eV}$ ), under the AM1.5G standard spectrum and  $T = 300^\circ\text{K}$ .



**Figure III.12:** Generation and recombination rate distributions through the Schottky barrier solar cell based on p-type CIGS material under the AM1.5G standard spectrum and  $T = 300^\circ\text{K}$ .

In the depletion region near the p-type CIGS/Al interface (Figure III.10), there is a high concentration of electrons due to the formation of a Schottky barrier for holes, resulting in a low holes carrier density. The high electron carrier density and the low hole carrier density create a gradient in carrier concentrations, leading to the recombination of minority carriers (holes) with majority carriers (electrons). This recombination process limits the overall efficiency of the solar cell. In the remaining part of the depletion region and the quasi-neutral region of the p-type CIGS layer, the concentration of holes increases, and the electron concentration remains lower than the hole concentration due to the p-type nature of the CIGS material (Figure III.10). Recombination occurs between the minority carriers (electrons) and the majority carriers (holes) in these regions as well, contributing to the overall recombination rate. To improve the performance of the solar cell, it is crucial to minimize recombination losses by optimizing the minority carrier densities in the different regions of the device. This can be achieved through various strategies such as reducing defect densities, optimizing the doping concentration, and carefully engineering the band structure of the CIGS absorber layer and the interface with the cathode material. Figures III.13, III.14 and III.15 show, respectively, the effect of the defect density ( $N_t$ ), the thickness ( $d$ ) and the doping concentration ( $N_A$ ) of the p-type CIGS layer on the recombination rate distribution.

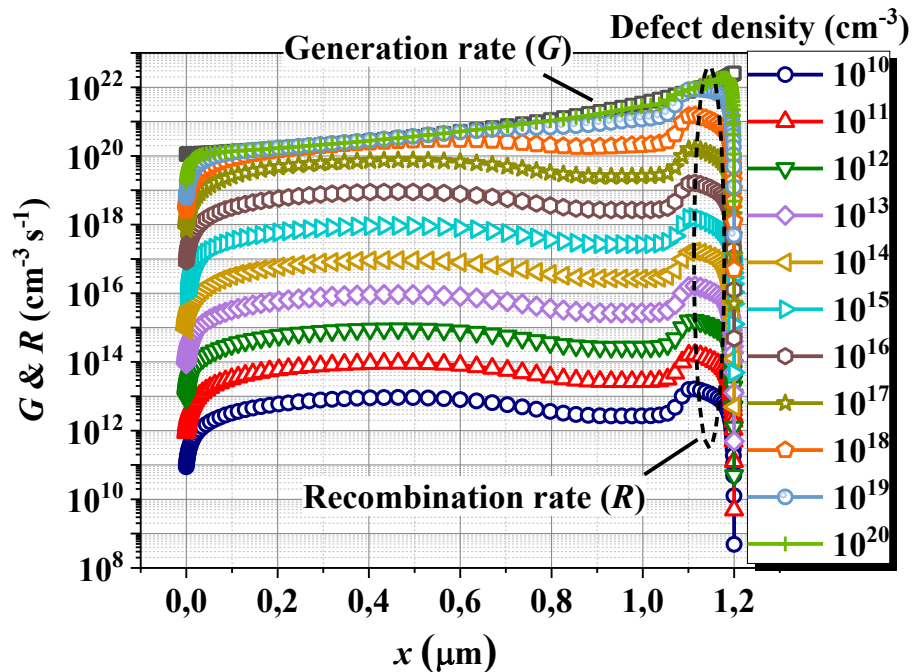


**Figure III.13:** Generation and recombination rate distributions through the Schottky barrier solar cell based on p-type CIGS material with the increase of the defect density ( $N_t$ ) within the range  $[10^{10} - 10^{20} \text{ cm}^{-3}]$ .

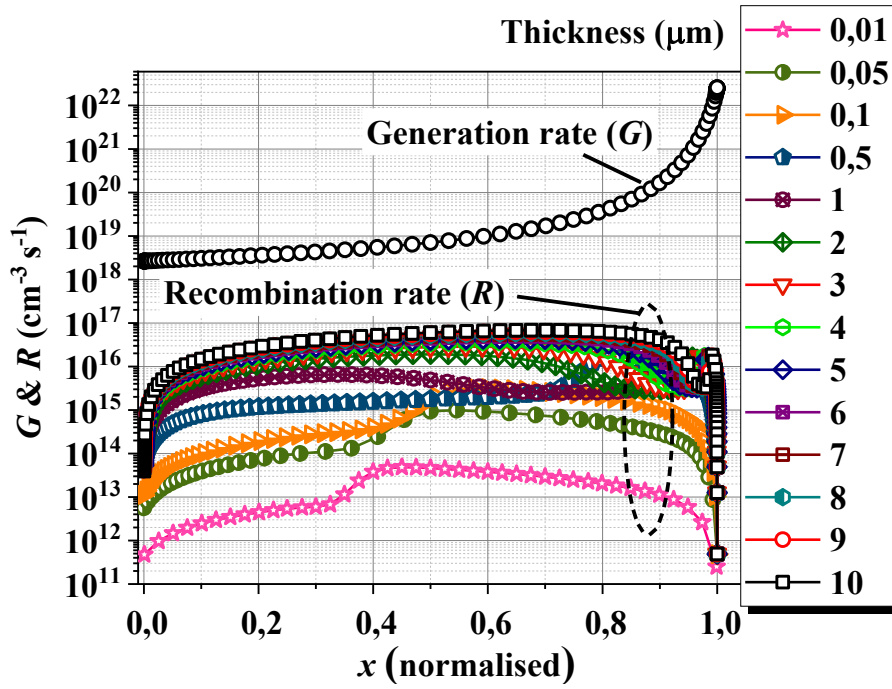


**Figure III.14:** Generation and recombination rate distributions through the Schottky barrier solar cell based on p-type CIGS material with the increase of the thickness ( $d$ ) within the range  $[0.01 - 10 \mu m]$ .

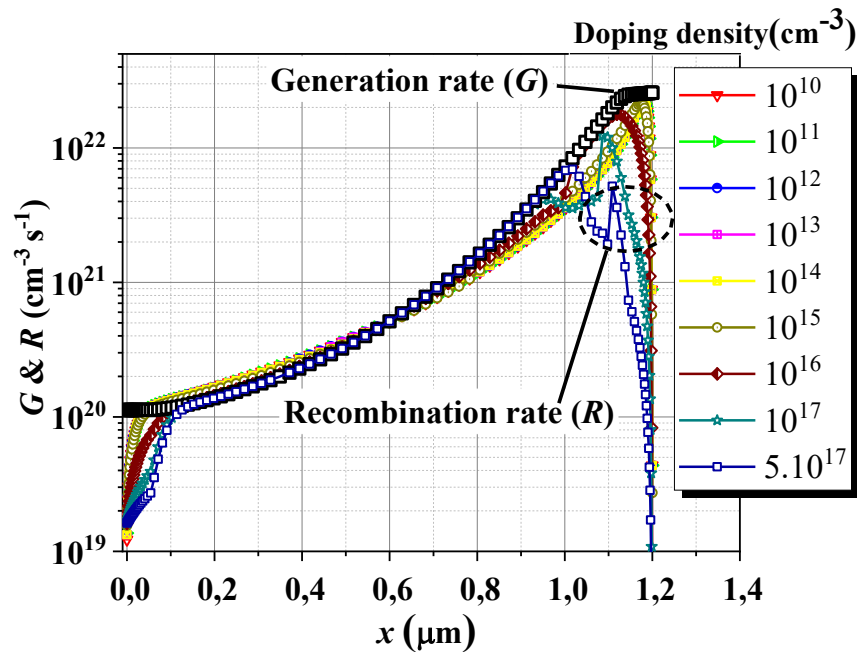


**Figure III.15:** Generation and recombination rate distributions through the Schottky barrier solar cell based on p-type CIGS material with the increase of the doping concentration ( $N_A$ ) within the range  $[10^{10} - 5 \times 10^{17} cm^{-3}]$ .

The increase of the defect density in the p-type CIGS layer (Figure III.13) leads to an increase in the recombination rate distribution along the layer. Defects in the semiconductor material, such as CIGS, can act as recombination centers. When the defect density in the p-type CIGS layer increases; there are more available recombination centers for charge carriers. This means that a higher number of electrons and holes will encounter these defects and recombine, rather than reaching the interface between the p-type CIGS and the Schottky contact (Al). The recombination rate distribution along the p-type CIGS layer will then increase, resulting in the loss of current and reduced efficiency of the solar cell. In the context of a solar cell, it is desirable to minimize recombination and maximize the collection of charge carriers at the electrodes to generate electrical current.

As shown in Figure III.16 and Table III.2; increasing the defect density in the p-type CIGS layer within the range  $[10^{10} - 10^{20} \text{cm}^{-3}]$  has, initially, little impact on the photovoltaic output parameters of the solar cell. The increase in recombination rate due to higher defect density does not have a significant negative impact on the photovoltaic output parameters. They remain relatively unaffected. However, once the defect density exceeds  $10^{15} \text{cm}^{-3}$ , negative effects start to emerge, leading to a decrease in the fill factor ( $FF$ ) and the open circuit voltage ( $V_{oc}$ ). This reduction is likely due to an increase in the recombination losses caused by the higher concentration of defects. The recombination of charge carriers at the defect sites hampers the effective separation and collection of the carriers, leading to a decrease in the fill factor and open circuit voltage. As the defect density increases further, exceeding  $10^{17} \text{cm}^{-3}$ , the short circuit current density ( $J_{sc}$ ) experiences a significant decrease. The higher defect density promotes more recombination events, leading to a reduction in the number of charge carriers available for contributing to the short circuit current. The decreases in fill factor, open circuit voltage, and short circuit current density all contribute to a reduction in the conversion efficiency ( $\eta$ ) of the Schottky barrier solar cell. The conversion efficiency represents the ability of the solar cell to convert incoming sunlight into electrical energy, and the negative effects caused by the higher defect density ultimately lead to a decrease in this efficiency.

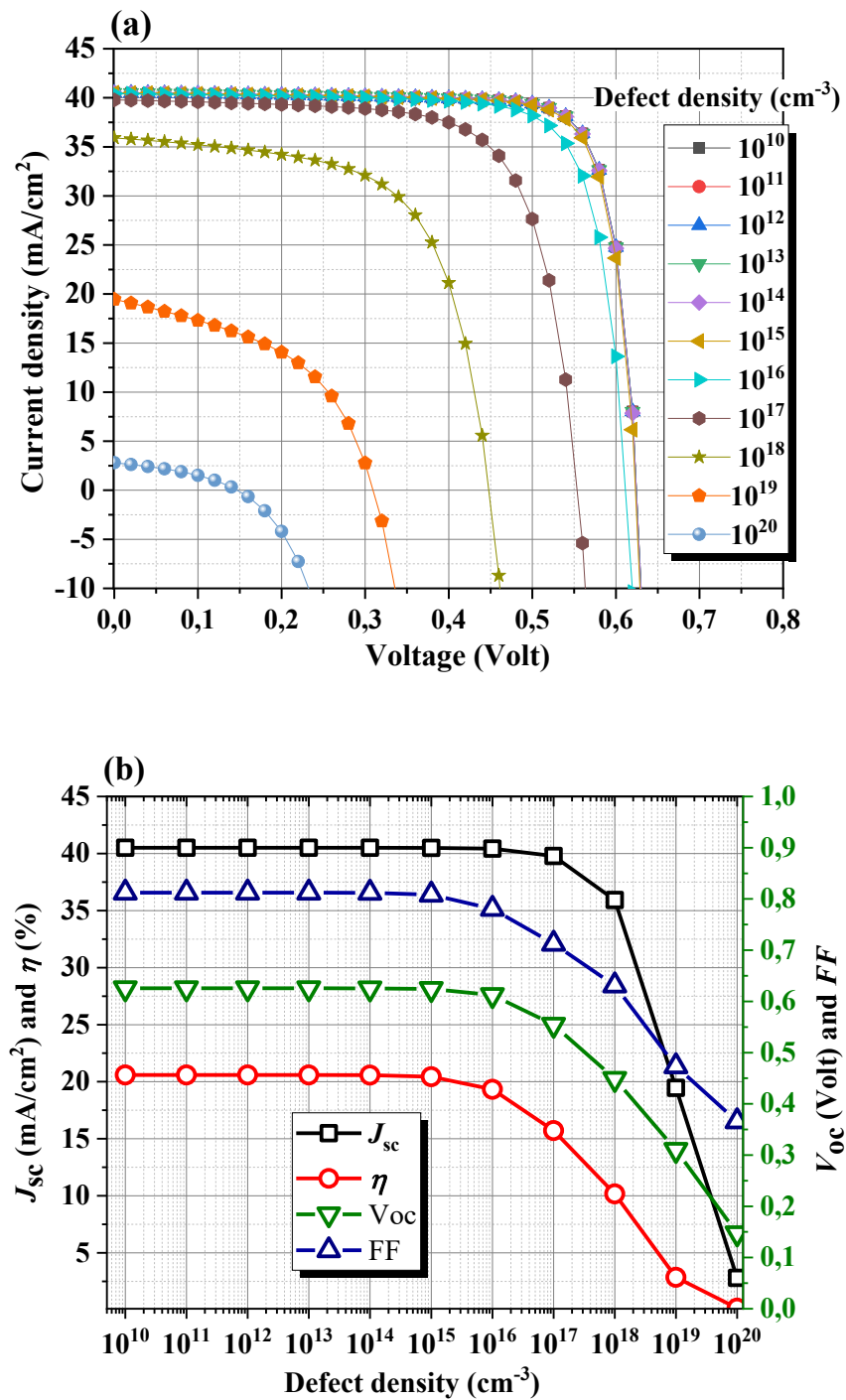


**Figure III.16:** Variation effect of the p-type CIGS layer defect density on : (a)  $(J - V)$  characteristics and (b) the photovoltaic output parameters of the Schottky barrier solar cell .

**Table III.2:** Variation effect of the p-type CIGS layer defect density on the photovoltaic output parameters of the Schottky barrier solar cell .

Defect density ( $cm^{-3}$ )	$J_{sc}(mA/cm^2)$	$V_{oc}(V)$	$FF$	$\eta(\%)$
$10^{10}$	40,505	0,62557	0,81241	20,5853
$10^{11}$	40,50499	0,62557	0,81241	20,5853
$10^{12}$	40,50499	0,62557	0,81241	20,5851
$10^{13}$	40,50491	0,62555	0,81237	20,5838
$10^{14}$	40,50419	0,62543	0,81201	20,5703
$10^{15}$	40,49692	0,62422	0,8084	20,4355
$10^{16}$	40,42521	0,61251	0,78049	19,3257
$10^{17}$	39,78487	0,55433	0,71254	15,7142
$10^{18}$	35,91831	0,44866	0,63095	10,1679
$10^{19}$	19,45698	0,31018	0,47316	2,8557
$10^{20}$	2,80793	0,14739	0,36594	0,1514

Therefore, minimizing the recombination rate distribution by reducing the defect density in the p-type CIGS layer is crucial to optimize the ( $J - V$ ) characteristics and improve the photovoltaic performance of the Schottky barrier solar cell. Techniques such as defect passivation, interface engineering, and material optimization are employed to mitigate recombination losses and enhance the efficiency of the solar cell [27-29].

Figure III.17 shows the variation effect of the p-type CIGS layer thickness on : (a) ( $J - V$ ) characteristics and (b) the photovoltaic output parameters of the Schottky barrier solar cell ( which are also presented in Table III.3)

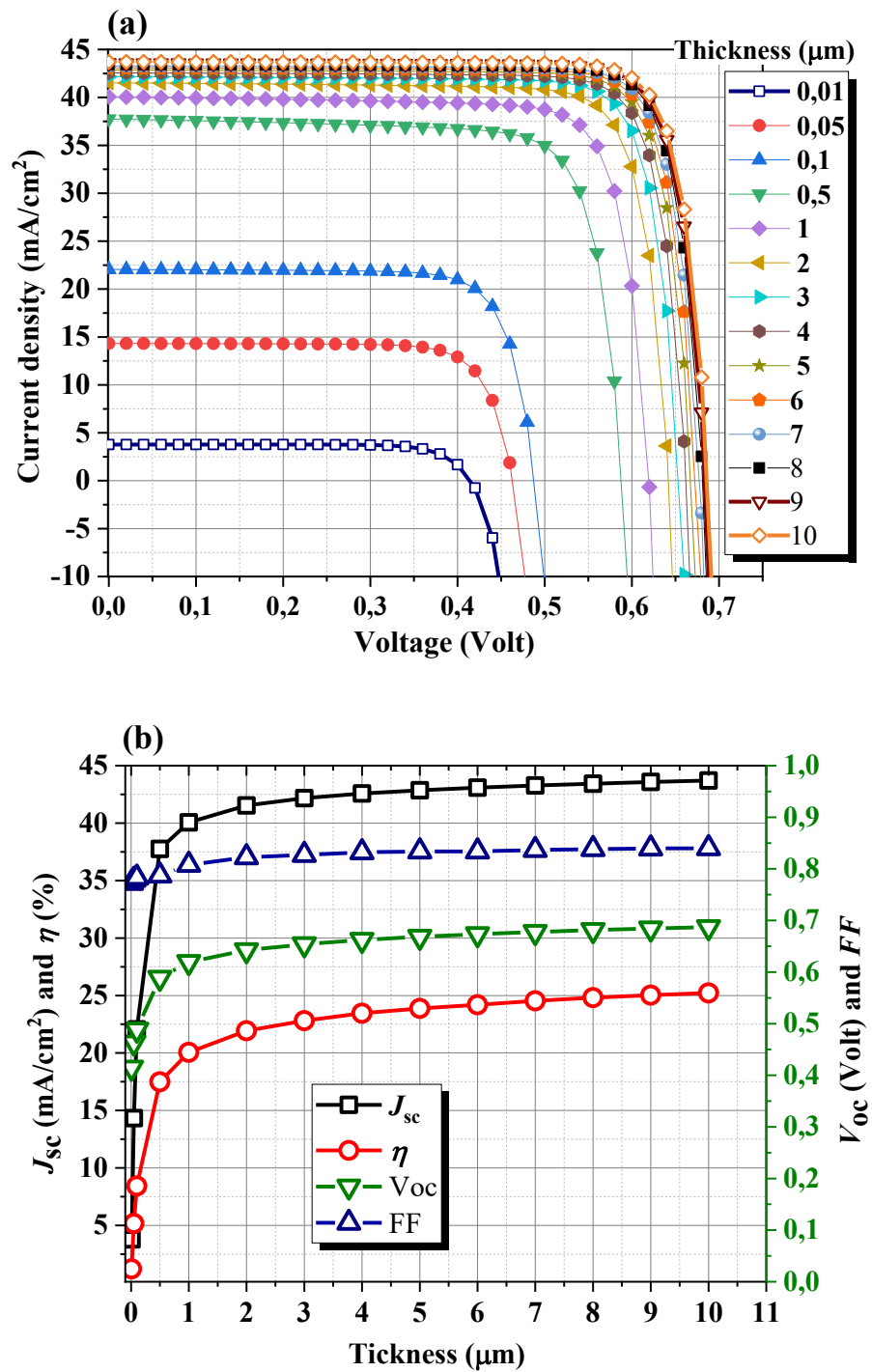


**Figure III.17:** Variation effect of the p-type CIGS layer thickness on : (a)  $(J - V)$  characteristics and (b) the photovoltaic output parameters of the Schottky barrier solar cell .

**Table III.3:** Variation effect of the p-type CIGS layer thickness on the photovoltaic output parameters of the Schottky barrier solar cell .

Thickness ( $\mu\text{m}$ )	$J_{sc}(\text{mA}/\text{cm}^2)$	$V_{oc}(V)$	$FF$	$\eta(\%)$
0,01	3,78002	0,41484	0,7726	1,2115
0,05	14,32666	0,4635	0,77855	5,1699
0,1	22,04841	0,48851	0,78278	8,4311
0,5	37,74838	0,58878	0,78704	17,4924
1	40,06296	0,6195	0,80785	20,05
2	41,52976	0,64223	0,82246	21,9365
3	42,17359	0,654	0,82685	22,806
4	42,56989	0,66245	0,83197	23,462
5	42,85512	0,66834	0,83363	23,8767
6	43,07992	0,67336	0,83381	24,1877
7	43,2677	0,6778	0,83666	24,5368
8	43,4309	0,68145	0,83829	24,8102
9	43,57676	0,68434	0,83943	25,0332
10	43,70994	0,68697	0,83993	25,2208

We can notice that increasing the thickness of the p-type CIGS layer has a positive effect on the photovoltaic output parameters of the cell despite the increase in the recombination rate distribution along the p-type CIGS layer as shown previously in Figure III.14.

On one hand, increasing the thickness of the p-type CIGS layer can improve light absorption within the semiconductor material. A thicker layer allows for a greater path length for incident photons, increasing the probability of photon absorption and generation of electron-hole pairs. This can result in a higher short-circuit current density ( $J_{sc}$ ) and an overall increase in the

photocurrent. However, increasing the thickness of the p-type CIGS layer can also lead to an increase in the recombination rate distribution along the layer (Figure III.14). This is due to the longer distance that the charge carriers have to travel before reaching the contacts, providing more opportunities for recombination. The net effect of the increased recombination rate distribution and improved light absorption depends on the specific characteristics of the solar cell and the compromise involved. In some cases, the positive impact of enhanced light absorption may outweigh the negative impact of increased recombination, leading to an overall improvement in the photovoltaic output parameters, which is fortunately satisfied as shown on Figure III.17 and Table III.3. However, if the recombination losses dominate, the overall performance of the solar cell may still be negatively affected despite the thicker p-type CIGS layer. Usually, to optimize the photovoltaic output parameters, it is important to find a balance between light absorption and recombination losses such as optimizing the layer thickness.

Figure III.18 shows the variation effect of the p-type CIGS layer doping concentration ( $N_A$ ) on : (a) ( $J - V$ ) characteristics and (b) the photovoltaic output parameters of the Schottky barrier solar cell ( which are also presented in Table III.4). Increasing the doping concentration of the p-type CIGS layer in a Schottky barrier solar cell can have several effects on the photovoltaic output parameters. Regarding the open circuit voltage ( $V_{oc}$ ); this latter is increased with increasing the doping concentration of the p-type CIGS layer. This is because higher doping levels can reduce the recombination rate at the interfaces (as shown on Figure III.15), allowing for a more efficient separation of photogenerated carriers. A higher  $V_{oc}$  corresponds to an increased potential difference between the terminals of the solar cell when no current is flowing. The fill factor ( $FF$ ) shows also an increase with increasing the doping concentration. The fill factor is a measure of how effectively the solar cell utilizes the available voltage and current. Higher doping levels can improve the charge carrier transport properties, reducing resistive losses and improving the  $FF$ . However, increasing the doping concentration of the p-type CIGS layer has, initially, not affected the short circuit current density ( $J_{sc}$ ). But, once the doping concentration reaches a certain threshold, typically around ( $10^{15} \text{ cm}^{-3}$ ), the short circuit current density starts to decrease. The short circuit current density ( $J_{sc}$ ) is primarily determined by the absorption of incident photons and the efficient collection of photo-generated carriers. Some works reported that higher doping concentration can leads to a decrease in short circuit current density  $J_{sc}$  due to the decrease in the minority carrier diffusion length [30].

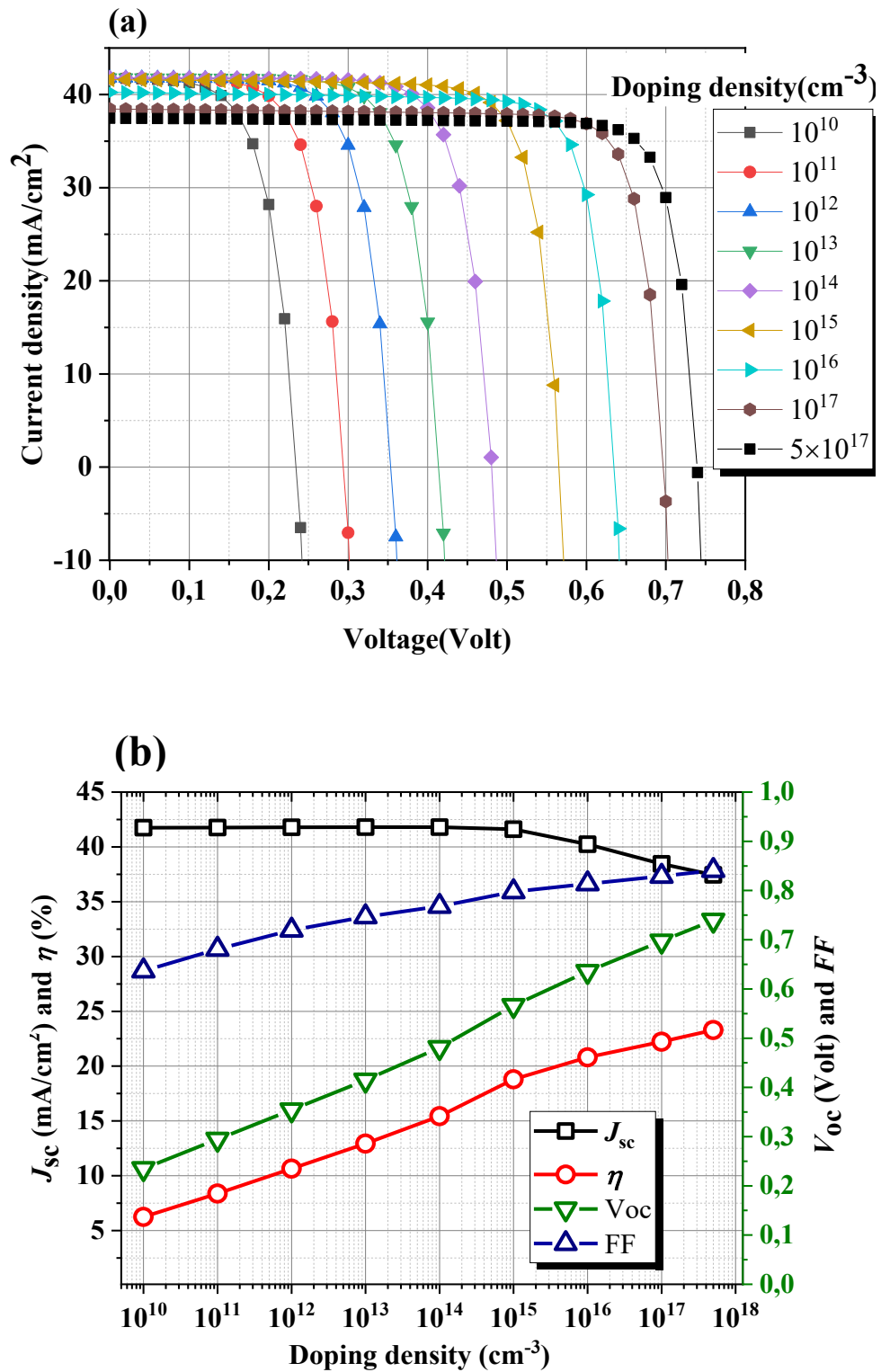


**Figure III.18:** Variation effect of the p-type CIGS layer doping concentration on : (a)  $(J - V)$  characteristics and (b) the photovoltaic output parameters of the Schottky barrier solar cell .

**Table III.4:** Variation effect of the p-type CIGS layer doping concentration on the photovoltaic output parameters of the Schottky barrier solar cell .

Doping concentration $N_A(cm^{-3})$	$J_{sc}(mA/cm^2)$	$V_{oc}(V)$	$FF$	$\eta(\%)$
$10^{10}$	41,74824	0,23505	0,63681	6,2489
$10^{11}$	41,76927	0,29468	0,68069	8,3782
$10^{12}$	41,78457	0,35437	0,7194	10,6522
$10^{13}$	41,79541	0,41463	0,74668	12,9397
$10^{14}$	41,79556	0,48079	0,76793	15,4314
$10^{15}$	41,60686	0,56638	0,79753	18,794
$10^{16}$	40,23901	0,63552	0,81365	20,8072
$10^{17}$	38,44502	0,69731	0,82902	22,2242
$5 \times 10^{17}$	37,45063	0,73954	0,84085	23,2883

Higher doping concentrations can also affect the absorption characteristics of the material. Indeed, Figure III.19 shows the optical generation rate distribution along the Schottky barrier solar cell with the increase of the doping concentration ( $N_A$ ) within the range [ $10^{10} - 5 \times 10^{17} cm^{-3}$ ]. Increasing the doping concentration in the p-type CIGS layer leads to the observed increase in the optical generation rate along the first half of the p-type CIGS layer, which is closer to the front side illuminated. We believe that this behavior contributes to the open circuit voltage ( $V_{oc}$ ) increase. When the doping levels are increased, more charge carriers (electrons and holes) are available in the material. This results in an increased generation of electron-hole pairs when the material absorbs light. The higher optical generation rate along the front side of the p-type CIGS layer means that more electron-hole pairs are generated in this region. Consequently, a higher number of charge carriers are available for separation, contributing to an improvement in the open circuit voltage.

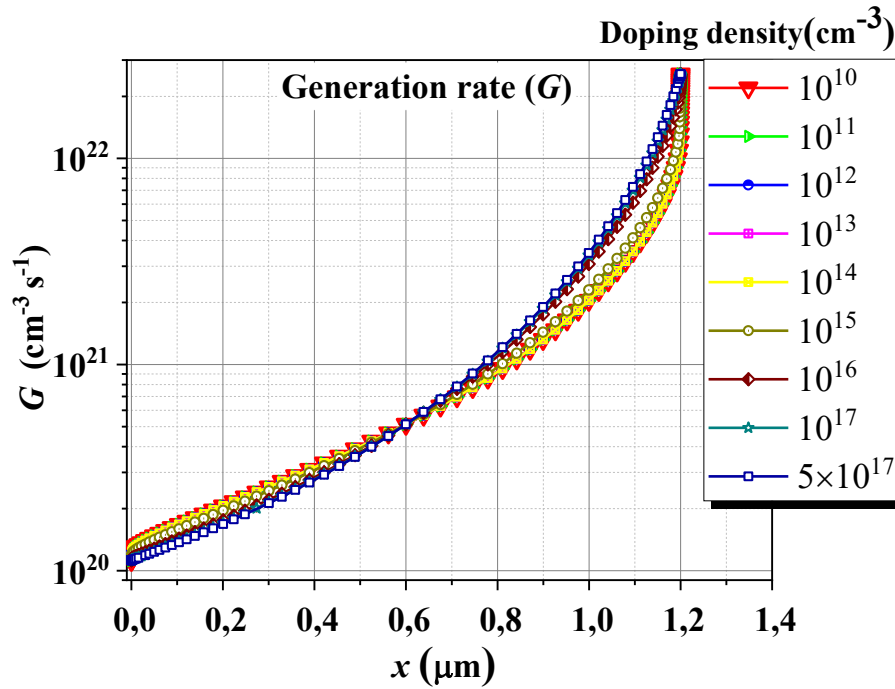


**Figure III.19:** Optical generation rate distribution along the Schottky barrier solar cell with the increase of the doping concentration ( $N_A$ ) within the range  $[10^{10} - 5 \times 10^{17} \text{ cm}^{-3}]$ .

Concerning the short circuit current density ( $J_{sc}$ ), as we mentioned previously, it does not show, initially, a sensitivity to the increase in doping levels until the concentration reaches around ( $10^{15} \text{ cm}^{-3}$ ). Beyond this value, the short circuit current density starts to decrease. This decrease can be attributed to the observed decrease in the optical generation rate along the second half of the p-type CIGS layer, which is closer to the back side of the solar cell. This means that fewer electron-hole pairs are generated and available for separation near the back side of the p-type CIGS layer. Consequently, there is a reduction in the number of charge carriers contributing to the short circuit current, leading to a decrease in the short circuit current density.

Overall, the increase in doping concentration affects the optical generation rate distribution along the p-type CIGS layer. In the front side, the increase of the optical generation rate contributes to the improvement in open circuit voltage, while, in the back side, the decrease of the optical generation rate leads to the reduction in short circuit current density beyond a certain doping concentration. These effects highlight the complex interplay between doping levels, optical generation rate, and the performance characteristics of the Schottky barrier solar cell based on Al/p-type CIGS material.

Regarding the distribution of the recombination rate (Figure III.15), increasing the doping concentration does not have a significant impact on the recombination rate in the bulk of the p-type CIGS layer. Then, the recombination processes in this region are mainly governed by other factors such as material quality, defects, and impurities present in the bulk material. However, the recombination rate at the front interface between the aluminum (Al) and p-type CIGS layer, as well as at the back interface of the p-type CIGS layer, decreases with increasing doping concentration. This decrease is beneficial as it indicates a reduction in recombination losses at the interfaces, improving the overall efficiency of the solar cell. It indicates also that it is not the cause of the short circuit current density reduction. This latter can be considered as a slight reduction since it does not alter the further improvement in  $V_{oc}$ ,  $FF$  and then in the power conversion efficiency ( $\eta$ ) with further increase of the doping concentration ( $N_A$ ) beyond the value of  $10^{15} \text{ cm}^{-3}$ .

For the ideal case when series and shunt resistances are neglected, we remind that:

$$V_{oc} \cong \frac{Ak_B T}{q} \ln \left( \frac{J_{sc}}{J_0} + 1 \right) \quad \text{Eq.III.10}$$

It is clear that open circuit voltage ( $V_{oc}$ ) depends on  $J_0$  (the saturation current density) and on  $J_{sc}$ , (the short circuit current density).  $J_0$  may be limited by diffusion, recombination or thermionic emission [31]. So,  $V_{oc}$  is a measure of the amount of the dominant mechanism in the solar cell (diffusion, recombination or thermionic emission).

Usually for the Schottky barrier solar cell,  $V_{oc}$  is dependent on the Schottky barrier height ( $\phi_B$ ) through the reverse bias saturation current density  $J_0$  which is limited by thermionic emission:

$$J_0 = A^* T^2 \exp\left(-\frac{\phi_B}{k_B T}\right) \quad \text{Eq.III.11}$$

Where  $A^*$  is the effective Richardson constant for the semiconductor. But we can see from Figure III.18 and Table III.4 that an increase in doping levels results in larger open circuit voltage. This means that  $V_{oc}$  is noticeably dependent on the doping levels; and this can occur only if the Schottky barrier solar cell behaves as an ideal  $n^+ - p$  junction diode in the voltage range of solar cell operation [30]. In an ideal  $n^+ - p$  junction diode, the  $V_{oc}$  is primarily determined by the difference in Fermi levels between the n-type and p-type regions. Higher doping levels can create a larger built-in potential across the junction, resulting in a higher  $V_{oc}$ . In the case of a Schottky barrier solar cell based on (Al/p-type CIGS material), the choice of aluminum (Al) as the cathode metal helps to establish a high Schottky barrier height ( $\phi_{bp} = 1.85 \text{ eV}$ ) at the Al/CIGS interface (see Eq.III.9). This high barrier height contributes to the formation of an

effective  $n^+$ -p junction-like behaviour. With a high Schottky barrier height, the Schottky barrier solar cell can exhibit characteristics similar to a minority carrier-dominated diode. This means that in the absence of illumination (dark conditions), the dark current can approach the ideal value with a saturation current density ( $J_0$ ) limited by diffusion. In other words, the dark current is primarily governed by the diffusion of minority carriers across the junction rather than recombination processes.

The behaviour of a minority carrier-dominated diode with a high Schottky barrier height allows for a higher  $V_{oc}$  and better performance in terms of open circuit voltage.

With the doping density increase, the saturation current density  $J_0$  will decrease according to Eq.III.12 and hence  $V_{oc}$  increases according to Eq.III.10.

$$J_0 = qn_i^2 \left( \frac{1}{N_A} \sqrt{\frac{D_n}{\tau_n}} + \frac{1}{N_D} \sqrt{\frac{D_p}{\tau_p}} \right) \cong qn_i^2 \left( \frac{1}{N_A} \sqrt{\frac{D_n}{\tau_n}} \right) \quad \text{Eq.III.12}$$

Where  $n_i$  is the intrinsic density ( $cm^{-3}$ ),  $D_n$  and  $D_p$  are the diffusion coefficients ( $cm^2s^{-1}$ ) of electrons and holes respectively.

The limiting open circuit voltages reached in such a structure are those of an ideal  $n^+$ -p junctions and their characteristics are determined solely by the p-type CIGS layer properties and do not depend critically on the barrier height ( $\phi_{bp}$ ) at the (Al/ p-type CIGS layer) interface. In other words, the dominant current is governed by the transport properties in the p-type CIGS layer via drift-diffusion of minority carriers.

Now we explore in Figure III.20 the behaviour of : (a) ( $J - V$ ) characteristics and (b) the photovoltaic output parameters of the Schottky barrier solar cell with changing the cathode work function ( $\phi_m$ ) within the range [4.1 – 4.7 eV]. For that purpose, we will consider different cathode metals, including Al, Ta, Ti, Zn, Mo, W, and Cu, respectively. [32]

The ( $J - V$ ) characteristics and the photovoltaic output parameters of the Schottky barrier solar cell show no dependency on the cathode work function ( $\phi_m$ ) change within the range [4.1 – 4.7 eV]. This can be attributed to the high barrier height ( $\phi_{bp}$ ) established at the metal/p-type CIGS interface. Following the equation for ( $\phi_{bp}$ ):

$$\phi_{bp} = (\chi_{sc} + E_g) - \phi_m \quad \text{Eq.III.13}$$

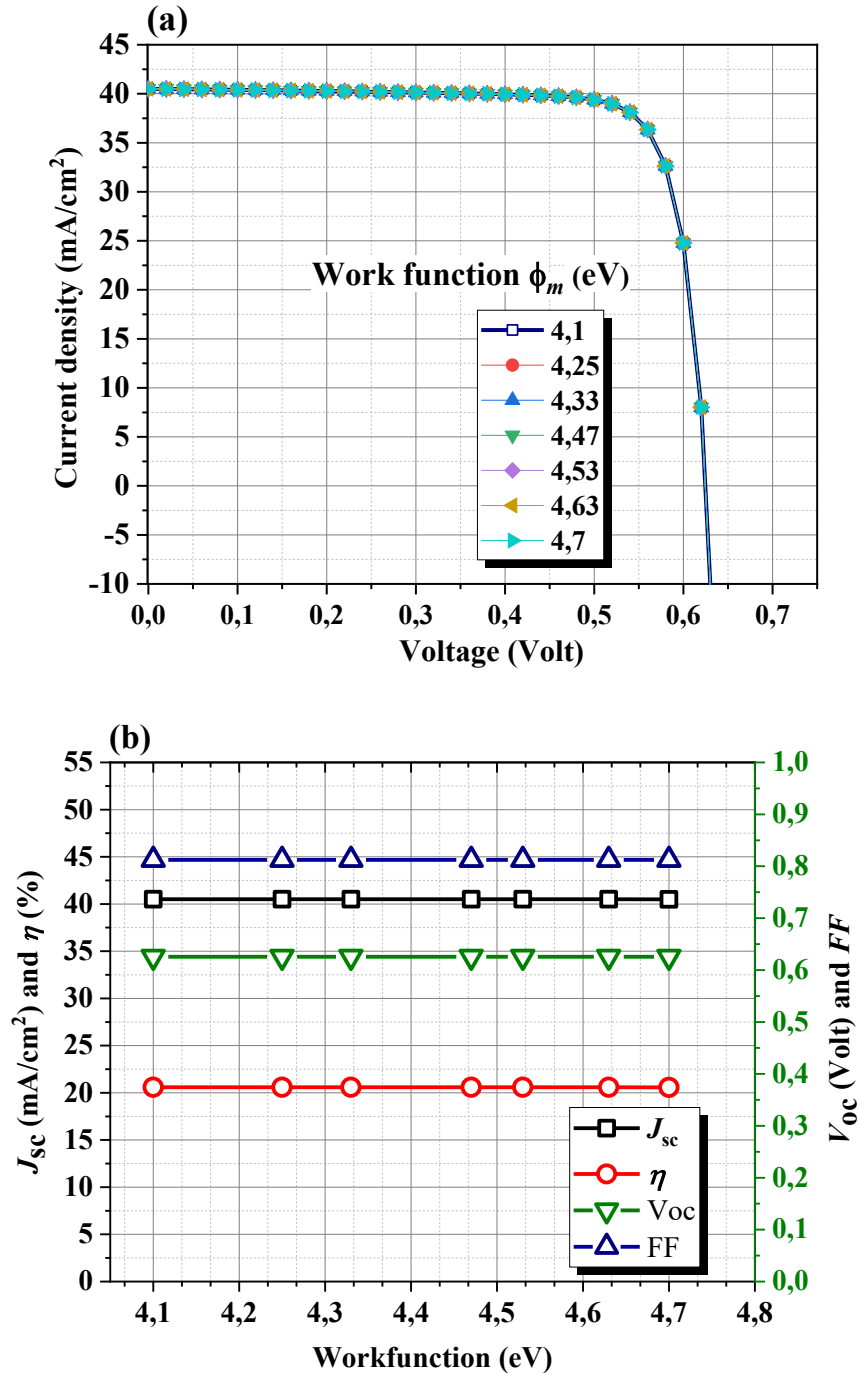


**Figure III.20:** Behaviour of : (a) ( $J - V$ ) characteristics and (b) the photovoltaic output parameters of the Schottky barrier solar cell with changing the cathode work function ( $\phi_m$ ) within the range [4.1 – 4.7 eV].

The high barrier height ( $\phi_{bp}$ ) is limited, to a significant extent, by the bandgap energy ( $E_g$ ) and the semiconductor electron affinity ( $\chi_{sc}$ ), particularly when ( $\phi_m$ ) is lower than ( $\chi_{sc}$ ). This means that the Schottky barrier height ( $\phi_{bp}$ ) is primarily governed by the intrinsic properties of the p-type CIGS material rather than the cathode work function ( $\phi_m$ ) in this range. As a result, when

the cathode work function ( $\phi_m$ ) falls within the specified range, the ( $J - V$ ) characteristics and the photovoltaic output parameters of the solar cell are not significantly influenced by changes in ( $\phi_m$ ). This is because the dominant factor determining the barrier height, ( $\phi_{bp}$ ), is related to the bandgap energy and the semiconductor electron affinity of the p-type CIGS material.

### III.6. Conclusion

We have investigated the Schottky barrier solar cell based on p-type Cu(In,Ga)Se<sub>2</sub> (CIGS) material, exposed to the AM1.5 G standard spectrum at ambient temperature (300°K). The cathode metal, which serves as the front contact of the cell, is Aluminum (Al) with a work function ( $\phi_m$ ) of 4.1 eV, lower than the electron affinity of the p-type CIGS material ( $\chi_{sc} = 4.8$  eV). This configuration forms a Schottky barrier for holes at the (Al/p-type CIGS) interface. The purpose of using a Schottky contact at the front contact is to create a barrier that allows selective carrier collection. In this case, the lower work function of Aluminum compared to the electron affinity of CIGS leads to a barrier for holes, allowing efficient collection of photogenerated electrons while blocking the flow of holes from the p-type CIGS layer to the front contact. On the other hand, the left (back) contact, which acts as the anode, is defined to be neutral and forms an Ohmic contact. The Ohmic contact allows both electrons and holes to pass through easily without any significant barrier. This condition ensures efficient carrier transport without hindrance. To conduct the investigation, we have utilized the numerical simulation software Scaps-1D. This software allowed us to perform steady-state calculations of various internal parameters of the solar cell, including the band diagram, electron and hole concentrations, and recombination rate. Additionally, it enables the calculation of external parameters such as current density-voltage ( $J - V$ ) and power-voltage ( $P - V$ ) characteristics. These calculations allowed us to extract important photovoltaic output parameters, namely the short circuit current density ( $J_{sc}$ ), the open circuit voltage ( $V_{oc}$ ), the fill factor ( $FF$ ), the maximum power ( $P_{max}$ ) provided by the cell and the photovoltaic conversion efficiency ( $\eta$ ).

Our investigation has focused on varying the parameters of the CIGS absorber layer, specifically the defect density ( $N_t$ ) within the range [ $10^{10} - 10^{20} \text{ cm}^{-3}$ ], the thickness ( $d$ ) within the range [0.01-10 $\mu\text{m}$ ], and the doping concentration ( $N_A$ ) within the range [ $10^{10} - 5 \times 10^{17} \text{ cm}^{-3}$ ].

The increase of the defect density in the p-type CIGS layer leads to an increase in the recombination rate distribution along the layer. However, it displays, initially, little impact on the photovoltaic output parameters of the cell. But, when the defect density exceeds  $10^{15} \text{ cm}^{-3}$ ,

negative effects start to emerge, leading to a decrease in the fill factor ( $FF$ ), open circuit voltage ( $V_{oc}$ ), and eventually the short circuit current density ( $J_{sc}$ ), resulting in a reduction in conversion efficiency ( $\eta$ ).

Increasing the thickness of the p-type CIGS layer has a positive effect on the photovoltaic output parameters of the cell despite the increase in the recombination rate distribution along the p-type CIGS layer. Increasing the thickness of the p-type CIGS layer improves the light absorption within the semiconductor material and the positive impact of enhanced light absorption has outweighed the negative impact of increased recombination, leading to an overall improvement in the photovoltaic output parameters.

Increasing the doping concentration of the p-type CIGS layer has several effects on the photovoltaic output parameters of the Schottky barrier solar cell. Regarding the open circuit voltage ( $V_{oc}$ ); this latter is increased with increasing the doping levels. The fill factor ( $FF$ ) shows also an increase with increasing the doping concentration. However, the short circuit current density ( $J_{sc}$ ), initially, is not affected by the doping concentration increase, but once the doping concentration reaches a certain threshold, typically around ( $10^{15} \text{ cm}^{-3}$ ), the short circuit current density starts to decrease. This fact can be considered as a slight reduction since it does not alter the further improvement in  $V_{oc}$ ,  $FF$  and then in the power conversion efficiency ( $\eta$ ) with further increase of the doping concentration ( $N_A$ ) beyond the value of  $10^{15} \text{ cm}^{-3}$ . The recombination rate distribution showed, at its turn, a decrease at the front and back interfaces with increasing doping concentration. This decrease is beneficial as it indicates a reduction in recombination losses at the interfaces, improving the overall efficiency of the solar cell.

By exploring the behaviour of ( $J - V$ ) characteristics and the photovoltaic output parameters of the Schottky barrier solar cell with changing the cathode work function ( $\phi_m$ ) within the range [4.1 – 4.7 eV], we have noticed that these latter show no dependency on the cathode work function ( $\phi_m$ ) change within the previous range. This can be attributed to the high barrier height ( $\phi_{bp}$ ) established at the metal/p-type CIGS interface, and because the dominant factor determining the barrier height, ( $\phi_{bp}$ ), is related to the bandgap energy and the semiconductor electron affinity of the p-type CIGS material, rather than the cathode work function ( $\phi_m$ ) in this range [4.1 – 4.7 eV].

In summary, the better photovoltaic conversion efficiency ( $\eta$ ) reached from increasing the doping concentration of the p-type CIGS layer is 23.28 %. Increasing the thickness of the p-type

CIGS layer allowed us to improve ( $\eta$ ) to 25.22 % . However, to avoid a significant degradation and to maintain better photovoltaic output parameters, it is advisable to limit the p-type CIGS layer defect density to a value not exceeding  $10^{15}cm^{-3}$ . This suggests that minimizing defects and optimizing the material quality during the fabrication process is crucial for achieving higher efficiency and performance in Schottky barrier solar cells based on Al/p-type CIGS material.

## References

- [1] A. Laoufi, D. Benmoussa, K. Oussama, and F. Mustafa, 'Numerical modeling of multi-junction solar cell-based CIGS with two sub-cells in parallel using silvaco TCAD', *Chalcogenide Letters*, vol. 18, pp. 297–301, Jun. 2021.
- [2] R. Prasad, A. K. Das, and U. P. Singh, 'Bilayer CIGS-based solar cell device for enhanced performance: a numerical approach', *Appl. Phys. A*, vol. 127, no. 2, p. 140, Jan. 2021, doi: 10.1007/s00339-021-04298-y.
- [3] T. Alzoubi and M. Moustafa, 'Simulation analysis of functional MoSe 2 layer for ultra-thin Cu(In,Ga)Se 2 solar cells architecture', *Mod. Phys. Lett. B*, vol. 34, no. 05, p. 2050065, Feb. 2020, doi: 10.1142/S0217984920500657.
- [4] M. Abdelfatah, W. Ismail, N. M. El-Shafai, and A. El-Shaer, 'Effect of thickness, bandgap, and carrier concentration on the basic parameters of Cu<sub>2</sub>O nanostructures photovoltaics: numerical simulation study', *Materials Technology*, vol. 36, no. 12, pp. 712–720, Oct. 2021, doi: 10.1080/10667857.2020.1793092.
- [5] M. A. Shafi et al., 'A Numerical Simulation for Efficiency Enhancement of CZTS Based Thin Film Solar Cell Using SCAPS-1D', *East European Journal of Physics*, no. 2, Art. no. 2, Jun. 2022, doi: 10.26565/2312-4334-2022-2-06.
- [6] M. Burgelman, K. Decock, S. Khelifi, and A. Abass, 'Advanced electrical simulation of thin film solar cells', *Thin Solid Films*, vol. 535, pp. 296–301, May 2013, doi: 10.1016/j.tsf.2012.10.032.
- [7] M. Moustafa, T. Al Zoubi, and S. Yasin, 'Optoelectronics Simulation of CIGS-Based Solar Cells Using a Cd-Free Nontoxic ZrS<sub>x</sub>Se<sub>2-x</sub> as a Novel Buffer Layer', *Braz J Phys*, vol. 52, no. 4, p. 141, Jun. 2022, doi: 10.1007/s13538-022-01146-z.
- [8] M. Moustafa and T. AlZoubi, 'Effect of the n-MoTe<sub>2</sub> interfacial layer in cadmium telluride solar cells using SCAPS', *Optik*, vol. 170, pp. 101–105, Oct. 2018, doi: 10.1016/j.ijleo.2018.05.112.
- [9] M. I. Hossain et al., 'E-beam evaporated hydrophobic metal oxide thin films as carrier transport materials for large scale perovskite solar cells', *Materials Technology*, vol. 37, no. 4, pp. 248–259, Mar. 2022, doi: 10.1080/10667857.2020.1830551.

- [10] T. AlZoubi, A. Moghrabi, M. Moustafa, and S. Yasin, 'Efficiency boost of CZTS solar cells based on double-absorber architecture: Device modeling and analysis', *Solar Energy*, vol. 225, pp. 44–52, Sep. 2021, doi: 10.1016/j.solener.2021.07.012.
- [11] M. Moustafa, T. AlZoubi, and S. Yasin, 'Towards high-efficiency CZTS solar cells via p-MoS<sub>2</sub> interfacial layer optimisation', *Materials Technology*, vol. 37, no. 10, pp. 1563–1572, Aug. 2022, doi: 10.1080/10667857.2021.1964214.
- [12] M. Mostefaoui, H. Mazari, S. Khelifi, A. Bouraiou, and R. Dabou, 'Simulation of High Efficiency CIGS Solar Cells with SCAPS-1D Software', *Energy Procedia*, vol. 74, pp. 736–744, Aug. 2015, doi: 10.1016/j.egypro.2015.07.809.
- [13] Marc Burgelman, Koen Decock, Alex Niemegeers, Johan Verschraegen, Stefaan Degraeve, SCAPS manual, Version: 26-11-2021, University of Gent, 'Belgium'.
- [14] K.-J. Hsiao, J.-D. Liu, H.-H. Hsieh, and T.-S. Jiang, 'Electrical impact of MoSe<sub>2</sub> on CIGS thin-film solar cells', *Phys. Chem. Chem. Phys.*, vol. 15, no. 41, pp. 18174–18178, Oct. 2013, doi: 10.1039/C3CP53310G.
- [15] B. Theys et al., 'Revisiting Schottky barriers for CIGS solar cells: Electrical characterization of the Al/Cu(InGa)Se<sub>2</sub> contact', *physica status solidi (a)*, vol. 213, no. 9, pp. 2425–2430, 2016, doi: 10.1002/pssa.201533063.
- [16] K. Chowdhury and R. Mandal, 'Advancement of schottky barrier solar cells: a review', in *contemporary issues in computing*, volkson press, Jan. 2020, pp. 93–98. doi: 10.26480/cic.01.2020.93.98.
- [17] M. Gloeckler, A. L. Fahrenbruch, and J. R. Sites, 'Numerical modeling of CIGS and CdTe solar cells: setting the baseline', in *Proceedings of 3rd World Conference on Photovoltaic Energy Conversion*, 2003, May 2003, pp. 491-494 Vol.1.
- [18] N. Khoshsirat, N. A. Md Yunus, M. N. Hamidon, S. Shafie, and N. Amin, 'Analysis of absorber layer properties effect on CIGS solar cell performance using SCAPS', *Optik*, vol. 126, no. 7, pp. 681–686, Apr. 2015, doi: 10.1016/j.ijleo.2015.02.037.
- [19] U. Rau, S. Siebentritt, *Wide-Gap Chalcopyrites*, Springer, 2006

- [20] M. Burgelman and J. Marlein, 'Analysis of Graded Band Gap Solar Cells With SCAPS', in 23rd European Photovoltaic Solar Energy Conference and Exhibition, WIP-Munich, 2008, p. 5 pages, 2185 kb. doi: 10.4229/23RDEUPVSEC2008-3DO.5.2.
- [21] A. Mouhoub, A. Bouloufa, K. Djessas, and A. Messous, 'Analytical modeling and optimization of original bifacial solar cells based on Cu(In,Ga)Se<sub>2</sub> thin films absorbers', *Superlattices and Microstructures*, vol. 122, pp. 434–443, Oct. 2018, doi: 10.1016/j.spmi.2018.06.068.
- [22] M. Gloeckler and J. R. Sites, 'Potential of submicrometer thickness Cu(In,Ga)Se<sub>2</sub> solar cells', *Journal of Applied Physics*, vol. 98, no. 10, p. 103703, Nov. 2005, doi: 10.1063/1.2128054.
- [23] Simulation of Heterojunction Solar Cells with AFORS-HET. [http://shodhganga.inflibnet.ac.in/bitstream/10603/42510/8/09\\_chapter%204.pdf](http://shodhganga.inflibnet.ac.in/bitstream/10603/42510/8/09_chapter%204.pdf)
- [24] A. Sylla, S. Touré, and J.-P. Vilcot, 'Numerical Modeling and Simulation of CIGS-Based Solar Cells with ZnS Buffer Layer', in *Open Journal of Modelling and Simulation*, 2017, pp. 218–231. doi: 10.4236/ojmsi.2017.54016.
- [25] W. Liu, H. Li, B. Qiao, S. Zhao, Z. Xu, and D. Song, 'Highly efficient CIGS solar cells based on a new CIGS bandgap gradient design characterized by numerical simulation', *Solar Energy*, vol. 233, pp. 337–344, Feb. 2022, doi: 10.1016/j.solener.2022.01.054.
- [26] S. R. Fatemi Shariat Panahi, A. Abbasi, V. Ghods, and M. Amirahmadi, 'Analysis and improvement of CIGS solar cell efficiency using multiple absorber substances simultaneously', *J Mater Sci: Mater Electron*, vol. 31, no. 14, pp. 11527–11537, Jul. 2020, doi: 10.1007/s10854-020-03700-4.
- [27] P. M. P. Salomé et al., 'Passivation of Interfaces in Thin Film Solar Cells: Understanding the Effects of a Nanostructured Rear Point Contact Layer', *Advanced Materials Interfaces*, vol. 5, no. 2, p. 1701101, 2018, doi: 10.1002/admi.201701101.
- [28] W. Li, W. Li, Y. Feng, and C. Yang, 'Numerical analysis of the back interface for high efficiency wide band gap chalcopyrite solar cells', *Solar Energy*, vol. 180, pp. 207–215, Mar. 2019, doi: 10.1016/j.solener.2019.01.018.

[29] N. E. I. Boukortt, S. Patanè, B. Hadri, and G. Crupi, ‘Graded Bandgap Ultrathin CIGS Solar Cells (Invited Paper)’, *Electronics*, vol. 12, no. 393, p. 393, Jan. 2023, doi: 10.3390/electronics12020393.

[30] J. Shewchun, R. Singh, and M. A. Green, ‘Theory of metal-insulator-semiconductor solar cells’, *Journal of Applied Physics*, vol. 48, no. 2, pp. 765–770, Aug. 2008, doi: 10.1063/1.323667.

[31] O. M. Nielsen, ‘Current mechanism of tunnel m.i.s. solar cells’, in *IEE Proceedings I Solid State and Electron Devices*, 1980, p. 301. doi: 10.1049/ip-i-1.1980.0059.

[32] B. Ofuonye, J. Lee, M. Yan, C. Sun, J.-M. Zuo, and I. Adesida, ‘Electrical and microstructural properties of thermally annealed Ni/Au and Ni/Pt/Au Schottky contacts on AlGaN/GaN heterostructures’, *Semiconductor Science and Technology*, vol. 29, no. 9, Sep. 2014, doi: 10.1088/0268-1242/29/9/095005.

# **General conclusion**

## General conclusion

We have investigated the Schottky barrier solar cell based on p-type Cu(In,Ga)Se<sub>2</sub> (CIGS) material, exposed to the AM1.5 G standard spectrum at ambient temperature (300°K). The solar cell consists of a p-type CIGS absorber layer with a front contact of Aluminum (Al) as cathode metal, and a back contact that acts as the anode. The work function ( $\phi_m$ ) of the cathode is 4.1 eV, lower than the electron affinity of the p-type CIGS material ( $\chi_{sc} = 4.8 \text{ eV}$ ). Consequently, the Al/p-type CIGS interface forms a Schottky barrier which blocks the flow of holes from the p-type CIGS layer toward the cathode; while enabling efficient collection of photogenerated electrons. The back contact forms an Ohmic contact, allowing easy passage of both electrons and holes for efficient carrier transport. In this investigation, we utilized the Scaps-1D numerical simulation software for steady-state calculations. Internal parameters such as band diagram, electron and hole concentrations, and recombination rate were evaluated. External parameters such as current density-voltage ( $J - V$ ) and power-voltage ( $P - V$ ) characteristics were calculated. Photovoltaic output parameters, including short circuit current density ( $J_{sc}$ ), open circuit voltage ( $V_{oc}$ ), fill factor ( $FF$ ), maximum power ( $P_{max}$ ), and photovoltaic conversion efficiency ( $\eta$ ), were extracted. The investigation focused on varying parameters of the p-type CIGS absorber layer: defect density ( $N_t$ ) within the range [ $10^{10} - 10^{20} \text{ cm}^{-3}$ ], the thickness ( $d$ ) within the range [0.01-10 $\mu\text{m}$ ], and the doping concentration ( $N_A$ ) within the range [ $10^{10} - 5 \times 10^{17} \text{ cm}^{-3}$ ].

Increasing the defect density in the p-type CIGS layer leads to an increase in recombination rates. Initially, the photovoltaic output parameters are not significantly affected. However, when the defect density exceeds  $10^{15} \text{ cm}^{-3}$ , negative effects start to emerge. High defect density results in a decrease in fill factor ( $FF$ ), open circuit voltage ( $V_{oc}$ ), short circuit current density ( $J_{sc}$ ), and conversion efficiency ( $\eta$ ). Minimizing defects and optimizing material quality during fabrication is crucial for achieving higher efficiency.

Increasing the thickness of the p-type CIGS layer has a positive effect on photovoltaic output parameters. Despite increased recombination rates, the enhanced light absorption outweighs the negative impact. Improved light absorption leads to better performance in terms of  $J_{sc}$ ,  $V_{oc}$ ,  $FF$ , and  $\eta$ .

Increasing the doping concentration of the p-type CIGS layer has several effects on photovoltaic output parameters. Open circuit voltage ( $V_{oc}$ ) increases with higher doping levels. Fill factor ( $FF$ ) also increases with increasing doping concentration. Short circuit current density ( $J_{sc}$ ) remains unaffected initially but starts to decrease once the doping concentration exceeds a certain threshold (around  $10^{15} cm^{-3}$ ). Recombination rate decreases at the front and back interfaces with increasing doping concentration, reducing recombination losses and improving overall efficiency.

The photovoltaic output parameters and ( $J - V$ ) characteristics show no dependency on the cathode work function ( $\phi_m$ ) in the range of 4.1-4.7 eV. This can be attributed to the high barrier height ( $\phi_{bp}$ ) established at the metal/p-type CIGS interface, and because the dominant factor determining the barrier height, ( $\phi_{bp}$ ), is related to the bandgap energy ( $E_g$ ) and the semiconductor electron affinity ( $\chi_{sc}$ ) of the p-type CIGS material, rather than the cathode work function ( $\phi_m$ ) within the range [4.1 – 4.7 eV].

In terms of achieving the highest photovoltaic conversion efficiency ( $\eta$ ), increasing the doping concentration of the p-type CIGS layer yielded 23.28%. Increasing the thickness of the p-type CIGS layer further improved efficiency to 25.22%. However, it is advisable to limit the defect density to avoid degradation, with a recommended value not exceeding  $10^{15} cm^{-3}$ . Minimizing defects and optimizing material quality during fabrication are crucial for achieving better efficiency and performance in Schottky barrier solar cells based on Al/p-type CIGS material.

قمنا بدراسة خلية شمسية ذات حاجز شوتكي بناء على مادة (Cu(In,Ga)Se<sub>2</sub>:CIGS) مطعمة من نوع P ، باستخدام برنامج المحاكاة الرقمية Scaps-1D و باعتبار النظام المستقر لحساب كل من الوسائط الداخلية المتمثلة في مخطط الطاقة ، تراكيز الإلكترونات و الثقوب و معدل الالتحام و الوسائط الخارجية المتمثلة في الخصائص كثافة تيار - جهد (J - V) و الخصائص إستطاعة - جهد (P - V) و من ثم استخلاص وسائط الخروج الفوطوفولطائية للخلية و المتمثلة في كثافة تيار الدارة القصيرة (J<sub>sc</sub>) ، جهد الدارة المفتوحة (V<sub>oc</sub>) ، معامل التعبئة (FF) ، الإستطاعة الكهربائية الأعظمية الممنوحة من طرف الخلية (P<sub>max</sub>) ومردود التحويل الفوطوفولطائي (η). ركزنا في الدراسة على تأثير تغيير كل من كثافة العيوب (N<sub>t</sub>) ، السمك (d) و تركيز التطعيم (N<sub>A</sub>) في المنطقة الممتصة p-type CIGS. من حيث تحقيق أعلى مردود تحويل فوطوفولطائي، فإن زيادة تركيز التطعيم أعطى مردود 23.28%. زيادة سمك المنطقة p-type CIGS حسن المردود أكثر إلى 25.22%. و مع ذلك ، من الأحسن الحد من كثافة العيوب من أجل تجنب تدهور الوسائط الفولطائية مع قيمة موصى بها لكثافة العيوب لا تتجاوز 10<sup>15</sup> cm<sup>-3</sup>. من جهة أخرى لم تظهر وسائط الخروج الفوطوفولطائية أي تأثير بعمل الإنتزاع (φ<sub>m</sub>) لمعدن الكاثود لدى تغييره في المجال [4.1-4.7 eV]. تسلط هذه النتائج الضوء على أهمية تحسين الوسائط مثل تركيز التطعيم والسمك وكثافة العيوب من أجل تحقيق أعلى مردود تحويل فوطوفولطائي في الخلايا الشمسية ذات حاجز شوتكي بناءً على مادة CIGS مطعمة من النوع p.

**كلمات مفتاحية:** CIGS ؛ خلية شمسية ؛ حاجز شوتكي ؛ محاكاة رقمية

## Abstract

We have investigated a Schottky barrier solar cell based on p-type Cu(In,Ga)Se<sub>2</sub> (CIGS) material, using the Scaps-1D numerical simulation software for steady-state calculations. Internal parameters such as band diagram, electron and hole concentrations, and recombination rate were evaluated. External parameters such as current density-voltage (J - V) and power-voltage (P - V) characteristics were calculated. Photovoltaic output parameters, including short circuit current density (J<sub>sc</sub>), open circuit voltage (V<sub>oc</sub>), fill factor (FF), maximum power (P<sub>max</sub>), and photovoltaic conversion efficiency (η), were extracted. The investigation focused on changing the defect density (N<sub>t</sub>), thickness (d), and doping concentration (N<sub>A</sub>) of the CIGS absorber layer. In terms of achieving the highest photovoltaic conversion efficiency (η), increasing the doping concentration yielded 23.28%. Increasing the thickness of the p-type CIGS layer further improved efficiency to 25.22%. However, it is advisable to limit the defect density to avoid degradation, with a recommended value not exceeding 10<sup>15</sup> cm<sup>-3</sup>. On the other hand, the photovoltaic output parameters of the cell show no dependency on the cathode work function (φ<sub>m</sub>) changing in the range [4.1-4.7 eV]. These findings highlight the importance of optimizing parameters such as doping concentration, thickness, and defect density in order to achieve the highest photovoltaic conversion efficiency in Schottky barrier solar cells based on p-type CIGS material.

**Keywords:** CIGS; solar cell; Schottky barrier; numerical simulation